


Spring 2010

Analysis of conjugated polymer nanotubules formed by template wetting nanofabrication

Steven D. Bearden Jr.
Louisiana Tech University

Follow this and additional works at: <https://digitalcommons.latech.edu/dissertations>

 Part of the [Chemical Engineering Commons](#), [Materials Science and Engineering Commons](#), and the [Nanoscience and Nanotechnology Commons](#)

Recommended Citation

Bearden, Steven D. Jr., "" (2010). *Dissertation*. 456.
<https://digitalcommons.latech.edu/dissertations/456>

This Dissertation is brought to you for free and open access by the Graduate School at Louisiana Tech Digital Commons. It has been accepted for inclusion in Doctoral Dissertations by an authorized administrator of Louisiana Tech Digital Commons. For more information, please contact digitalcommons@latech.edu.

NOTE TO USERS

This reproduction is the best copy available.

UMI[®]



**ANALYSIS OF CONJUGATED POLYMER NANOTUBULES
FORMED BY TEMPLATE WETTING NANOFABRICATION**

by

STEVEN D. BEARDEN, JR., M. S.

A Dissertation Presented in Partial Fulfillment
of the Requirements for the Degree
Doctor of Philosophy

COLLEGE OF ENGINEERING AND SCIENCE
LOUISIANA TECH UNIVERSITY

May 2010

UMI Number: 3411208

All rights reserved

INFORMATION TO ALL USERS

The quality of this reproduction is dependent upon the quality of the copy submitted.

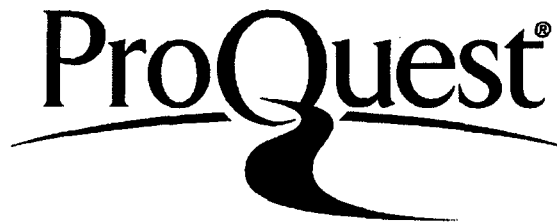
In the unlikely event that the author did not send a complete manuscript and there are missing pages, these will be noted. Also, if material had to be removed, a note will indicate the deletion.



UMI 3411208

Copyright 2010 by ProQuest LLC.

All rights reserved. This edition of the work is protected against unauthorized copying under Title 17, United States Code.



ProQuest LLC
789 East Eisenhower Parkway
P.O. Box 1346
Ann Arbor, MI 48106-1346

APPROVAL FOR SCHOLARLY DISSEMINATION

The author grants to the Prescott Memorial Library of Louisiana Tech University the right to reproduce, by appropriate methods, upon request, any or all portions of this Dissertation. It is understood that the "proper request" consists of the agreement, on the part of the requesting party, that said reproduction is for his personal use and that subsequent reproduction will not occur without written approval of the author of this Dissertation. Further, any portion of the Dissertation used in books, papers, and other works must be appropriately referenced to this Dissertation.

Finally, the author of this Dissertation reserves the right to publish freely, in the literature, at any time, any or all portions of this Dissertation.

Author Steven T. Bush

Date 04-25-2010

LOUISIANA TECH UNIVERSITY

THE GRADUATE SCHOOL

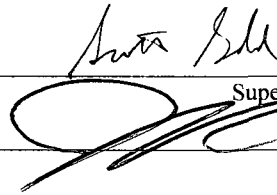
04/06/2010

Date

We hereby recommend that the dissertation prepared under our supervision
by Steven D. Bearden, Jr.

entitled ANALYSIS OF CONJUGATED POLYMER NANOTUBULES FORMED BY
TEMPLATE WETTING NANOFABRICATION

be accepted in partial fulfillment of the requirements for the Degree of
Doctor of Philosophy in Engineering

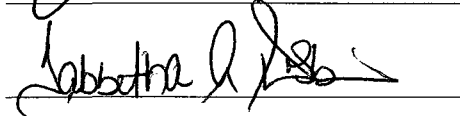
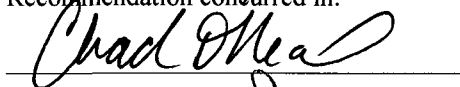


Supervisor of Dissertation Research

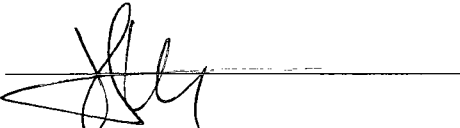
Head of Department

Department

Recommendation concurred in:



Advisory Committee




Approved:

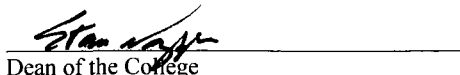


Director of Graduate Studies

Approved:



Dean of the Graduate School



Dean of the College

ABSTRACT

Semiconducting and optoelectric conjugated polymers have potential in micro and nano-electronic applications. Their widely tunable physical conformations and orientations make these polymers ideal material for engineering small scale devices. The polymers have been incorporated into several electronic devices including light-emitting diodes, solar cells, and field-effect transistors. Widespread adoption of these materials will not be a reality until the issues of poor device performance, short lifespans, and device degradation are resolved.

Nanostructures have been demonstrated to have improvements in molecular ordering and electronic transport. In the work presented here, tubular nanostructures of conjugated polymers fabricated by the template wetting nanofabrication process are analyzed for their structural and electronic properties. Analysis focused on the optical absorbance of these materials and the effects of confinement, filtration, and solvent choice have on disordered and ordered polymers. Other analyses include the effects of polymer blending, orientation, and solvent evaporation determined from vibrational spectroscopy, thermogravimetric analysis, and mobility characteristics.

Improvements in optical bandgap of MEH-PPV and P3HT ranging from ~ 0.12 eV to 0.05 eV, respectively, were found for nanotubes cast chloroform. The improvements in bandgap from all solvents were found to be, on average, 0.08 eV for MEH-PPV and 0.05 eV for P3HT. Enhancement due to nanostructuring of P3HT were

found to be independent of pore size but dependent on molecule size as low molecular weight fractions obtained from DC filtration were found to have spectrum similar to drop-cast films. Solvent choice in MEH-PPV was found to be highly important as the non-aromatic solvents THF and chloroform were found to have dichroic ratios greater than 10 indicating a highly aligned structure that increased the optical bandgaps and mobilities of the samples. Order was shown to also be dependent on the gel solvent evaporation time fraction which was 0.17 for chloroform and 0.58 for THF. Solvent choice for P3HT was shown to increase when cast from THF with a dichroic ratio ~ 16 and a $t_{\text{gel}}/t_{\text{total}}$ of 0.75. The order in THF samples of P3HT, however, did not noticeably affect the optical properties.

This dissertation shows that the nanostructuring of amorphous and semi-crystalline conjugated polymers leads to increased order, enhanced optical properties, as well as longer effective conjugation lengths that have not been noted in device created from these polymers before.

TABLE OF CONTENTS

ABSTRACT	iv
LIST OF TABLES	ix
LIST OF FIGURES	x
ACKNOWLEDGMENTS	xiii
CHAPTER 1 INTRODUCTION.....	1
CHAPTER 2 LITERATURE REVIEW.....	6
Properties of Conjugated Polymers	7
Optical Absorbance.....	7
Electrical Properties.....	13
Luminescence	15
Solvent Interactions	17
Nanostructuring of Organic Materials	20
Electrospinning.....	21
Template Synthesis.....	23
Template Wetting	25
CHAPTER 3 EXPERIMENTAL METHODS.....	28
Materials	28
Template Wetting of Porous Anodized Aluminum Oxide with Polymer Solutions.....	30
Ultraviolet-Visible Spectroscopy.....	34
Infrared Spectroscopy.....	39

Thermogravimetric Analysis	43
Electrical Testing	44
CHAPTER 4 CHARACTERIZATION OF CONJUGATED POLYMER NANOSTRUCTURES FABRICATED VIA TEMPLATE WETTING....	46
Introduction.....	46
Experimental.....	48
Materials	48
Methods	48
Results and Discussion	50
Conclusions.....	55
CHAPTER 5 SPECTROSCOPIC AND ELECTRICAL EVALUATION OF POLY(3-HEXYLTHIOPHENE) NANOTUBES	57
Introduction.....	57
Experimental.....	58
Materials	58
Methods	58
Results and Discussion	60
Electrical Characterization.....	60
Hole Mobility.....	64
Polarized FTIR.....	64
Conclusions.....	65
CHAPTER 6 IMPACT OF PURIFICATION BY SOXHLET EXTRACTION OF POLYTHIOPHENE NANOTUBES	67
Introduction.....	67
Experimental.....	69
Materials	69

Methods	69
Results and Discussion	71
Electronic Spectra	71
Electrical Characterization.....	75
Conclusion	76
CHAPTER 7 WATCHING PAINT DRY: THE EFFECTS OF CASTING SOLVENT ON THE FORMATION OF CONJUGATED POLYMER NANOTUBES CREATED WITH TEMPLATE WETTING NANOFABRICATION	78
Introduction.....	78
Experimental	80
Materials	80
Methods	81
Results and Discussion	83
Electrical Characterization.....	83
UV-Visible Spectroscopy	84
Polarized Infrared Spectroscopy	89
Solution Evaporation Characteristics.....	93
Conclusion	97
CHAPTER 8 CONCLUSION	100
Future Work.....	103
REFERENCES	105

LIST OF TABLES

Table 5.1.	Quantitative comparison of P3HT thin film and nanotubule spectra, illustrating the peak narrowing and redshift of the nanotubule spectra relative to films	60
Table 5.2.	Peak locations in UV-Vis absorption band as identified from minima in 2 nd derivative of absorption spectrum.....	62
Table 6.1.	Percentage of material extracted in each cycle of the Soxhlet extraction procedure for experimental work done here and elsewhere	70
Table 6.2.	Quantitative comparison of P3HT thin film and nanotubule spectra, illustrating the peak narrowing and redshift of the nanotubule spectra relative to films	73
Table 6.3.	Peak locations in UV-Vis absorption band identified from minima in 2 nd derivative of absorption spectrum. Film data denoted with * is from Trznadel et al. [9].....	74
Table 7.1.	Hole mobility determined from analysis of space-charge-limited currents in MEH-PPV and P3HT nanotube-based electronic devices	84
Table 7.2.	Peak absorption and optical bandgap for MEH-PPV and P3HT thin films and 100 nm nanotubules determined from UV-Vis spectra	86
Table 7.3.	Peak locations in P3HT UV-Vis absorption band as identified from minima in 2 nd derivative of absorption spectrum. Relative peak location is designated with a vertical dashed line.....	88
Table 7.4.	Peak locations in MEH-PPV UV-Vis absorption band as identified from minima in 2 nd derivative of absorption spectrum. Relative peak location is designated with a vertical dashed line.....	89
Table 7.5.	Dichroic ratio of MEH-PPV and P3HT nanotubules determined by polarized FTIR shown with the measured absorbances for each orientation. Dichroic ratio calculated using Equation 7.2	90

LIST OF FIGURES

Figure 2.1. Single and overlapping p -orbitals from the sp^2 carbons along the backbone of a conjugated polymer form π -bonding and π -anti-bonding molecular orbitals, allowing for transfer from one band to another due to absorbed energy	8
Figure 2.2. Kuhn's model for the potential energy of a chromophore with alternating bond length. The potential energy is seen as a sine wave with V_0 as the amplitude and the minimum excitation energy for an infinitely long conjugation length	10
Figure 2.3. Relative interchain excitation energy levels for π - π^* transition for two cofacial polymers.....	12
Figure 2.4. Illustration of the excitation energy and energy necessary to initially transport an electron/hole. An electron-hole pair is created a) by initial excitation or absorption of a photon. The electron and hole have a columbic attraction b) that must be overcome to separate the charges and induce conduction.....	14
Figure 3.1. General chemical structure of a) PPV, b) polythiophene, c) MEH-PPV, and d) P3HT.....	29
Figure 3.2. Description of the solution-based template wetting procedure carried out in this work. The process shown is for the fabrication of MEH-PPV nanotubes from a MEH-PPV/chloroform wetting solution.....	32
Figure 3.3. SEM micrograph of a template wetted with MEH-PPV a) with residual polymer on the top of the template and b) with the residual polymer removed by plasma. Figure 3.3b is courtesy of CAMD at LSU Baton Rouge.....	33
Figure 3.4. SEM imaging of a) MEH-PPV and b) P3HT nanotubes created using solution-based template wetting procedures.....	34
Figure 3.5. Illustration of the location of the optical bandgap (E_g) as the intersection of the linear regions just before and after the onset of absorption.....	39
Figure 3.6. Setup for polarized FTIR to calculate the R for polymer orientation normal to the surface of the film surface	43

Figure 3.7. The generalized device structure used is illustrated in a), while b) illustrates the barrier height minimization due to anode and cathode material choice of Au in the construction of hole-only devices. Gray sections in a) represent the template and the squiggly lines represent incorporated polymer [146]	45
Figure 4.1. SEM photo of P3HT nanotubes partially released from the AAO template.....	49
Figure 4.2. <i>J-V</i> curves for nanocomposites of a 100 nm pore diameter AAO with MEH-PPV, a 50:50 blend MEH-PPV and P3HT, and P3HT [108].....	51
Figure 4.3. Mobilities calculated from the SCLC model for nanocomposites of MEH-PPV/aluminum oxide, 50:50 (by vol.) blend of MEH-PPV and P3HT/aluminum oxide, and P3HT/aluminum oxide [108]	52
Figure 4.4. UV-Vis spectra of P3HT solution, film, and composite.....	53
Figure 4.5. UV-Vis spectra of MEH-PPV solution, film, and composite.....	53
Figure 4.6. UV-Vis spectra of the three polymer composites.....	54
Figure 4.7. FTIR spectra in the double bond region of the three polymer composites....	55
Figure 5.1. Representative SEM photo of P3HT nanotubes.....	59
Figure 5.2. UV-Vis spectra of P3HT thin films compared to those of 200 nm and 100 nm nanotubes fabricated via template wetting nanofabrication	60
Figure 5.3. UV-Vis spectra (solid line) showing 2 nd derivative of absorbance (dashed line) used to identify peak locations for P3HT in a) thin films, b) 200 nm nanotubes, and c) 100 nm nanotubes.....	63
Figure 5.4. The C-C inter-ring vibrational band for the \perp (dashed line) and 30° (solid line) polarizations. The full FTIR spectra are shown in the inset.....	65
Figure 6.1. UV-Vis spectra of P3HT as received (UNF), and fractions extracted with dichloromethane (DC) and tetrahydrofuran (THF) via Soxhlet extraction a) cast into films, b) in 200 nm diameter nanotubes, and c) 100 nm diameter nanotubes.....	72
Figure 6.2. Representative UV-Vis spectra (solid line) showing the 2 nd derivative of absorbance (dashed line) used to identify peak locations for P3HT in a) 200 nm nanotubes cast from the THF fraction and b) 200 nm nanotubes cast from the DC fraction. The vertical dotted lines represent minima in the 2 nd derivative of the spectrum.....	75

Figure 6.3. J - V characteristics for nanotube-based electronic devices created with various fractions of P3HT material for a) 100 nm and b) 200 nm nanotubes. Solid lines represent regression fits to Equation 3.5 [146].....	76
Figure 7.1. Scanning electron micrographs of a) MEH-PPV and b)P3HT nanotubes created using template wetting in 100 nm diameter alumina nanopores with chloroform as the solvent for the wetting solution.....	81
Figure 7.2. Average J - V characteristics for electronic devices fabricated from 100 nm nanotubes of a) MEH-PPV and b) P3HT, created by template wetting from various solvents. Solid lines represent least-squares-regression fits to Equation 3.5 [146].....	83
Figure 7.3. UV-Vis absorbance spectra for a) thin films and c) 100 nm nanotubules of MEH-PPV and b) thin films and d) 100 nm nanotubules of P3HT in four solvents.....	85
Figure 7.4. Hole mobility (μ_p) [146] and optical bandgap E_g for 100 nm nanotubules of a) MEH-PPV and b) P3HT. The closed symbols correspond to the μ_p and the open symbols correspond to E_g	87
Figure 7.5. Mobility data [146] plotted as a function of dichroic ratio in a) MEH-PPV and b) P3HT as well as optical bandgap as a function of dichroic ratio in c) MEH-PPV and d) P3HT.....	92
Figure 7.6. Illustration showing the three phases that make up the drying of the MEH-PPV and P3HT in various solvents	93
Figure 7.7. Gel drying fraction (t_{gel}/t_{total}) for MEH-PPV and P3HT polymer solutions compared with the a-b) dichroic ratio, c-d) optical bandgap (E_g), and e-f) hole mobility (μ_p) [146]	96

ACKNOWLEDGMENTS

First, I would like to thank my research advisor and mentor, Dr. Scott A. Gold, who has continually and unyieldingly provided the support, encouragement, and direction necessary to the completion of my dissertation.

I would also like to extend my heartfelt thanks to my wife Katie. Without her support and encouragement I never would have been able to attempt an undertaking of this magnitude. My extended family must also share in that thanks as they instilled in me the importance of education and never once doubted my efforts.

Thanks must also be given to my committee members, Dr. Pedro Derosa, Dr. Tabbetha Dobbins, Dr. Chad O'Neal, and Dr. Sandra Zivanovic, who helped to direct and support this work and whose efforts made it better.

An additional thank you must be given to Joey Cannon who was the instigation of this work and who provided supportive efforts and contributions to some of the work contained in this dissertation. I would also like to thank the faculty and staff of the IfM, especially Dee Tatum, Deb Wood, and the late Scott Williams who aided me with anything that I needed to complete my work.

A final thanks is extended to Dr. David Mills and Dr. Daniela Mainardi who provided me with financial support and extremely beneficial professional development through the NSF GK-12 Teaching Fellows program. Their efforts through the GK-12 program helped me to finish my work and prepare for whatever comes after.

CHAPTER 1

INTRODUCTION

With the discovery of electrically conductive polyacetylene [1-3], the field of synthetic metals was born [4], and with it, great interest into the field of organic electronic devices. The conductivity of polyacetylene was small, but it inspired a host of other organic electronic materials with better properties. In polythiophenes, for example, the electronic transport has increased by five orders of magnitude in as few as 15 years [5-7]. These material advances have stemmed from basic research into the production of higher yields of regioregular structures [8], purity [9], and the fundamentals molecular ordering to increase electron/hole transport [10].

Conjugated polymers have found applications in a variety of commercial and consumer electronics including: light-emitting diodes (OLEDs) [11-13], solar cells [13-15], and field-effect transistors [5, 16, 17]. Conjugated polymers have largely generated interest due to their inexpensive processing from solutions at room temperature using methods such as inkjet printing [18], electrospinning [19], and template wetting [20, 21]. This has led to a few commercially available products being adopted by industries in the last few years. These applications are, as of now, limited in scope [7, 20, 22].

Devices created from conjugated polymers are hampered by relatively poor performance; limited lifespans, lower reliability, and susceptibility to degradation under ambient conditions continue to frustrate and to inspire new areas of research [7, 20, 23].

Applications in the fields of radio frequency identification tags and smart cards are promising as they are low-cost and disposable electronics well suited to the characteristics of conjugated polymers [21]. A growing field of conjugated polymer electronic devices, as well as one of the first commercial applications, is that of rechargeable batteries and energy storage [24].

The inherent optoelectric properties of conjugated polymers has held great promise in the last decade to create OLED displays for cell phones, notebook computers, and hand-held devices and is the subject of a large amount of industrial research [22, 25]. For example, IBM has put a large number of resources into the development of inexpensive and flexible displays [21] as well as entertainment headsets [25]. Though it would certainly appear to be a large future market for these materials, further research into the device characteristics and fabrication techniques is needed to move from the research lab and into the marketplace.

In order to create devices from conjugated polymers, many material deficiencies must be overcome. Polymer chain aggregation hampers the production of OLEDs [26] while insufficient chain aggregation and high bandgaps prevent the production of photovoltaic devices [27]. These deficiencies are small compared to the poor charge transport properties in solid-state devices [28].

The semiconducting properties of conjugated polymers are a function of the alternating double and single carbon bonds that are the primary components of the polymer backbone. The delocalization of the π bonds along the backbone from the valence band to the conduction band [29], creates an environment that allows for electron transport along the polymer backbone and from one polymer to another [7, 10]. More

ordered polymer chains that reduce interchain distance while extending the conformation of the polymer in a oriented direction is key to the creation of polymer devices with better transport processes [10].

The nanostructuring of conjugated polymers has been found to have advantageous properties. This advantage is due to the forced packing and order of these polymers on the nanoscale. This induced order prevents the polymer from being able to relax into conformations with unfavorable electronic properties. The work presented here examines the effect of confinement on two widely studied conjugated polymers, MEH-PPV and P3HT, by imbedding them into nanoporous anodized aluminum oxide membranes using the template wetting nanofabrication process [30]. The goal of this dissertation is to examine the optical, infrared, and electrical properties of template wetted MEH-PPV and P3HT nanotubules constructed using template wetting nanofabrication in order to determine the effects of the nanostructuring, decreasing nanopore diameter, filtration of impurities, and solvent choice on the structure of the MEH-PPV and P3HT nanotubes.

Chapter 2 gives an overview of the background work related to research and experimental methods presented in this dissertation. Optical absorption, electronic transport properties, and luminescence are reviewed as it pertains to the molecular order of solid-state conjugated polymers. The particulars of molecular ordering from solution casting are detailed in a section on solvent interactions. Nanofabrication methods of conjugated polymer devices are reviewed with the focus of creating cylindrical structures (nanotubes and nanowires) at this scale. The template wetting nanofabrication technique as well as the underlying science behind it is detailed at the end of the chapter.

Chapter 3 explains the experimental methods used in this work including the details of template wetting techniques with respect to device fabrication. Methods for collecting and analyzing ultraviolet-visible spectroscopy (UV-Vis) and Fourier transform infrared spectroscopy (FTIR) are described. Brief discussions on the mathematical analysis of space-charge-limited (SCL) current and thermogravimetric analysis (TGA) of the solvent drying characteristics are also presented.

Chapter 4 discusses the fabrication of nanocomposites from two commonly studied conjugated polymers and porous anodized aluminum oxide. Optical bandgaps of the conjugated polymers in these composites was found to be at a lower energy which suggests a more ordered polymer with higher degrees of alignment and chain packing. A blend of the two polymers in the porous template was found to be a simple mixture of the two polymers without any noticeable electrical interactions.

Chapter 5 investigates the nanostructuring of a commonly studied derivative of polythiophene by solution based template wetting. UV-Vis optical absorption revealed a more ordered structure with a narrower region of electronic states. Further analysis of the absorption spectrum revealed that the nanostructured polythiophene had absorption bands not seen in thin film devices indicated a change in the self-orientation of this semi-crystalline conjugated polymer. Polarized infrared spectroscopy found that the polythiophene backbone was aligned with the wall of the nanopore.

Chapter 6 determines the impact of impurities on the optical and electrical properties of nanotubule polythiophene. Purification by Soxhlet extraction is known as an effective technique for the removal of residual catalyst and other impurities for polythiophenes. In this study, Soxhlet extraction was used to filter out these impurities

before nanostructuring by template wetting. UV-Vis absorbance was used to determine the effect of the contaminants/purification on the effective conjugation length of the polymer.

Chapter 7 investigates the role that solvents will have on the formation and properties of conjugated polymer nanotubes fabricated by solution based template wetting. It is well known that polymer conformations in solid state devices depend on the solvent used and the fabrication process employed. The effect that differing solvents play in the template wetting process is not been well studied. Nanotubules from two commonly studied conjugated polymers are studied for their electronic transport, optical absorption, orientation, and solvent evaporation characteristics. The effects of amorphous and semi-crystalline polymers as well as the aromatic and non-aromatic solvents are discussed.

Chapter 8 concludes the dissertation work with a final discussion of key results and brief remarks about possible future research projects.

CHAPTER 2

LITERATURE REVIEW

Semiconducting polymers have been studied widely in recent years for a variety of applications in electronic devices. Their electroluminescent properties have been researched for potential light-emitting diodes [11, 12] while their optoelectric properties have found interest in photovoltaics [14, 15]. Their semiconducting nature has lead more researchers to study them for use in field effect transistors [5, 16, 17]. Optimism for these polymers to be used in commercial applications has mainly been hampered by poor electronic performance due (among other issues) to the lack of a regular structure in the solid state. This has made it essential to increase the molecular order of these materials in order to create viable devices [10, 31].

Chapter 2 is organized into two major sections; Properties of Conjugated Polymers and Nanostructuring of Conjugated Polymers. The first section covers the optical absorbance of these materials and the polymer conformations that bring about those properties, a brief discussion about the electrical transport characteristics of conjugated polymers, a discussion on the luminescence, and the solvent interactions that effect the structural conformation of the conjugated polymers and the effects that this has on devices cast from these solvents. Nanostructuring of Conjugated Polymers briefly reviews three major techniques for fabricating tubular and cylindrical nanostructures with a discussion on the properties of polymers created by these methods.

Properties of Conjugated Polymers

Optical Absorbance

The ability for semiconducting polymers to absorb light in the UV and Visible regions is derived from the conjugated structure of the polymer. This is an alternating of double (π and σ) and single (σ) bonds along the polymer chain. The π bond is composed of two p-orbitals that arise from two double bonded carbon atoms and is relatively weak when compared to the σ bond formed from the s-orbitals. When the π bond is excited, via thermal or optical effects, it converts to a higher energy π^* anti-bonding orbital [28]. Therefore, the π bond will only convert to a π^* bond if the excitation of the bond is equal to the energy gap between the two levels. This excitation from the highest occupied molecular orbit (HOMO) to the lowest unoccupied molecular orbit (LUMO) is sometimes used interchangeably with bandgap (E_g) [32].

Trans-polyacetylene is the simplest case of a conjugated polymer. The excitation in a conjugated polymer differ from traditional electron-electron excitation in that the energy absorbed is the energy necessary to create an electron-hole pair. This pair, otherwise known as an exciton, is part of the transport mechanism that will be discussed in a later section. The energy required to create the electron-hole pair depends very strongly on the length of conjugation present as the delocalization will occur along the length of the polymer chain. Since the polymer is conjugated, single bonds and double bonds can move relative to one another. This allows for the configuration of the electrons to change based on the energy applied. In general, the greater the number of double bonds, the lower the energy necessary to excite the electron to the LUMO level and create a hole. Figure 2.1 illustrates the relative difference in orbital levels between a single π bond and two π bonds in conjugation. A single π bond only has only one

excitation energy. A series of two π bonds has four possible excitation energies with the lowest occurring at a lower energy than a single π bond.

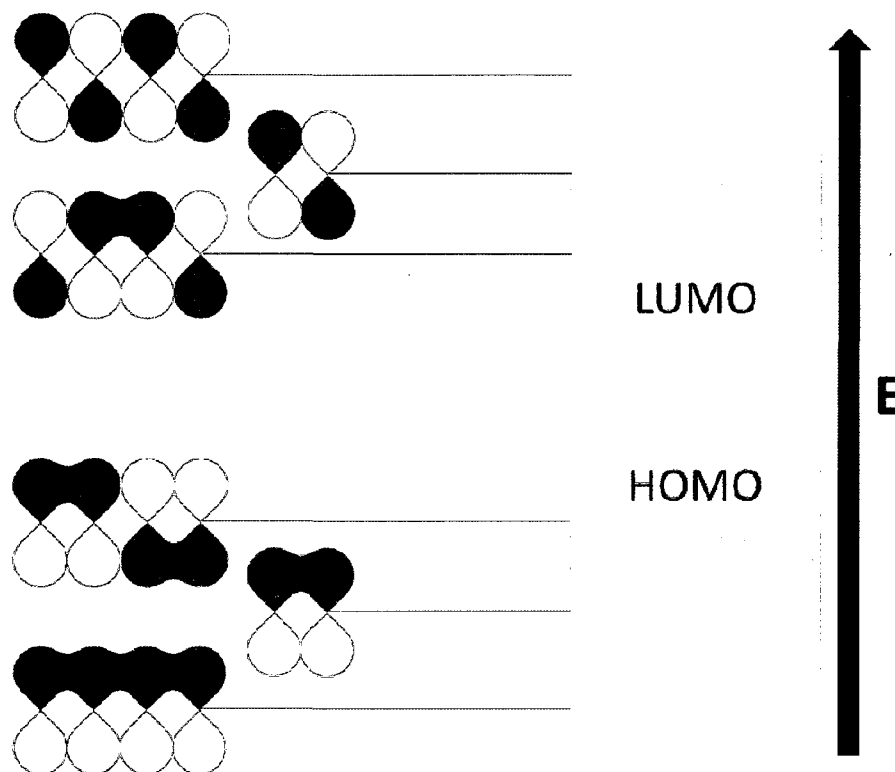


Figure 2.1. Single and overlapping p -orbitals from the sp^2 carbons along the backbone of a conjugated polymer form π -bonding and π -anti-bonding molecular orbitals, allowing for transfer from one band to another due to absorbed energy.

Kuhn described this tendency using methods similar to those used to determine the functional groups associated with chromophores in organic dyes [33, 34]. This assumed that the electron conformed to a model of being in a gas contained within an energy well that is a function of the size of the conjugation. The electron is then subject to a potential energy function from the atoms that create the conjugation and conforms to a sinusoidal wave pattern as shown in Figure 2.2. Using this method Kuhn developed the equation for the minimum absorption energy

$$\Delta E_1 = \frac{h^2}{8mL^2} (N+1) + V_0 \left(1 - \frac{1}{N}\right), \quad (2.1)$$

where h is the Plank's constant, m is the mass of an electron, L is the length of the conjugated chromophore, N is the number of π electrons, and V_0 is a constant [34]. This equation was updated years later by Taubmann to correct for the conjugation length of non polyenic polymers by

$$L = (N+l)d, \quad (2.2)$$

where d is the average bond length for C-C and C=C bonds and l is a correction factor accounting for the difference between the actual conjugation length and the one calculated by $N*d$ [35]. Combining Equations 2.1 and 2.2 yields

$$\Delta E_1 = \frac{h^2}{8md^2} \frac{(N+1)}{(N+l)^2} + V_0 \left(1 - \frac{1}{N}\right) \quad [36]. \quad (2.3)$$

Equations 2.1 and 2.3 show that an increase in the conjugation length reduces the excitation energy by a factor of $1/N$ resulting in a minimum energy, V_0 . Though conjugated polymers are generally much larger molecules than chromophores found in organic dyes, the general method provides a reasonably good approximation and is used regularly as a common association in the literature [36-38].

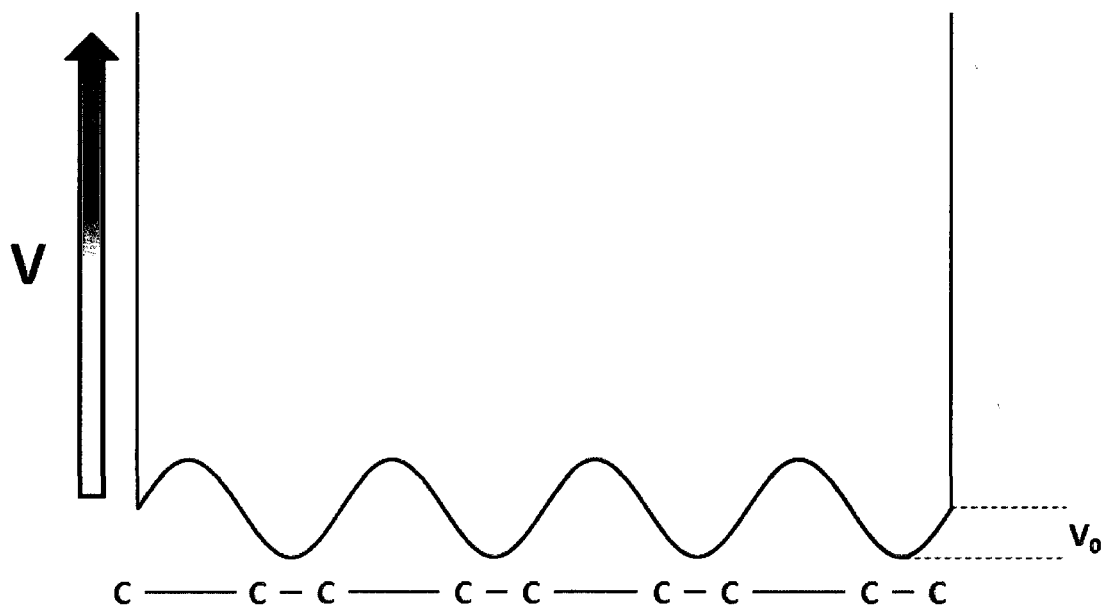


Figure 2.2. Kuhn's model for the potential energy of a chromophore with alternating bond length. The potential energy is seen as a sine wave with V_0 as the amplitude and the minimum excitation energy for an infinitely long conjugation length.

As polymers increase in molecular weight and chain length, the probability of defects within the chain rises. Polymer chains are known to be susceptible to a variety of conditions like tetrahedral sp^3 errors in polymerization where a double bond is replaced by a single bond inducing physical folding of the polymer chain [39]. These defects are particularly common in polymer chains that have been adsorbed onto the surface of some solid where the polymer will have aptly descriptive defects called loops, curls, and tails [40].

Defects in the chain will have the effect of lowering the overall conjugation length of the polymer [26]. Isolated chain sections will thus excite at different discrete energy levels. If there is sufficient energy, the conjugation can extend across a defect. This leads to a condition where the particular section is absorbing at an energy lower than that of the two related sections, but higher than if there was no defect [26]. This energy

will appear to correlate to a conjugation length that does not actually exist physically. Therefore, it is sometimes helpful to describe an excitation in terms of its effective conjugation length [41]. Since the actual conjugation length is not helpful or accurate in describing the excitation energy, it can be referred to be the number of conjugations that would be associated with an excitation at its particular energy [42]. It is rarely helpful to attempt to calculate the effective conjugation length since there is no physical definition [42]. The effective conjugation length allows for a qualitative comparison where one might describe a polymer with a longer effective conjugation length.

All of these different states can be described as a statistical distribution of absorption energies. Whereas a pure element will only show absorptions at discrete energy levels, a polymer chain will show a combination of every possible absorption energy [43] resulting in a near Gaussian curve where the energy at the onset of the curve is thought to be the optical band gap (E_g) and the peak is the highest concentration of electronic states or effective conjugation lengths [32].

Neighboring polymer chains will also interact electrically. Just as the excitation energy can be affected due to interactions across a defect within the polymer; it can also interact across the space between polymers as illustrated in Figure 2.3. The energy needed to cross this gap depends on the chain alignment and the energy needed to tunnel between chains is greater than the energy needed to cross an intrachain defect [44]. The closer two chains are to each other, the lower the energy needed for excitation due to the overlapping p-orbitals [26, 45]. This may be disrupted by defects in both chains causing chain alignment to only be in sections. However, the nearby presence of another

conjugated polymer with overlapping p-orbitals will have the effect of further lengthening the effective conjugation length.

Chain proximity is not always the dominating factor in reducing absorption energy. Orientation of one polymer with respect to another can have profound effects, especially on conjugated polymers that contain ring structures. A polymer chain that is aligned with another nearby chain is said to be in cofacial alignment. If stacked polymer chains are skewed or at an angle, then cofacial alignment is decreased as is the effective conjugation length. The more cofacial two polymers are the more states are able to interact. This has the effect of further increasing the effective conjugation length and decreasing the optical bandgap [46].

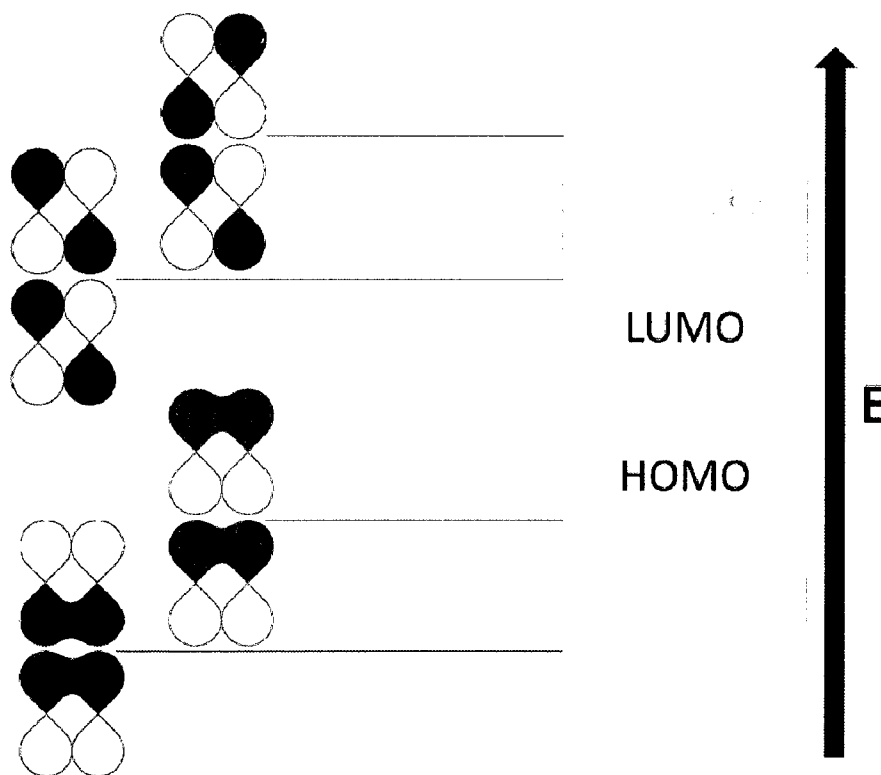


Figure 2.3. Relative interchain excitation energy levels for π - π^* transition for two cofacial polymers.

Electrical Properties

The semiconducting nature of conjugated polymers is closely related to the same material properties that drive optical absorption. A conducting charge delocalizes the π bond to create an electron hole pair just as in optical absorption. The energy level needed for this delocalization is lowered as the effective conjugation length increases. Therefore, for the initial excitation, the optical and electrical bandgaps are thought to be identical [4].

Unlike optical absorption, the charge carrier must pass through the medium. In order to do this a second mechanism must be considered. When an electron is elevated to the LUMO level an electron-hole pair is formed. A columbic attraction exists between the electron and the hole that must be overcome to transport either charge [47] as illustrated in Figure 2.4. A π bond delocalization also creates a repulsion between the p orbitals where there had once been an attraction. This repulsion results in the σ bond being stretched. As the exciton moves through the polymer, it travels with this “stretching” mechanism that causes a physical wave (or phonon) to move with the electron-hole pair [48]. In order to pass charge through the polymer, the electrical energy must be high enough to create the exciton, overcome the columbic attraction to split the exciton, and then transport the phonon. The electron-phonon transport can tunnel across chain defects and spaces between chains. This typically results in an electrical bandgap that is 0.5 to 1 eV larger than the optical bandgap [4, 48]. This further underscores the overall importance the chain organization and the effective conjugation length in creating a device.

These effects are valid for most conjugated polymers. However, most of the polymers considered up until now conform to the polyenic category in which the polymer

backbone is made up of alternating double and single bonds only (as in polyacetylene). For non-polyenes, such as poly(p-phenylene-vinylene) (PPV) or polythiophene (PT), the aromatic ring structure alters some of the electronic properties. The double bonds will localize in the ring structure of the polymer backbone which is the most energetically stable configuration[49]. The ability of the bonds to conjugate, allows for the polymer to form a quinoid configuration in which the double bonds will localize outside of the ring structure. The quinoid structure has a higher energy and thus a possible, but not energetically stable, lower bandgap [49, 50].

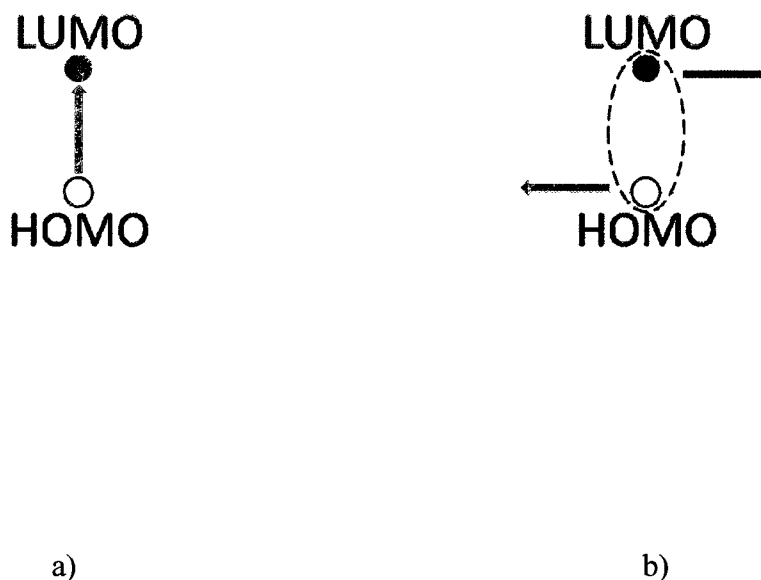


Figure 2.4. Illustration of the excitation energy and energy necessary to initially transport an electron/hole. An electron-hole pair is created a) by initial excitation or absorption of a photon. The electron and hole have a coulombic attraction b) that must be overcome to separate the charges and induce conduction.

The conductivity of conjugated polymers can vary depending on a couple of factors. As described before, chain organization in a bulk polymer structure can alter the effective conjugation length and affect device performance. More crystalline polymers, such as regioregular poly(3-hexylthiophene) (P3HT) [10, 51], generally exhibit a higher conductivity than the more amorphous non-regioregular P3HT [5] even though the chemical makeup of the two are identical. Beyond those reasons already studied, a significant barrier to larger conductivities is the fact that the π -bonds are not intrinsically delocalized which supplies relatively few free carriers that are available for transport [52]. In order to increase the number of carriers, doping the conjugated polymer with electron acceptors such as bromine or iodine; or electron donors such as alkali metals have been shown to increase conductivities several orders of magnitude to a point where they have been referred to as synthetic metals [1, 52-54]. Though the doping of these polymers is of interest to the subject as a whole, it is only included here for completeness.

Luminescence

The luminescence of conjugated polymers is of primary interest in relation to the development of inexpensive organic light-emitting diodes (OLEDs) [11-13]. There are two general mechanisms of luminescence in conjugated polymers: stimulated emission from absorbed photons (photoluminescence) and emission due to electronic charge transfer within the bulk polymer structure (electroluminescence) [55].

Photoluminescence (PL) occurs by the decay of an exciton that is created by the absorption of a photon. As described earlier, the absorption of the photon is highly dependent on the energy of that photon as well as the effective conjugation lengths available in the bulk polymer. The created exciton may decay back to the ground state that it excited from with a longer wavelength photon being emitted (due to a Stokes shift)

[55]. This is not the only available radiative decay available to the polymer structure. The exciton may move to another conjugation length with a lower energy and radiate from there with a different emitting wavelength [45]. Other paths the exciton may take is to nonradiatively transition the conjugation to the quinoid form and then decay with a lower energy photon [56] or simply decay to bipolarons and triplet excitons without the benefit of radiation [4, 29, 57]. The intra and interchain transport, as well as the usual distribution of effective conjugation lengths, make the PL complex than optical absorption.

Electroluminescence (EL) is no less complex. Holes that are injected into the HOMO band from positively charge polarons while negative polarons are created by electrons injected into the LUMO band. When these charged species combine, they will form an exciton [55]. This exciton can behave just as one that is created by photoexcitation as discussed in the previous paragraph. The EL spectrum is different from the PL spectrum in that it will not significantly overlap the absorption spectrum. Higher energy photons emitted by EL have a potential to be reabsorbed by the polymer while in PL the lower energy conjugation lengths are already excited by the injected photons [55]. EL is also limited by having a quantum yield approximately one quarter of that of PL as injected charge will only form excitons on average one in four times [55].

In either case, the yield of luminescence is highly dependent on the orientation and configuration of the polymer strands. Polymer structures with long effective conjugation lengths that contain interchain transport will generally have lower luminescence efficiency than those with short effective conjugation lengths [4, 29, 45, 50,

58, 59]. The more isolated the polymer strands and the more conformational defects that exist in the polymer structure the higher the quantum yields [56].

Solvent Interactions

Conjugated polymers have generated interest due to their inexpensive processing from solutions at room temperature using methods such as inkjet printing [18], electrospinning [19], and template wetting [20, 21]. Many devices created from conjugated polymers are created from a solution of the polymer dissolved in an appropriate solvent. In order to understand how devices created from conjugated polymers form it is necessary to review the reaction of these polymers in solution and during the solvent drying process [39]. The details of some solvent casting techniques are discussed at a greater length in the later in this chapter.

Polymers dissolve into a solvent via a two-step process. The solvent must diffuse into the bulk polymer causing the polymer to swell and form into a gel state [60]. From this point, the polymer slowly dissolves into the solution with sections of the polymer dissolving until the entire polymer chain becomes solvated and diffuses into the solution [40]. For a polymer chain to dissolve from a bulk a large amount of the polymer chain must interact with the, relatively, much smaller solvent molecules and overcome the intermolecular forces that are binding the bulk polymer together. For these reasons the degree of cross-linking, the crystallinity, and the molecular weight will all affect the solubility in a particular solvent [40, 60].

If the polymer is soluble in a solvent (solubility in this case meaning that a polymer chain will isolate and diffuse away from the bulk) then the solvent can be described by how it affects the conformation of the dissolved polymer chain. A “good” solvent (illustrated in Figure 2.5a) is one where the solvent interaction with the polymer

is greater than the polymer interaction with itself [40, 60, 61]. This causes the chain to be relatively extended. In contrast, a “bad” solvent (Figure 2.5b) is one where it is energetically favorable for the chain to either partially or completely collapse in on itself or another polymer [39, 60, 62, 63].

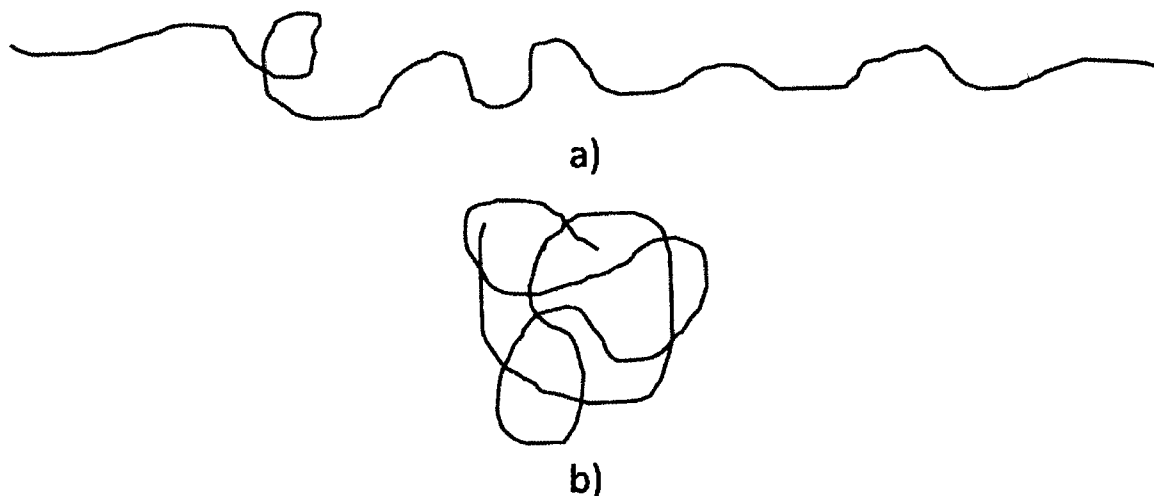


Figure 2.5. Illustration of polymer conformation in a solvent. A polymer chain in a good solvent (a) will have an extended conformation. A polymer chain in a bad solvent (b) will fold in on itself creating a collapsed coil.

Conformational changes of conjugated polymers in solution will alter the properties of that polymer. Conjugated polymers in good solvents will have little or no amount of interchain reaction and all properties will be solely from intrachain transport. In bad solvents, the chains begin to collapse on themselves [39] or sections of other polymer chains. A single chain that collapses in on itself is referred to as a collapsed coil. If more than one chain folds together it either be an aggregate, where the chains will fold together inducing charge transfer from one chromophore (effective conjugation length) to another, or an agglomerates, where the chains will fold together, but there will be no interchain interactions [61]. It has been suggested in literature that agglomeration

is the dominant form of chain folding [61]. In terms of absorption, an aggregate will absorb at a lower energy (or red shift) due to the longer effective conjugation length caused by the interchain reaction [61, 64] similar to the structure that the polymer would have in a solid [65]. The collapsed coil or a single polymer chain will absorb at a higher energy (blue shift) due to conformational defects shortening the effective conjugation length [66]. The absorption properties of agglomerates, lacking interactions between polymer chains, will not be changed [61].

The effects of solvent on the polymer chains and chain alignment affect the films cast from them [51, 67]. This is due to the polymer chains retaining a “memory” of the solvent that they are cast from [66, 68]. If the polymer chains, in a bad solvent, were to aggregate in solution, those aggregations would be deposited onto the surface. These aggregations can form together, but not interact electrically as the π bonds do not overlap [51, 68]. Agglomerations can create deformities on the surface of thin films and collapsed coils can create single chain polymer nanostructures [39, 62]. The solvent effect can be used to engineer the properties of the device. Luminescent devices can be fabricated from polymers with coupled interchain interactions; increasing the quantum efficiency of EL [4, 69]. Field-effect transistors and photovoltaics can be fabricated from good solvents creating very uniform films that exhibit a high level of interchain π bond overlap [67, 70].

When casting films of conjugated polymers from a solution, the factors of solubility [63], conformation within the solvent [39], solution concentration [66], molecular weight [70, 71], and solvent evaporation time [72] must all be taken into consideration. During the deposition of a semiconducting polymer solution, the solvent

evaporates from the polymer solution such that the conjugated backbone can align to the conjugated backbone of another polymer chain creating a supramolecular structure [62]. The ability for this alignment to occur is partially a function of the solvent evaporation time. A good solvent that has a low boiling point may evaporate too quickly not allowing for the formation of aggregates at the surface [66]. This can be thought of as a quenching of the deposited polymer in its solvated conformation [73]. A high boiling point solvent will allow for the conjugated backbones to align over time as they evaporate more slowly [51, 66, 70, 72]. With this in mind, several groups have found methods of slowing the evaporation time of low boiling point solvents from polymer solutions to enable the conjugated polymer chains to more readily align [62, 70-72, 74].

Nanostructuring of Organic Materials

With the advent of Iijima's discovery of carbon nanotubes [75], an ever increasing attention has been drawn to cylindrical structures on the nanoscale. Carbon nanotubes (CNTs) have been used for applications in electronics, medical devices, and structural components [76]. This has led to the development of nanotubes created from many different materials as carbon is not an ideal material for all applications. Cylindrical nanostructures are naturally one dimensional in nature. This makes nanotubes attractive for their uses in fields such as catalysis, electronics, or fluidics [77]. Nanotubes are attractive for their unique properties including extremely high aspect ratios, electrical properties that may be inherently different than that of the bulk, and anisotropic structure. Nanotubes have a distinct advantage over nanoparticles in that they can act as capsules or cavities [78]. In order to fully take advantage of these material properties, many different fabrication techniques have been developed to create

nanotubes, such as: rolled thin films [79], modular self-assembly [80], electrospinning [81], template synthesis [82], and template wetting [30]. The last three are the most relevant for the creation of polymer nanotubes. The template based methods have been the most widely used to create nanotubes from various conjugated polymers and are the most relevant to this work.

Electrospinning

Electrospinning, a process with roots in the textile industry dating back nearly a century [83], was first described as a technique for the creation of nanometer scale polymer fibers by Reneker and Chun [81]. The fibers are created by passing a stream or drop of a polymer solution between two electrodes under a large potential difference (on the order of 10^5 V) and can yield polymer strands with diameters on the order of 40 nm to 20 μm . A polymer solution is supplied to a nozzle which may serve as one of the electrodes. At the nozzle outlet, the polymer solution forms a hemispherical drop which is deformed into a conical shape, necessary for the formation of nanofibers, as the applied field overcomes the surface tension of the drop. [84]. Once the applied field completely overcomes the surface tension of the droplet, it is propelled as a jet off of the tip and toward the second electrode. The solvent in the jet evaporates in the space between the two electrodes. If the solvent loss becomes sufficient, then the jet can branch into two or more fibers under an electrical field greater than the cohesive forces of the liquid jet. This process can happen several times to create smaller and smaller fiber jets before the polymer collects on the electrode[81]. Thus, the charge applied to the solution, the makeup of that solution, and the distance between the electrodes, will alter the branching of this jet and, consequently, the final diameter of the polymer strand [85]. When the fibers reach the electrode, they will assemble in a random fashion due to the charge from

the applied field that often leads to an appearance of a woven mesh [84] making it difficult to separate individual strands [81].

Renecker and Chun used electrospinning to create fibers from electrically conductive polyaniline [81]. Sulfuric acid acts as the solvent and is the charge carrier in the solution to allow the formation of a jet from the droplet. However, the most widely studied conjugated polymers have low solubility in such electrolytes and thus have had not been used in electrospinning applications. This requirement greatly limits the number of conjugated polymers that can be electrospun [86]. One approach to this problem has been the creation of block co-polymers with conjugated blocks combined with additional block(s) to confer solubility in the electrospinning solution [87]. Li et al. developed another method that uses a carrier polymer to transport the conjugated polymer [19]. Since commonly studied polymers (e.g. MEH-PPV, P3HT, and PFO) are not soluble in solvents suitable for electrospinning, they were injected in the jet of poly(vinyl pyrrolidone) (PVP). This allowed the group to create MEH-PPV/PVP and P3HT/PVP composites that retained the optical properties of the conjugated polymers. PVP could be removed from the polymer, leaving behind only structures of the conjugated polymers.

Devices constructed from blends of conjugated polymers were created using this method. MEH-PPV was mixed with P3HT and PFO to determine what, if any, effect electrospinning had on the tendency of polymers to phase separate out of solutions [19, 86, 88]. UV-Vis spectroscopy of the blends yielded interesting characteristics. The blends showed features of both polymers. Characteristic peaks exhibited by each polymer would be in the spectrum. By altering the concentrations of the polymers in each of the blends, it was possible for the optical properties to be tuned to have the

characteristics of both polymers by either increasing or decreasing a peak height relative to another. P3HT/MEH-PPV blends differed from PFO/MEH-PPV blends in that they formed different structures [86]. The PFO/MEH-PPV blends phase separated into a shell/core arrangement. This produced a diode-like reaction when studied electrically [86]. The P3HT/MEH-PPV blend was different in that the P3HT phase separated to ~ 50 nm beads along the MEH-PPV fibers. When the optical properties were studied, it was found that the relative absorbance of the MEH-PPV to P3HT was smaller than that exhibited in a P3HT/MEH-PPV blend cast into a film [19, 86]. The authors suggest that this is due to an enhancement of the charge transfer between the MEH-PPV and the P3HT. This enhancement was thought to have been due to forced alignment of MEH-PPV chains as the polymer was subjected to shearing forces in the jet [86]. Hole mobilities obtained from the P3HT/MEH-PPV blends were found to vary from $\sim 10^{-5}$ cm² V⁻¹ s⁻¹ in 70 %wt. MEH-PPV to 10^{-3} cm² V⁻¹ s⁻¹ in 20 %wt. MEH-PPV [86].

Template Synthesis

The use of a templating structure to create tubular or rod-like structures on the nanoscale is found to be a far simpler fabrication technique that can be used for a larger variety of materials. Beyond the versatility, the formation of nanotubes within a porous membrane creates a nanostructured composite that has a large surface area and is easy to handle [78]. C. R. Martin was one of the first to use and apply a template synthesis process [82, 89]. Electro-polymerization, electrodeposition, and chemical synthesis are techniques that have been used to create tubular and fiber-like structures in porous media. Template synthesis, in particular, has been shown as an appropriate fabrication technique for metals [90, 91], semiconductor [92], and conjugated polymers [93-95]. The nano-

fabrication of conjugated polymer structures is accomplished by either chemical synthesis or electropolymerization.

Chemical synthesis is a process in which a porous template serves as a membrane between two fluids. The first fluid is a solution comprised of the monomer units needed to create a nanotube of a particular polymer. The second fluid is a solution that contains an oxidant. The two fluids mix in the porous membrane where the monomer and the oxidant react in polymerization [95, 96]. The reacting species polymerize preferentially at the surfaces of the porous template including the pore walls [97]. This method has been used in the formation of several different conjugated polymers [93, 94, 96-98].

Electro-polymerization differs from chemical synthesis in that it is an electrochemical synthesis which does not use an oxidant. Instead, one side of the porous template is coated in metal that will act as an electrode. The template is placed into an electrolytic solution containing a monomer. A current is passed through the solution and the monomer polymerizes inside of the pores of the template. This process will form nanotubes or nanowires with material properties that can be tuned by changing the temperature, current, polymerization time, and the solution concentration [99, 100]. This method has seen a growth in popularity over the past few years because of the amount of control that can be exerted over the tube/wire formation. Several conjugated polymer nanotubes have been created using this process [96, 100, 101] including poly(p-phenylene vinylene) (PPV) [100] and polythiophene (PT)[102].

The work by Martin discovered enhancements in the conductivity of the conjugated polymers created within the templates. These enhancements were due to increased alignment and order of the polymer chains within the pores. Using X-ray

diffraction and polarized light infrared spectroscopy, Martin found that the polymer chains were forming parallel to the length of the tube in some polymers [94] and perpendicular with the length in others [97]. Originally it was thought that parallel alignment (as a result of stretching) of the chains within the tube should mean that charge carriers should be able to travel preferentially down the length of the polymer chain which would account for the increase in conductivity [94]. The alignment of the polymers within the pores of the templates seemed to be further effected by the size of the pore. Tubes with diameters larger than 400 nm behaved largely like cast films of the polymers. Below 400 nm, however, the smaller the diameter the more alignment is observed [82, 89, 95, 97]. The conductivities of the structures also show enhancement. Eventually Martin concluded that the smaller diameter pores contained a larger amount of aligned polymer chains relative to the bulk [97]. It did not seem to matter whether the alignment was perpendicular or parallel, enhancement in conductivity was shown in both cases [97].

Template Wetting

Template wetting as a nanofabrication process was first introduced by Steinhart, et al. and has proven to be an uncomplicated method of building nanostructures [30]. This process uses common wetting phenomena to coat the pores of porous template. Low surface energy solutions (or melts) are deposited onto high surface energy oxides where the solution is drawn into the pores of the oxide and evaporates to leave behind the solute material. This method has been shown to be extremely effective at creating nanotubes out of “high-performance” polymers such as poly(oxy-1,4-phenyleneoxy-1,4-phenylenecarbonyl-1,4-phenylene) (PEEK) and polytetrafluoroethylene (PTFE) [30, 77].

Conjugated organic semiconductors have been used to create nanotubes [103] using this process including those that have good absorbance and luminescent properties [104-108].

Template wetting has been shown to create polymer nanostructures with properties different from those of the bulk material. Molecular ordering has been shown to increase in nanotubes created by template wetting with orientations either parallel [109, 110] or perpendicular [106] to the pore wall. One study of the effects of wetting a template with poly (vinylidene difluoride) (PVDF) found two different effects. Melt-assisted wetting produced a largely ordered structure that formed a brush-like structure along the wall. This order also seemed to increase as the diameter of the pore decreased. This effect was known as curvature-induced order. Solution wetting seemed to be more amorphous than the melt-assisted wetting. Steinhart, et al. hypothesized that this was largely due to problems with solvent quality [110]. Schlitt, et al. discovered that solvent quality greatly effects the formation of the tubes. Poor solvent conditions would result in tubes that would collapse and be ill formed and favorable solvent conditions were more likely to produce stable polymer nanotubes [111].

Solution based template wetting of conjugate polymer nanotubes have been of interest to researchers in the last few years with the first papers being published in 2005-2006 [104, 112, 113]. These early papers gave way to a more in depth study of poly(9,9-dioctylfluorene-2,7-diyl) (PFO) nanotubes created via template wetting. The study revealed that PFO, a conjugate polymer that can have a variety of crystal phases, shows an increase in molecular ordering [106]. The molecules were determined to align parallel to the pore walls [106] similar to results observed in polyacetylene that had been template synthesized [94]. Moynihan, et al. determined that a red shift in the PL of nanotubes

relative to thin films was indicative of a characteristic increase in effective conjugation length in the polymer [106].

Increased order in conjugated polymers, especially amorphous polymers, could yield interesting electrical and optical properties. Template-wetting-induced order on these polymers could increase the effective conjugation length and lower the bandgap. It is known that P3HT self-orders by a stacking of the thiophene rings that make up the backbone of the polymer [10]. It is of particular interest as to whether template wetting nanofabrication will result in curvature-induced order on amorphous polymers (i.e. MEH-PPV) that have not shown an ability to self-align.

CHAPTER 3

EXPERIMENTAL METHODS

The majority of the work presented in this dissertation concerns the characterization of nanostructured tubules fabricated from conjugated polymers. Solution wetting of porous templates is used to create the nanotubes presented throughout the entirety of this study. Ultraviolet-visible-near infrared (UV-Vis) spectroscopy is used to determine the electronic structure of the nanotubes. Fourier transform infrared spectroscopy (FTIR) is used to determine the chemical structure of the wetted conjugated polymer nanostructures. In particular, polarized infrared absorbance spectroscopy (PIRAS) is used to determine the alignment of the polymers in the nanopores. Thermogravimetric analysis (TGA) was also performed, but is only discussed in Chapter 7. Effects of solvent, pore diameter, and filtration are presented for semi-crystalline and amorphous conjugated polymers. Details on the methods used to create and analyze these nanotubules are presented here.

Materials

The semiconducting properties of conjugated polymers arise from the conjugation found along the backbone of the polymer. Many of these conjugated polymers are polyenes, or have a conjugated backbone similar to that of polyacetylene discussed in Chapter 1 [1-3]. Non-polyenic conjugated polymers also exist and will demonstrate the

same phenomena. Non-polyenes include many aromatic five and six carbon rings [114, 115]. This ring structure is the basis for the conjugated structure in poly(phenylene vinylene) (PPV), polythiophene, and their chemical derivatives. PPV and polythiophene are both crystalline polymers that exhibit a very low solubility in most solvents at or near room temperature [5, 11]. Derivatives of these polymers, in which side chains are added, are found to be soluble in a variety of organic solvents [12, 114, 116, 117]. Figure 3.1, illustrates the chemical structure of PPV (Figure 3.1a) and polythiophene (Figure 3.1b) as well as two common derivatives poly (2-methoxy-5-(2'-ethylhexyloxy)-1,4-phenylene vinylene) (MEH-PPV) (Figure 3.1c) and poly (3-hexylthiophene-2,5-diyl) (P3HT) Figure (3.1d).

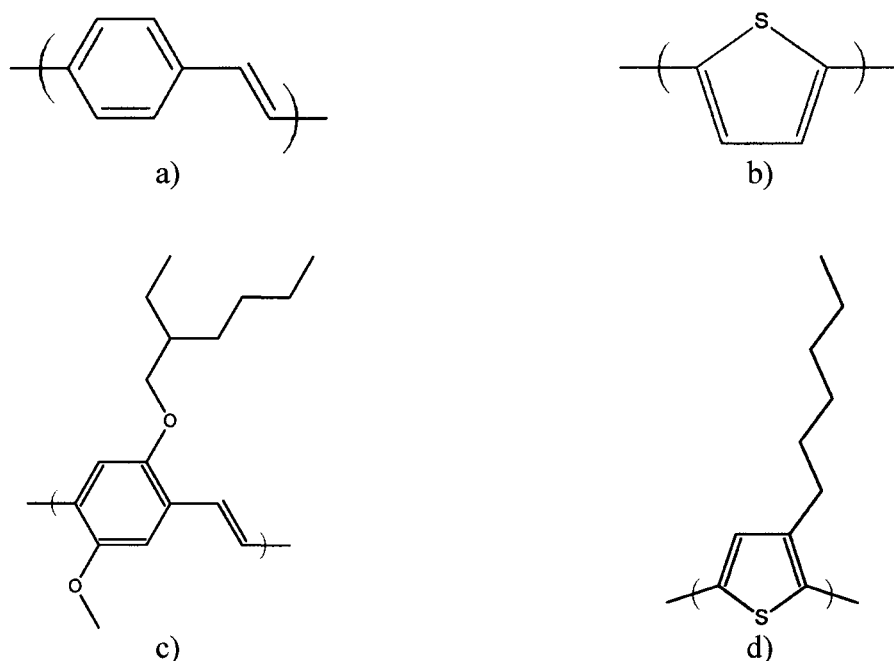


Figure 3.1. General chemical structure of a) PPV, b) polythiophene, c) MEH-PPV, and d) P3HT.

Used throughout this work, soluble MEH-PPV, shown in Figure 3.1c, is an amorphous conjugated polymer that has been widely studied for its luminescent [12, 13] and photovoltaic properties [13, 15]. Regioregular P3HT, depicted in Figure 3.1d, is a semi-crystalline polymer studied for uses as a photovoltaic material [118] as well as a field-effect transistor [10]. The MEH-PPV used here was purchased from Sigma-Aldrich ($M_n = 70,000 - 100,000$, as powder) and was used without modification. The P3HT was also purchased from Sigma-Aldrich ($M_n = \sim 64,000$, as powder) and was used without modification and filtered by Soxhlet extraction in Chapter 6.

Template Wetting of Porous Anodized Aluminum Oxide with Polymer Solutions

Steinhart, et al. first reported on the creation of nanotubes created via the template wetting nanofabrication process and demonstrated its ability to create nanotubules from a wide variety of materials [30]. The use of nanoscale porous oxides, such as alumina or silica, as a template have been shown to be very effective at creating well defined nanostructures from low energy solutions and materials. Polymers, generally regarded as low energy materials, have been found to be good substances from which to create nanotubes [78]. The physical processes behind the creation of the nanotubes and controlling variables have been rigorously reviewed in the literature [111, 119-121].

Wetting from polymeric melts has proven to be an effective method in creating nanostructures from polystyrene and solvent resistant polymers such as PTFE [30]. The polymer, in some type of bulk state, is deposited on to the porous template and then heated to a temperature slightly above its melting temperature. The viscous polymer melt then wets into the template, coating the surface of the nanopores. The template and polymer are then cooled, leaving behind nanostructures of the once melted polymer. This

process of template wetting is reviewed in detail in the literature [77, 122]. This method is quite capable of creating nanotubules from a wide array of materials but is not practical for some biomaterials, electronic, or thermally active polymers. Wetting with a polymeric solution is a more appropriate alternative.

Template wetting was shown by Steinhart to create nanotubes from PVDF [110]. However, these nanotubes were largely amorphous when cast from a solvent, in contrast with the increased order that was found when PVDF was melt casted into a porous template [110]. It is of interest that solution wetting forms tubes, as this has been used to create nanotubes, at room temperature, from other materials, including conjugated polymers [106, 112, 113]. More recent studies have found that it is possible to control the formation of the nanostructures by closely controlling the solvent selection, polymer molecular weight, solution concentration [111], and wetting conditions [123].

In the work presented here, aluminum oxide membranes (Anodisc®, Whatman Co.) were used as the porous templates. The templates are 60 μm deep, 13 mm in diameter, and have pores of 100 or 200 nm diameters. The pore densities are 10^{10} cm^{-2} for 100 nm pores and 10^9 cm^{-2} for 200 nm. The wetting process entails a precursor solution film that wets the entire surface of the template [78]. This will cause a polymer film to dry on the bottom surface of the template which can cause the template to stick to the surface it was wetted on. To resolve this issue, templates were wetted on top of a level PTFE surface. The polymeric solution is applied to the top of the template with a pipette and allowed to evaporate for several hours (often overnight) to facilitate the complete escape of the solvent. Other wetting techniques entail depositing the wetting solution on a surface and placing the template onto the drop [106, 111] or placing the

entire template into a solution and then removing it to dry [123]. The method used in this work, shown in Figure 3.2, is the most widely used method in the literature and is expected to improve repeatability as well as remove the difficulty of templates surfacing when placed onto a solution.

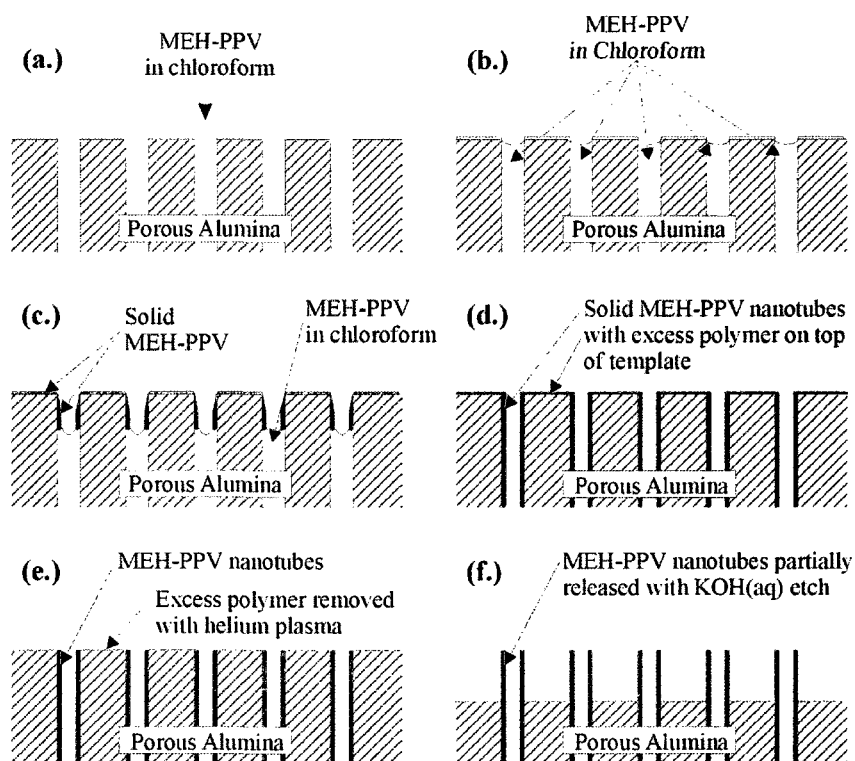


Figure 3.2. Description of the solution-based template wetting procedure carried out in this work. The process shown is for the fabrication of MEH-PPV nanotubes from a MEH-PPV/chloroform wetting solution.

In this work, the entire polymer deposited onto the template is assumed to penetrate into the template and form into tubes. However, scanning electron micrographs of the template surface after drying (Figure 3.3a) showed a residual polymer film on the side of the template in which the wetting solution was applied. In order to determine the properties of the nanostructures in the pores of the template and not that of the deposited

film; it is necessary to remove this excess polymer from the template. Template surfaces were cleaned and non-reactive ion etched similar to the method described in [124]. He atoms bombard the surface of the template and physically remove the excess polymer. This process was completed using a PlasmaTherm RIE with a 100 W He plasma at 200 mtorr for 10 minutes on each surface (top and bottom) of the template. Figure 3.3b provides a visual verification that most of the polymer is removed so that pores of the template are visible.

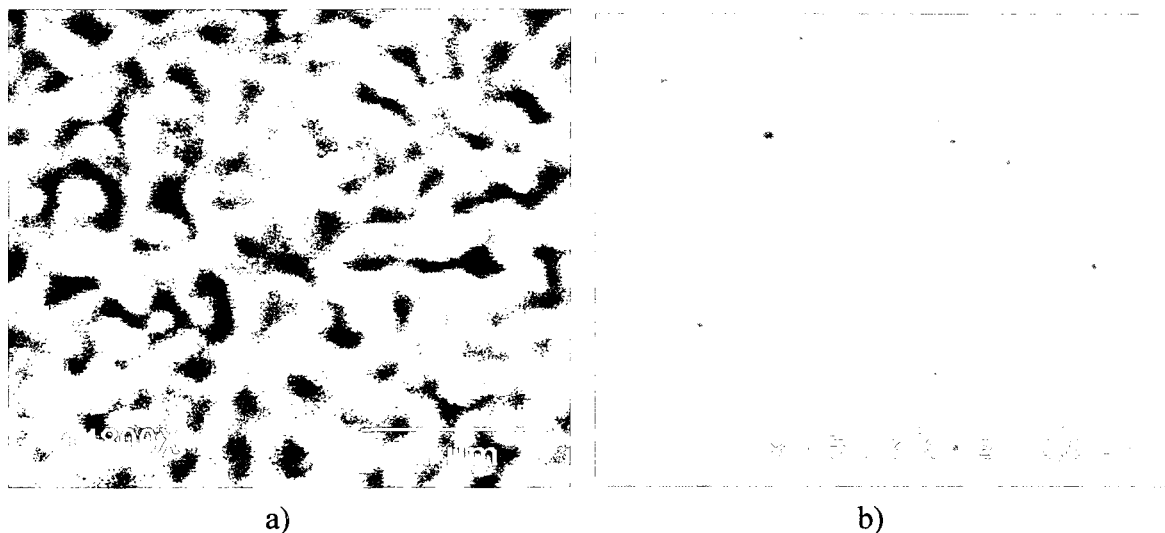


Figure 3.3. SEM micrograph of a template wetted with MEH-PPV a) with residual polymer on the top of the template and b) with the residual polymer removed by plasma. Figure 3.3b is courtesy of CAMD at LSU Baton Rouge.

In order to verify that tubular structures were created, SEM micrographs of the tubes were taken to determine the shape and morphology of the deposited polymer. This physical characterization was done with a Hitachi S-4800 field-emission-gun SEM at Louisiana Tech University. Samples were prepared for the SEM by etching the template in 25 % (by weight) aqueous KOH. This removed some of the alumina template and

allowed the nanostructures to be partially released (as in Figure 3.2f). Representative SEM micrographs of MEH-PPV and P3HT are presented in Figure 3.4.

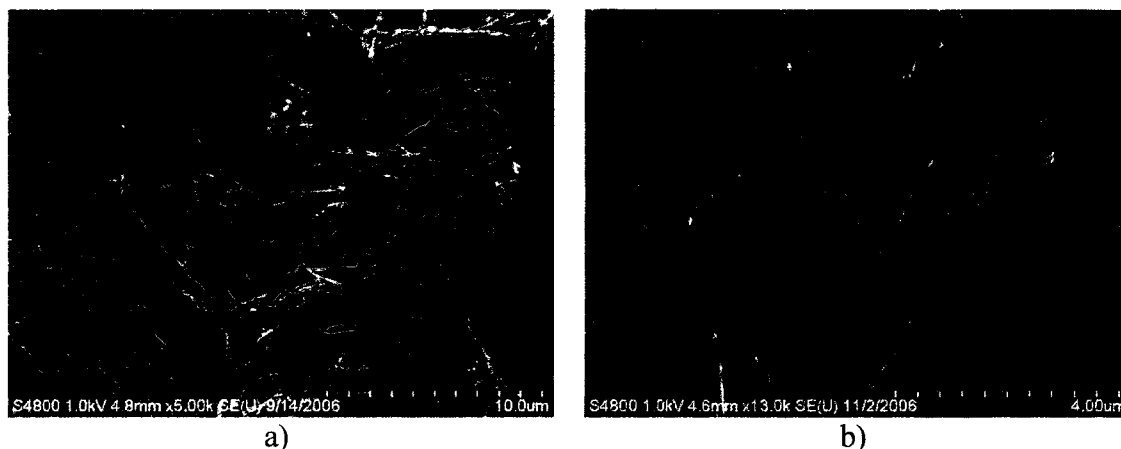


Figure 3.4. SEM imaging of a) MEH-PPV and b) P3HT nanotubes created using solution-based template wetting procedures.

Ultraviolet-Visible Spectroscopy

Characterization of organic compounds via spectroscopy can be accomplished with a number of different techniques. Ultraviolet-visible-near infrared spectroscopy (UV-Vis) is unique in its ability to characterize and provide insight into the π -electron configuration of conjugated organic molecules [125]. UV-Vis spectroscopy is the process by which an incident beam of monochromatic light is passed through a substance and the absorbance of that material (A) is determined by the Beer-Lambert law

$$A = \log\left(\frac{I}{I_0}\right) = \epsilon cl, \quad (3.1)$$

where I is the intensity of the incident light that passes through the material and I_0 is the intensity of the light from the source. For a solution, ϵ is the molar absorptivity (extinction coefficient), c is the concentration of the solution, and l is the path length that the light takes through the sample. For organic molecules, the absorption of light takes

place as the energy is sufficient to excite an electron from its ground state in the valence band to an energy level within the conduction band. These transitions can be characterized as $\sigma\text{-}\sigma^*$ for a bonded σ to an antibonded σ^* , $\pi\text{-}\pi^*$ for a bonded π to an antibonded π^* , or from non-bonded electron, n , to either a σ^* or π^* state ($n\text{-}\sigma^*$ or $n\text{-}\pi^*$ respectively). For a non-conjugated system, these transitions take place at relatively high energies (~ 6.5 eV). Since the absorbances of particular chemical structures can be determined experimentally, UV-Vis is a very useful tool to determine the chemical structure of a molecule. Woodward-Fieser rules were developed to use the known structure of a chemical to predict the absorbance or resolve chemical structures from the experimentally calculated absorbance by adding together the absorption contributions of individual chemical components of a molecule [126, 127].

In conjugated organic molecules, the energy of absorption is lowered by a factor of $1/N$ for each (N) conjugation that is added to the molecule as described in Chapter 2. Thus, at lower energies, (i.e. inside the visible light range, 4.13 to 1.55 eV) only the $\pi\text{-}\pi^*$ transitions are found. These transitions are indicative of the available electronic states in the structure. In conjugated polymers, this equates to the different available conjugation lengths.

The conjugated backbone of polymers and the $\pi\text{-}\pi^*$ excitation found in UV-Vis spectroscopy is used throughout this work. Just as the smaller organic molecules absorb at lower energies with increasing conjugation length, semiconducting and optoelectric polymers will exhibit the same relationship. However, as noted in Chapter 2, it is unlikely at the entire backbone of the polymer will act as a continuous conjugated system due to breaks in the conjugation [44, 128]. This separates the polymer absorbance into

discrete π - π^* transition states. These states are often broad and will overlap to form a continuous curve in the UV-Vis spectrum[129]. The relative energies of these spectra can give useful information as to the conformation of the conjugated polymer. A polymer in solution will often have a unique conformation in that solution and thus can exhibit a different UV-Vis absorption. This effect is known as solvatochromism [64]. A polymer in solution that absorbs a lower energy relative to another polymer in solution will have a longer conjugation length. This shift in the spectra is known as a bathochromic shift or (or redshift) [130]. Similarly, the higher energy absorbance of a polymer is due to a shortening of the effective conjugation length and thus displays a hypsochromic shift (or blueshifted) [130].

Until the conjugated polymer is irradiated with enough energy to create a π - π^* transition, the polymer will not absorb. In UV-Vis spectroscopy, the transition from the polymer not absorbing to absorbing is called the onset and is equated with the optical bandgap (E_g) [131]. The E_g is the lowest energy required to excite an electron from the HOMO level to the LUMO level. Often the E_g energy is not the most prevalently absorbed electronic state of the conjugated polymer. The conjugation length with the highest concentration in the solution will have the largest absorbance (as can be seen in Equation 3.1) and thus will form the peak in the UV-Vis spectrum [32]. This peak location, will then give information as to the length of the most numerous conjugation length in the solution and allow for another comparison between polymers in different solvents.

UV-Vis spectroscopy of conjugated polymers in solution displays the electronic states of the individual polymers chains. Polymers in dilute solutions are electronically

isolated from other polymers. This means that the effective conjugation length found from UV-Vis of polymer solutions will only show the intrachain interactions. Because of this, the UV-Vis spectra will typically be a Gaussian peak of the statistically available conjugation lengths. In contrast, UV-Vis of solid state samples will have different features. Conjugated polymers in solid state (i.e. thin films) will have features like those found from solutions such as the onset and a peak. However, some conjugated polymers will also have shoulders or multiple, well-defined peaks [32]. These features arise due to the formation of interchain interactions where the π -orbitals of one chain will interact with the π -orbitals of another, nearby chain. Formation of these types of features in the UV-Vis spectrum is usually indicative of some type of self-ordering in the solid state. This can be seen when comparing the spectra of semi-crystalline regioregular P3HT and amorphous nonregioregular P3HT, where rr-P3HT forms fine structures and is redshifted with respect to the broad, featureless absorption of ir-P3HT [32].

Films cast from conjugated polymers are often redshifted from the isolated polymer in dilute solution. Since it is unlikely that the conjugated polymer is more aligned and with fewer defects in the film state; the bathochromic shift must be due to intermolecular π -electron interactions [125]. This leads to states that interact electrically but are not of the same conjugation length. As in Chapter 2, this is referred to as the effective conjugation length and can be at a lower energy than the dilute polymer solution [42]. The effective conjugation length can be “elongated” by increased chain packing and interchain alignment [132, 133]. Therefore, UV-Vis can be an extremely useful analysis technique to detect relative changes in intra and interchain conformation of the conjugated polymers.

The UV-Vis spectroscopy in this work is carried out in order to determine the relative changes in solid state polymer structure. Absorbance spectra will be used to compare MEH-PPV and P3HT nanotubes formed via template wetting nanofabrication with the more traditional thin films. Thin film samples in this work were created by drop casting the polymer solution onto the surface of a quartz slide and allowing it to completely dry in air. Nanotube samples were examined in template directly after He plasma etching without any further modification. Nanotube and thin film samples were examined with a Shimadzu UV-1650PC UV-Visible Spectrophotometer. Both types of samples were placed in the UV-Vis system such that the sample would be normal to the beam and the entire beam would fall on the sample. Scans were taken from 1100 nm to 200 nm (= ~ 1.2 -6.2 eV).

The optical bandgap, as defined earlier, is taken to be the onset of absorption. In this work, that onset is found by finding the intersection of the lines formed from the region of the spectrum just before absorption and the first linear region after the onset. Figure 3.5 is an illustration of this analysis. This is believed to be a more accurate method than simply extending the first linear region to the x-axis and calculating the energy at zero absorbance. As can be seen in Figure 3.5, the onset does not always rise from zero absorbance and an E_g calculated by zero absorbance would return a skewed result.

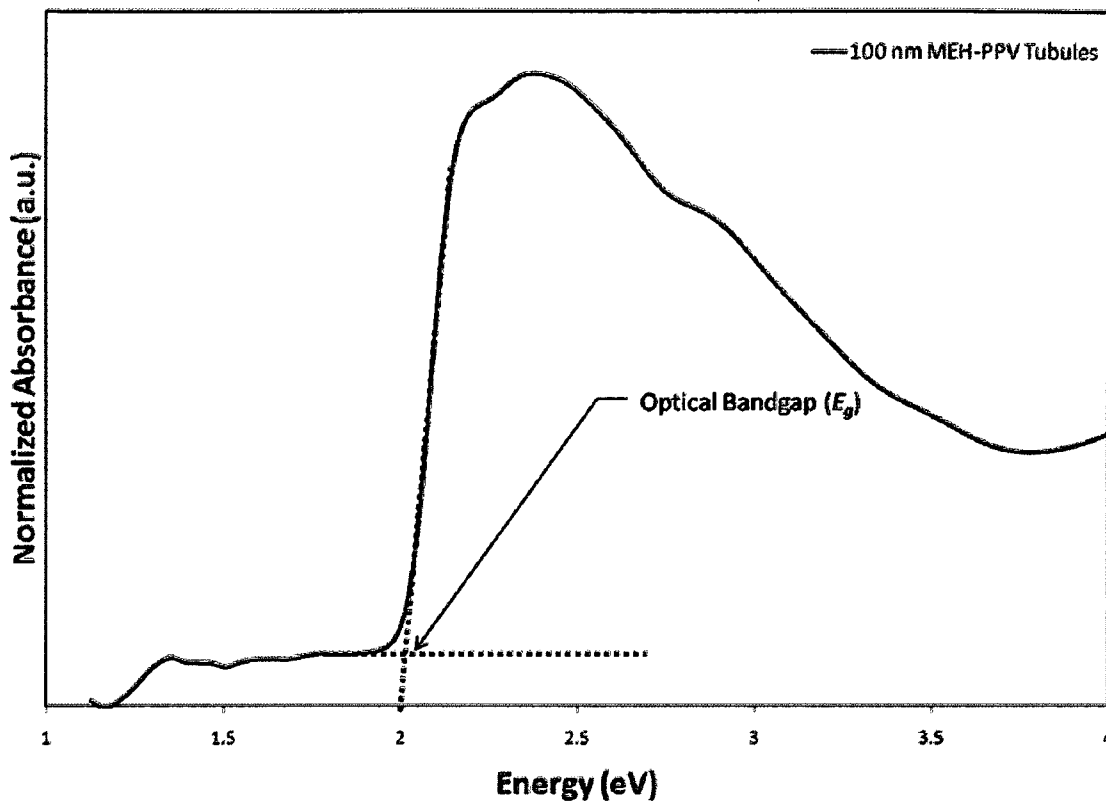


Figure 3.5. Illustration of the location of the optical bandgap (E_g) as the intersection of the linear regions just before and after the onset of absorption.

Infrared Spectroscopy

Infrared spectroscopy is a useful tool to determine the chemical structures of a substance. Infrared (IR) radiation is directed at a substance and this energy will be absorbed by molecules undergoing a transition between quantum states that are associated with different molecular vibrations or vibration-rotations at certain energy levels [60, 134]. The amount of energy required to cause the absorption is based on the dipole moment of the chemical [135]. Vibrations can only be at discrete energy levels as in optical absorption [135]. These vibrational modes can be thought of as a spring-mass system with the atoms as masses and the bond as a “spring” and the energy necessary to

produce a sustained vibration can only be at discrete levels corresponding to the natural frequency. The energy (usually quantified by the wavenumber) of this IR absorption can be detected and associated with a particular chemical bond or chemical structural fragment (functional group) [134]. Individual bond types will often have different absorption energies based on the type of vibration. Just as in spring-mass systems, the number of vibrations is based on the degrees of freedom [135]. The term, vibration, is a generic term that describes the variances in bond length (stretching) or the movement of atom out of its present plane (bending). Therefore, a particular molecule can have several different absorption energies that each correspond to a different type of vibration with the total number of absorption energies being limited by the degrees of the freedom of the bond [135].

Within polymers, IR spectroscopy can be used to identify and characterize the chemical bonds present in the polymer. The vibrational energies of side chains will absorb at nearly constant wavenumbers regardless of the structure of the rest of molecule [134]. This does not hold true for the polymer backbone. Returning to the understanding of the vibration as being a spring-mass system; it is possible to think of polymer backbones as several springs and masses connected together in series. This will affect the vibration frequency and thus the absorption energy [136]. As the number of repeat unit increases, the polymer will eventually vibrate as some minimum energy [136]. Since most polymer systems are larger than 20-30 repeating units, a change may not be noticed [136]. It is with this in mind that this work uses IR spectroscopy to focus on the chemical group sidechains that branch off the backbone [60] and the backbone elements of polymer chains [136].

Another application of IR spectroscopy that is used in this work is the determination of polymer orientation. Polymers that form with any induced strain will have an alignment preferential to the direction of the strain [60]. Polymers cast from solvents with no external force may crystallize, but the polymer direction will often be isotropic. If the polymer is subjected to an external force during or after the solvent drying, then the polymer will often align to that external force [60]. IR spectroscopy can be used to detect the presence of an orientation and to quantify it [137]. This analysis is known as polarized infrared absorbance spectroscopy (PIRAS) or simply as polarized FTIR. The detection is due to the polarization of the IR beam. If the periodic change in the dipole moment of the absorbing bond is parallel to the electric vector of IR radiation, then there will be absorption. If this is not the case, then there will not be absorption. Therefore, the polarization of an IR beam in directions parallel and perpendicular to an induced strain on a polymer can yield two detected absorbances. The ratio of these absorbances is referred to as the dichroic ratio (R). The dichroic ratio is defined as

$$R = \frac{I_{\parallel}}{I_{\perp}} = \frac{A_{\parallel}}{A_{\perp}}, \quad (3.2)$$

where I is the intensity of the absorption, A is the quantified absorbance, \parallel and \perp represent the parallel and perpendicular directions [137]. The parallel direction is usually taken as parallel to the orientation of the bond [60, 137], however parallel can also be a direction on the sample that is being tested for dichroism [138]. A polymer feature (such as a backbone or a side chain) that is oriented in the parallel direction will tend toward an R of infinity as the I_{\parallel} is extremely large and the I_{\perp} is very small. Likewise, for perpendicular orientation, R will tend towards zero [60, 137].

With most polymer films, the fiber formation or chain alignment is likely to appear in a direction parallel to the plane of the surface. However, for samples in which it is desired to know the orientation perpendicular to the surface, typical IR spectroscopy will not work as it is usually impractical to prepare and test thin cross-sections. In order for the IR beam to pass through a polymer sample, the sample must be very thin and oriented normal to the beam in order to minimize the path length. This would cause polymers oriented perpendicular to the surface of the film to appear to have an isotropic dichroic ratio ($R=1$) [138]. To correct for this the sample can be placed at an angle and then the perpendicular absorbance (A_{\perp}) can be replaced by the absorbance at the known sample angle A_{θ} . A_{θ} is defined as

$$A_{\theta} = A_{\perp} \cos^2(\theta) + A_{\parallel} \sin^2(\theta), \quad (3.3)$$

where θ is the angle of the sample [138]. By choosing the sample to be at an angle of 30° and rearranging to find A_{\parallel} , Equation 3.3 reduces to [94, 95]

$$A_{\parallel} = \frac{1}{3} \left(\frac{4A_{30}}{A_{\perp}} - 1 \right). \quad (3.4)$$

Figure 3.6 illustrates this experimental technique. Martin, et al. used polarized FTIR of an oriented sample to determine the alignment of polypyrrole nanotubes chemically synthesized in a template [94, 95].

Infrared spectroscopy measurements in this work were carried out with a Thermo Nicolet Nexus 470 FT-IR E.S.P using a MCT/A liquid N_2 cooled detector. MEH-PPV and P3HT nanotubes were analyzed in template after non-reactive He plasma etch without further modification. For alignment measurements, the experimental setup illustrated in Figure 3.6 was used to determine the dichroic ratio of the nanotubes in order

to discover if template wetting nanofabrication results in an alignment of the conjugated polymers in the pores of the template.

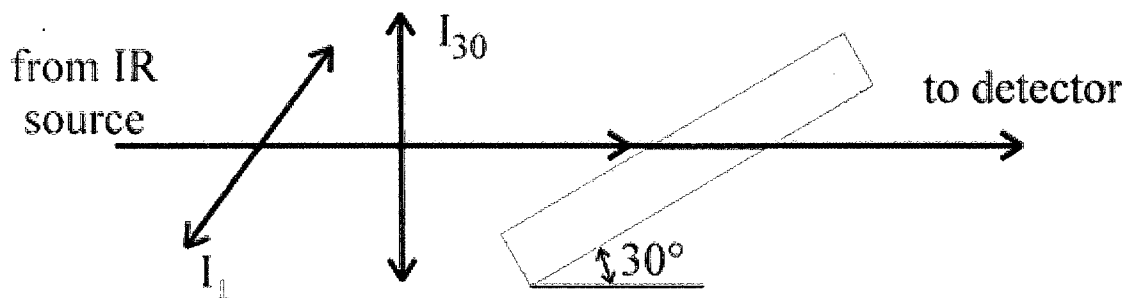


Figure 3.6. Setup for polarized FTIR to calculate the R for polymer orientation normal to the surface of the film surface.

Thermogravimetric Analysis

As discussed in Chapter 2, the interaction of the solvent with a conjugated polymer can alter or tune the properties of that polymer in the solid state. Polymer solutions that evaporate quickly will not form aggregates [66] at the surface and will “quench” in the solvent conformation as they dry [73]. Likewise, polymer films that are allowed to evaporate more slowly will organize more slowly going through a process of “solvent annealing” [139]. The effect of this annealing will generally result in a more ordered organization of the polymer chains with a longer effective conjugation length [51, 66].

It is of interest to this work to understand the solvent evaporation characteristics from films of conjugated polymers. These experiments were carried using thermogravimetric analysis (TGA). TGA uses a very accurate microbalance to record the weight change in a sample as a function of temperature [60] or over time at a constant temperature [140]. Solution drying measurements included in this work were measured

using a TA Q50-0816 TGA at 30° C in an alumina pan. Solution was applied directly to the pan and the mass of the drying drop was recorded until the weight change was less than 0.0 %/min at which point the solvent evaporation rate has slowed to a point where it can be considered negligible.

Electrical Testing

Most of the experiments and analysis carried out in this work involve spectroscopic studies of conjugated polymer nanostructures. Electrical testing is included as a comparison and is a more minor aspect of this study. The devices examined for their electrical properties were fabricated as in Figure 3.7a. All devices are considered to be single carrier devices following [141]. Single carrier devices were constructed by aligning the work function of the electrode material to that of the valence band of MEH-PPV and P3HT (a deviation of less than 0.4 eV) [142]. Conduction and valence band edges for P3HT [143] and MEH-PPV [144] are shown in Figure 3.7b. Au was chosen as the electrode material as its work function is close to that of the two polymers.

Au's work function alignment with the valence band edge of the polymers allows for the formation of the hole only devices use in this work. These devices were created by wetting the template with a solution of the polymer to be tested, the residual surface polymer was removed via He plasma etch, and Au was evaporated onto both sides. The cathode consisted of a large continuous area with the Au being evaporated through an 8 mm circular shadow mask. Anodes were patterned on the opposite side in a hexagonal pattern with 1.58 mm diameters. The analysis of the hole current densities in the single-carrier devices was carried out following the work of Chiguvare et al. [145] where single

carrier ohmic behavior with the Mott-Gurney trap free space charge limited conduction model (TF-SCLC) to yield

$$J = q\mu_p p \frac{V}{L} + \frac{9}{8} \varepsilon_0 \varepsilon_r \mu_p \frac{V^2}{L^3}, \quad (3.5)$$

where J is the current density, q is the electronic charge, μ_p is the hole mobility, p is the number of free holes per cm^3 of material, V is the applied bias, L is the device length, ε_0 is the permittivity of free space and, ε_r is the permittivity of the material. A more detailed derivation of this equation can be found in reference [146].

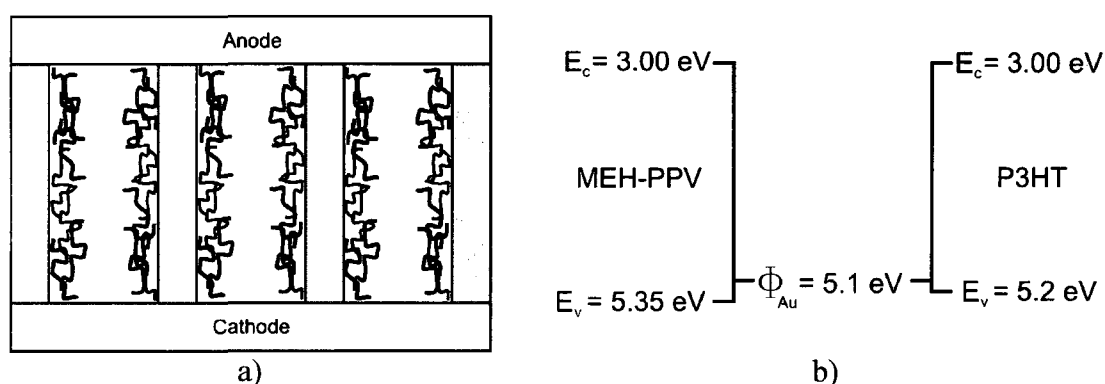


Figure 3.7. The generalized device structure used is illustrated in a), while b) illustrates the barrier height minimization due to anode and cathode material choice of Au in the construction of hole-only devices. Gray sections in a) represent the template and the squiggly lines represent incorporated polymer [146].

Devices were tested using a Keithley 236 source-measure unit. These hole only devices were examined by sweeping the applied voltage from 0 V to +100 V, +100 V to -100 V, and then from -100 V to 0 V. These measurements were carried out in three cycles in total darkness. The cathodes were attached to ground with the bias applied to the anode. Increments of 5 V were recorded with a 250 ms delay time. Multiple devices were tested per template in order to account for statistical variation.

CHAPTER 4

CHARACTERIZATION OF CONJUGATED POLYMER NANOSTRUCTURES FABRICATED VIA TEMPLATE WETTING

Introduction

Conjugated polymers have drawn considerable research interest for potential applications in a wide range of low-cost electronic devices [147-151] as they are amenable to a range of inexpensive melt and solution processing techniques, such as inkjet printing, spin casting, microstamping, and reel-to-reel fabrication [148, 149, 152]. Numerous material deficiencies exist for conjugated polymer systems depending on the desired device design. For example, contact limited injection properties hinder LED efficiencies, [153] while high band gaps and narrow absorption bandwidths limit polymers in photovoltaic performance [27]. However, the issue of poor charge carrier transport properties within the bulk material presents a far more universal problem [148, 149, 152, 154]. Improved synthesis procedures which produced greater regioregularity and purity have led to improved material properties [8, 155] while functionalization and the use of polymer blends [156-158] have provided means of tuning material properties.

Nanostructured inorganic/conjugated polymer composites have also shown promise as a vehicle for tuning and improving the electronic and optical material properties [104, 159-162]. Composites from porous, anodic aluminum oxide (AAO) and

conjugated polymers produced using template-based nanofabrication methods exhibit very different properties from those of bulk polymers. For example, Qi *et al.* [163] created a composite of poly(2-methoxy-5-(2'-ethylhexyloxy)-1,4-phenylene vinylene (MEH-PPV) by vapor deposition of the polymer onto an AAO membrane and observed a blue shift in the UV-Vis absorbance spectrum of MEH-PPV chains isolated within nanoporous alumina membranes; an effect attributed to a reduction of polymer-polymer intermolecular interactions. In a similar manner, Kahn *et al.* utilized a solvent based deposition process to prepare a MEH-PPV/AAO composite, observing a blue-shift in the photoluminescence spectrum as the nominal AAO pore diameter decreased [104].

Here, solution-based template wetting is demonstrated as an effective means of producing semiconductor/insulator nanocomposites from two of the most commonly examined semiconducting polymers, MEH-PPV and regioregular poly(3-hexylthiophene-2,5-diyl) (P3HT), as well as a blend of these two polymers. Template wetting nanofabrication, initially demonstrated by Steinhart *et al.*, has been shown to be a simple, effective, low cost method of making polymer/metal oxide nanocomposites [30, 77]. The process utilizes wetting phenomena to create a uniform coating of a low surface energy material, such as a polymer solution or melts, on porous template materials with high surface energy such as AAO. Composites fabricated in this manner have been shown to possess enhanced characteristics when compared to bulk materials; including curvature induced molecular order and crystallinity of polymers within the nanopores [107, 110]. In this chapter, the electronic and spectroscopic properties of semiconducting polymer/AAO nanocomposites fabricated via template wetting are described.

Experimental

Materials

The MEH-PPV and P3HT used in this study were obtained from Sigma-Aldrich, and used as received. Wetting solutions were created by dissolving each polymer individually, and in an equal weight blend of the two, in chloroform (2 mg/ml). Commercially available AAO membranes (Anodisc[®], Whatman Co.) were used as templates. These templates were 60 microns thick and 13 mm in diameter, having nominal pore diameters of 100 nm and a surface pore density of 10^{10} cm^{-2} .

Methods

The template wetting process used to fabricate the composites. The first step in the procedure was to pipette the polymer solution onto the top AAO template surface. The solvent was allowed to evaporate in air before further processing. While most of the applied polymer entered the template pores via surface tension effects, a noticeable amount of residual polymer was observed on the template surface after complete evaporation of the solvent. Removal of this residual layer was necessary in order to clearly observe individual polymer nanotubules, and confirm that any characteristics observed from the polymer were strictly from polymer confined in the pores of the AAO membrane. This was accomplished by etching in a non-reactive helium plasma at 100 W and 200 mtorr for 10 minutes in a PlasmaTherm RIE system [124]. It was presumed that the plasma had no significant effect on the polymer in the pores, given the low temperature, short time of the etching process, and high aspect ratio of the pores [107, 124]. Select samples were further etched in 25 wt. % aqueous KOH to selectively remove part of the AAO template to better enable imaging of the resulting polymer nanotubes. A representative scanning electron micrograph shown in Figure 4.2 illustrates

that nearly all the pores of the template membrane are filled and that the polymer conforms to the relatively cylindrical pore geometry.

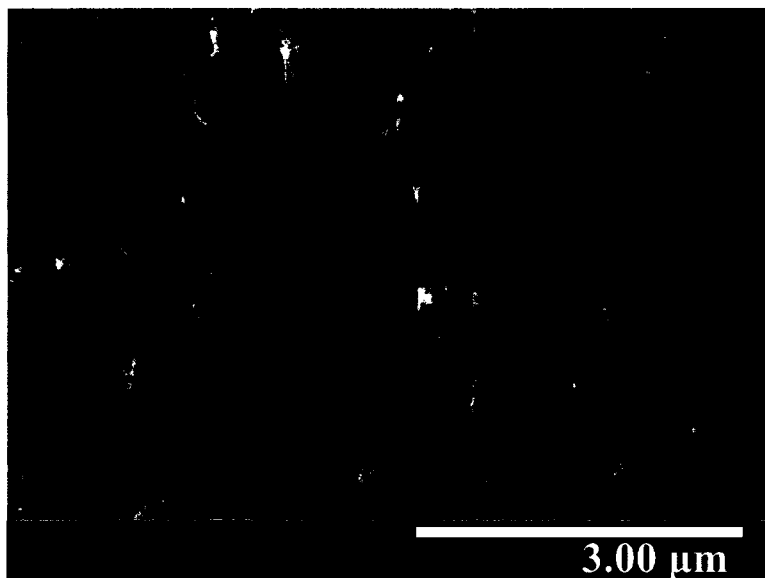


Figure 4.1. SEM photo of P3HT nanotubules partially released from the AAO template.

Simple resistors for electrical characterization were created by evaporation of gold electrodes onto the composite surfaces immediately after completion of the He plasma etch. Large area continuous cathodes were formed by depositing Au through an 8 mm circular shadow mask, centered on the template while multiple anodes were patterned on the opposite side of the template in a hexagonal pattern which produced seven devices. The close alignment of the Au work function with the valence band edges in MEH-PPV and P3HT produces hole injection barriers of only 0.25 eV and 0.1 eV, respectively, while maximizing the electron injection barrier in each case. This configuration produces electronic systems in which hole dominate conduction, effectively resulting in a single-carrier or “hole-only” device [141]. Single-carrier device structures such as this greatly simplify analysis of charge transport by eliminating the need to

disentangle convoluted effects of the simultaneous flow of holes and electrons present in more traditional two-carrier device structures.

Spectroscopic analysis was used to provide information about the π -electron system present in the conjugated, organic materials [34]. UV-Vis spectroscopy was used to determine optical absorbance spectra and to approximate optical band gaps of the polymers in various forms. Nanocomposites samples were examined immediately after He plasma etching, with no further modification. Thin-film samples were created by drop casting the polymer solutions onto quartz slides. All samples were oriented in the UV/Vis spectrometer (Shimadzu UV 1650PC) such that the incident beam was normal to the large flat surface of the sample. Vibrational spectra were also collected using transmission mode in a Nicolet Nexus FTIR spectrometer, providing useful chemical information about the samples.

Results and Discussion

Electrical behavior of the nanocomposite examined here was found to be well described by space charge limited conduction (SCLC) models, which have been widely applied to semiconducting polymer systems, including MEH-PPV [141, 142, 164] and P3HT [118, 145, 165] and is given in Equation 3.5. Current-voltage characteristics for the polymer/AAO devices as well as least squares regression fits to the SCLC model for each nanocomposite sample group [108] are shown in Figure 4.2.

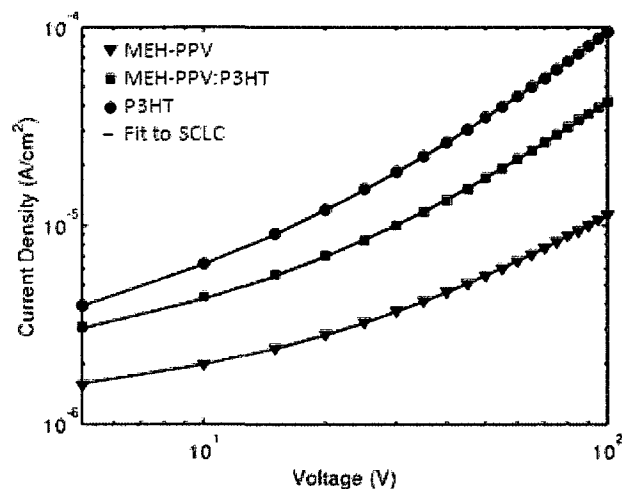


Figure 4.2. J - V curves for nanocomposites of a 100 nm pore diameter AAO with MEH-PPV, a 50:50 blend MEH-PPV and P3HT, and P3HT [108].

Hole mobilities obtained from this model are presented graphically in Figure 4.3. The P3HT/AAO blend is shown to have a much higher free hole mobility ($\sim 5.4 \times 10^{-3} \text{ cm}^2 \text{ V}^{-1} \text{ s}^{-1}$) than the MEH-PPV/AAO structure ($\sim 2.4 \times 10^{-4} \text{ cm}^2 \text{ V}^{-1} \text{ s}^{-1}$), which is expected given that P3HT is known to be a more ordered polymer than MEH-PPV. As expected, mobilities measured in the MEH-PPV:P3HT/AAO composite are between those found for the two homopolymer systems. With the exception of the MEH-PPV/AAO group, the mobility values found here are in excellent agreement with those found for thin film transistors fabricated using P3HT, MEH-PPV, and blends there from [88]. The hole mobilities observed for the MEH-PPV/AAO nanocomposite samples were found to be one to two orders of magnitude higher than those typically reported for MEH-PPV thin films [88, 166, 167]. This is thought to be the result of increased packing or molecular ordering of the polymer molecules due to confinement in the nanoscale pores in the AAO template, leading to a greater degree of intermolecular π -orbital interaction and reduced barriers to interchain transport [107, 168]. Close agreement of hole mobility for the

P3HT/AAO nanocomposites and thin film data reported elsewhere suggests that molecular order of this polymer is not increased due to confinement within the AAO pores [7, 10, 17, 88]. P3HT is, however, is a self-organizing, semi-crystalline polymer, [10] unlike the amorphous MEH-PPV, and thus less improvement in ordering or molecular packing is possible for this polymer.

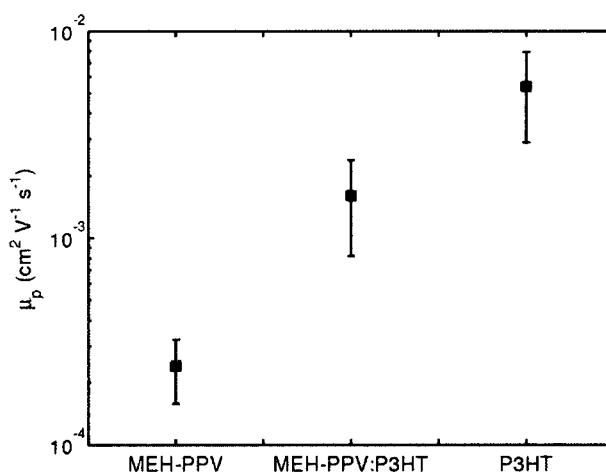


Figure 4.3. Mobilities calculated from the SCLC model for nanocomposites of MEH-PPV/aluminum oxide, 50:50 (by vol.) blend of MEH-PPV and P3HT/aluminum oxide, and P3HT/aluminum oxide [108].

Figure 4.4 shows representative UV-Vis absorbance spectra for a P3HT/AAO nanocomposite, as well as for a P3HT film drop cast on a quartz surface and P3HT dissolved in chloroform. The same information for MEH-PPV is shown in Figure 4.5. The onset of absorption in the UV-Vis spectrum allows direct observation of the minimum energy required to excite an electron from the valence band to the conduction band, which occurs via a π - π^* transition, and is approximately equal to the bandgap of the material. Lowering of the absorption onset is indicative of longer effective conjugation lengths and can correspond to increased carrier mobility [169]. In Figures

4.4 and 4.5, the value of the onset is taken as the intersection of the baseline section of the spectrum immediately before absorption and the approximately linear region of the absorption leading edge. The observed optical bandgaps of the solid phase is significantly lower than that of the solution for each polymer. This is expected as the molecules are electronically isolated from one another in the dilute solution and behave essentially as a statistical ensemble of individual molecules. However, only a small difference was observed between the adsorption onset energy of the films and the polymer in the AAO nanocomposites of P3HT of only ~ 0.05 eV when compared to the ~ 0.12 eV shift found between the MEH-PPV film and composites.

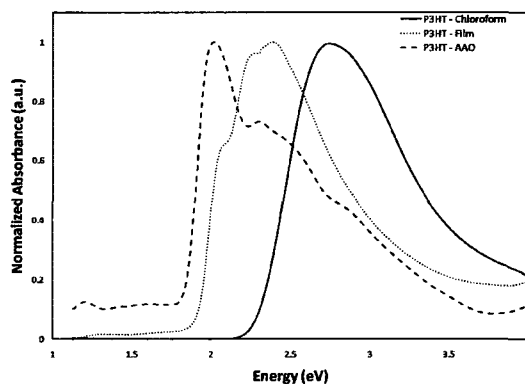


Figure 4.4. UV-Vis spectra of P3HT solution, film, and composite.

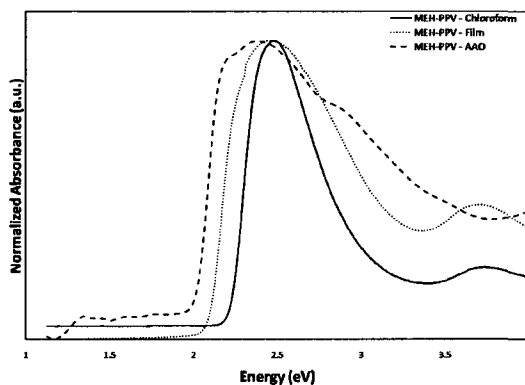


Figure 4.5. UV-Vis spectra of MEH-PPV solution, film, and composite.

In Figure 4.6, the UV-Vis spectra of the MEH-PPV:P3HT blend/AAO composite is compared to that of the homopolymer composites. Shoulders and peaks in the lower energy regions of the blend composite spectra, as well as the approximate band gap, are closely correlated with those of the P3HT/AAO composite, but are more closely related to those of the MEH-PPV/AAO composite as absorption energy is increased.

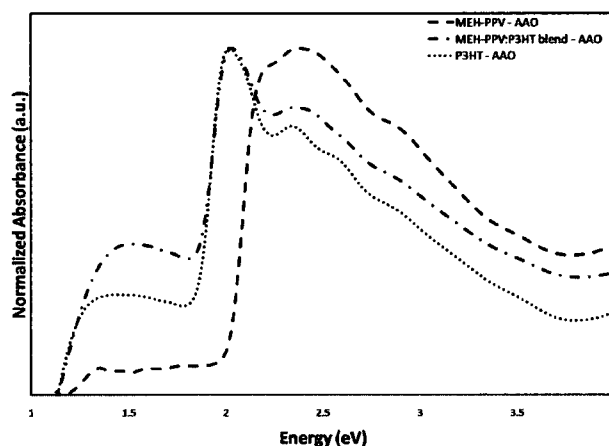


Figure 4.6. UV-Vis spectra of the three polymer composites.

The blend composite spectrum greatly resembles that of the P3HT-AAO, suggesting that there is little or no electronic interaction between the two polymer species, as no new energy states appear to be added to the system due to the MEH-PPV. This along with the previously discussed electrical properties of the blend would seem to indicate that the two polymers are segregated in the composite and there are no additional electronic states produced as a result of interaction between the two polymers.

Infrared spectra shown in Figure 4.7 further indicate phase segregation in the blend. The MEH-PPV:P3HT/AAO composite spectrum is similar in structure to both of the homopolymer composite spectra, and can indeed be obtained by addition of those spectra. The lack of changes in the FTIR spectrum is indicative of minimal if any

chemical interactions between the two polymers in the MEH-PPV:P3HT/AAO and is in agreement with similar observations reported in the literature with films and electrospun nanowires of MEH-PPV/P3HT blends [19, 170].

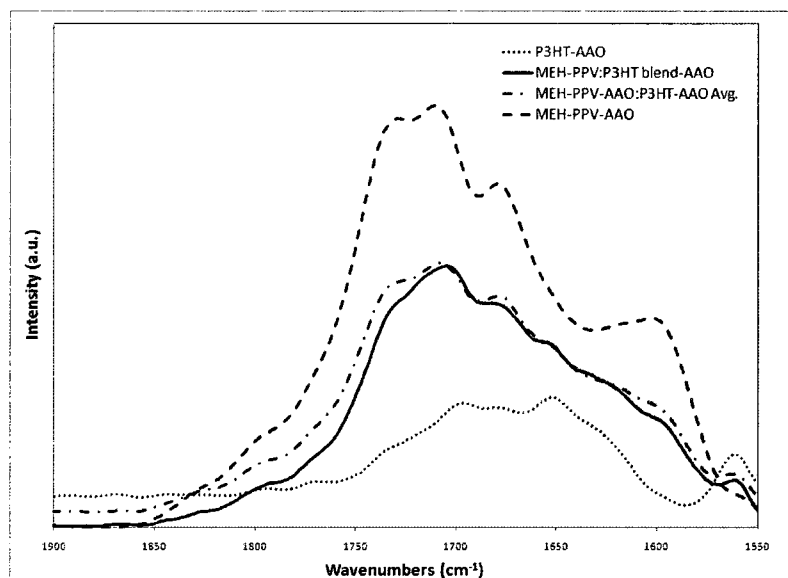


Figure 4.7. FTIR spectra in the double bond region of the three polymer composites.

Conclusions

Template wetting nanofabrication has been demonstrated as a simple, solution-based means of producing semiconductor/insulator nanocomposites using nanoporous metal oxides and the conjugated polymers MEH-PPV and P3HT. Hole mobilities in the MEH-PPV/AAO composite are improved when compared to thin films of that material, suggesting that confinement and curvature-induced molecular ordering of the polymer molecules may be present within the nanoscale pores of the AAO membrane. Unlike amorphous MEH-PPV, the semi-crystalline, self-ordering polymer P3HT shows no significant improvement in hole mobility when in the nanocomposite form, indicating that this polymer is ordered in a single fashion in both the composite and in thin films.

Further evidence of enhanced ordering in MEH-PPV nanocomposites, and lack thereof in P3HT-based samples, is observed by comparing the sharpness of the UV-Vis absorption bands. Nanocomposites formed from a blend of MEH-PPV and P3HT in an AAO membrane showed carrier mobilities intermediate to that of the individual polymer composites, suggesting that each polymer penetrates the nanoporous matrix equally well. Further, spectroscopic information from UV-Vis and FTIR analysis provides evidence that no chemical or electrical interactions occur between the two polymers when blended, a result indicative of phase segregation.

CHAPTER 5

SPECTROSCOPIC AND ELECTRICAL EVALUATION OF POLY(3-HEXYLTHIOPHENE) NANOTUBES

Introduction

Conjugated polymers, while attracting widespread attention due to their promise for a wide range of semiconductor device applications, are typically limited by poor charge transport properties [44]. Increasing the degree of molecular order can increase exciton lifetimes and carrier mobility as well providing a means of controlling optical absorption and emission. To this end, a variety of processing methods, nanofabrication techniques among them, have been employed. Some of these include the use of alignment substrates, [171] electrospinning, [19] nanofluidic-lithographic methods, [172] template synthesis, [82, 94] and template wetting [107, 112]. Among the simplest of these techniques is template wetting nanofabrication [77]. Template wetting has been found to produce polymer nanotubules and nanowires with very different material properties from thin films and other configurations of the same material [30, 77]. For example, some materials have shown curvature-induced molecular order and crystallinity within the nanopore [110] and in the case of conjugated polymers, enhanced carrier transport has been observed [107]. In this work, 100 and 200 nm diameter poly(3-hexylthiophene) (P3HT) nanotubules were fabricated using template wetting

nanofabrication and compared their optoelectronic properties with those of thin films of the same material in order to determine any curvature-induced effects.

Experimental

Materials

Anodic alumina membranes (Whatman Co.) were used as received as templates for the nanofabrication process. These had pore densities of approximately of 10^{10} pores per cm^2 and 10^9 pores per cm^2 , for templates with nominal pore diameters of 100 nm and 200 nm, respectively, and were ~ 60 μm thick. ACS reagent grade chloroform and regioregular P3HT (>98.5% head-to-tail linkages, Rieke Metal, Inc.) were obtained from Sigma-Aldrich and used as received to make wetting solutions by dissolving 2 mg/mL polymer in the chloroform.

Methods

The template wetting nanofabrication process begins with by pipetting 100 μL of the wetting solution onto a template. Excess polymer is removed from the exterior surface of the template via reaction ion etching in helium plasma. The resulting nanotubules, confined within the template pores, were evaluated spectroscopically in this form. For comparison, thin films were drop cast on a smooth quartz substrate from the same wetting solution.

To verify nanotubule formation, samples were inspected in the SEM. This was facilitated by etching in a 0.1 M aqueous KOH solution to selectively remove part of the alumina template, revealing the polymer. This etching process was only performed on samples examined in the SEM. A representative SEM photo is shown in Figure 5.1.

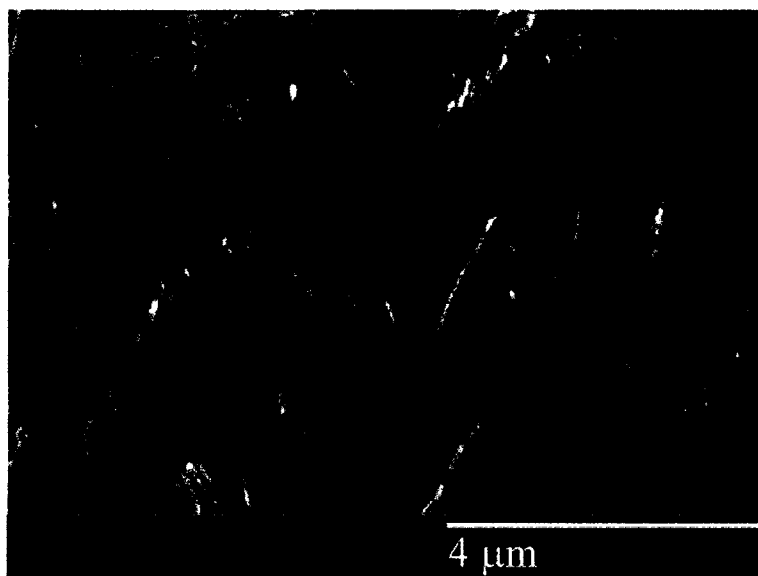


Figure 5.1. Representative SEM photo of P3HT nanotubules.

Hole mobility measurements were accomplished using a simple diodes created by depositing 150 nm Au layers on each side of the wetted templates by electron beam evaporation through a shadow mask. Multiple devices were created on each substrate. Current-voltage characteristics of these devices were fit to space-charge limited conduction models (Equation 3.5) to obtain the hole mobility of the material.

Polarized FTIR spectroscopy was used here to study P3HT in the nanotubular configuration. A Thermo-Nicolet Nexus 470 spectrometer with a slide mount polarizer was employed with the sample aligned 30° from parallel with the IR beam. Light polarized orthogonal to the axes of the nanotubules I_{\perp} and its absorbance A_{\perp} . The parallel polarized absorbance, $A_{//}$, is a component of the absorbance obtained from absorbance of the beam labeled I_{30} , which is oriented at an angle of 30° with respect to the tube axis, using Equation 3.3. A quantitative measure of chain orientation is the dichroic ratio, R , defined as the ratio of $A_{//}$ to A_{\perp} . The dichroic ratio can be readily solved for from the infrared absorbance as shown in Equation 3.4.

Results and Discussion

Electrical Characterization

Representative UV-Vis spectra shown in Figure 5.2 for thin films, 200 nm, and 100 nm diameter nanotubules, readily show a significant difference between the thin films and nanotubules. Notably, the spectral bands in the nanotubules appear to be narrower and redshifted in comparison to the thin films. Quantitative measures of these observations are summarized in Table 5.1.

Table 5.1. Quantitative comparison of P3HT thin film and nanotubule spectra, illustrating the peak narrowing and redshift of the nanotubule spectra relative to films.

Sample	Width at 3/4 Max (eV)	Fraction of Band Area from 1.8 to 2.25 eV	Onset of Absorption (eV)
Film	0.47	27.3%	1.89
200 nm	0.21	37.6%	1.85
100 nm	0.20	37.7%	1.84

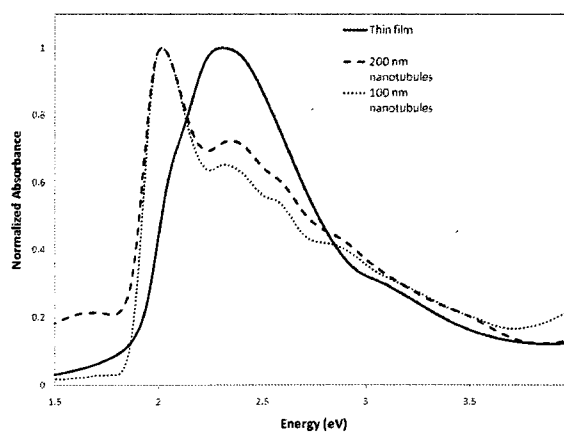


Figure 5.2. UV-Vis spectra of P3HT thin films compared to those of 200 nm and 100 nm nanotubules fabricated via template wetting nanofabrication.

While the absorption bands for all samples span approximately the same energy range, the nanotubule spectra show a sharp, narrow absorption band between ~ 1.80 and 2.25 eV with broad lower intensity absorption at higher energy in comparison with the

broader, more familiar shaped absorption band of the film. The full width at $\frac{3}{4}$ max illustrates the relative sharpness of the of the nanotubule bands (0.20-0.21 eV) in comparison to the film (0.47 eV). This suggests that narrower distribution of electronic states in the nanotubes than in the films, indicative of a higher degree of molecular order.

A bathochromic shift in the absorption of the nanotubes relative to the thin films is also apparent by inspection of Figure 5.2. One way to quantify this shift is to compare the relative area of the absorption band in the region from 1.80 to 2.25 eV (the location of the sharp portion of the nanotubule absorption band) to that of the entire absorption band from 1.8 to 3.5 eV. The low energy region comprises $\sim 38\%$ of the total absorption band area for the nanotubes but only $\sim 27\%$ of the total area for the thin film absorption band.

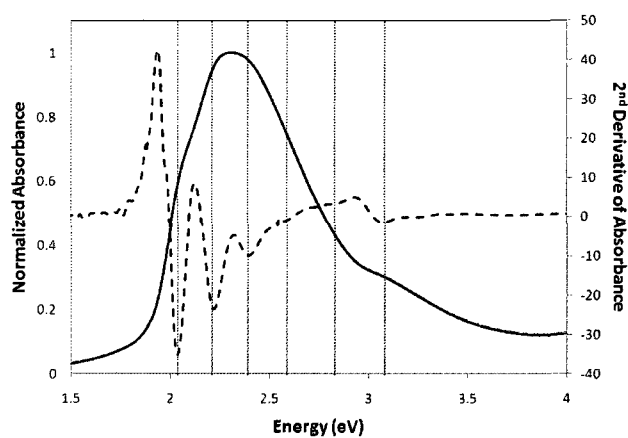
The onset of absorption, a more common and useful measure of the bathochromic shift, is found from the intersection of a tangent line to the low energy side of the absorption band with the x-axis of the spectrum. This onset energy, sometimes referred to as the optical bandgap, is equivalent to the minimum excitation energy for a π - π^* transition in the polymer. This energy shifts from 1.89 eV in P3HT films to 1.85 and 1.84 eV respectively in the 200 nm and 100 nm nanotubes. This redshift in the optical excitation energy is usually attributed to an increase in the effective conjugation length of the polymer.

Taking mathematical derivatives of the spectra is a useful approach to revealing the fine structure of the absorption bands, further elucidating differences between the thin films and nanotubes. This fine structure is related to the physical and electronic structure of the material [173]. In Figure 5.3, each representative spectrum is overlaid with its second derivative. The minima in the 2nd derivative provide the location of the

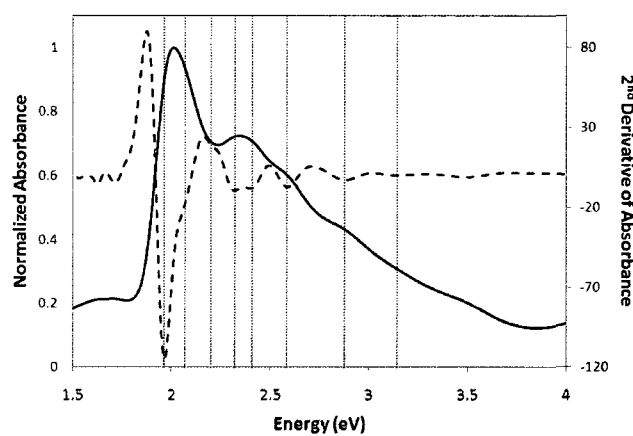
constituent peaks that make up the absorption band, and are summarized in Table 2 and by the dotted vertical lines in Figure 5.3. The four lowest energy film peaks are in good agreement with results reported Trznadel et al. for P3HT purified by Soxhlet extraction [9, 133]. Brown et al. however report a peak at 2.27 eV, rather than the ~ 2.2 eV seen in this work and elsewhere, however films in that work were annealed at 100°C and spin cast rather than drop-cast [133]. Two additional peaks, not seen in thin films, are resolved in the nanotubule samples, at 1.97 and ~ 2.3 eV, indicative of a change in physical structure from the film to the nanotube. The redshift of the lowest energy absorption feature is again evidence of increased order and a greater effective conjugation length. In comparing spectra of the two different diameter nanotubule samples, little difference is seen except at the two highest energy absorption peaks. The differences are insufficient to draw any conclusions however about the effect of nanotubule diameter.

Table 5.2. Peak locations in UV-Vis absorption band as identified from minima in 2nd derivative of absorption spectrum.

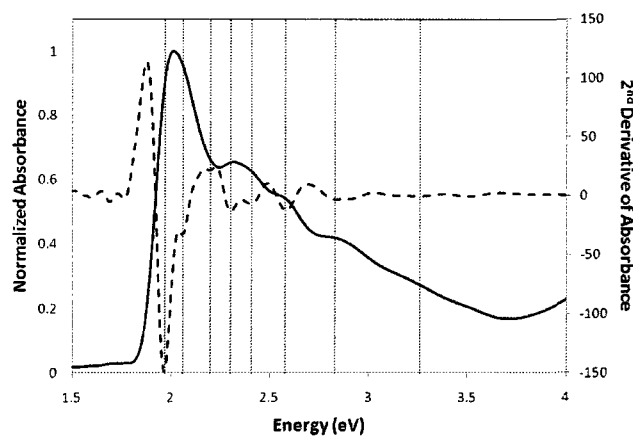
Sample		Absorption peak energy (eV)						
Film		2.04	2.21		2.39	2.59	2.83	3.08
200 nm	1.97	2.07	2.20	2.32	2.41	2.59	2.88	3.15
100 nm	1.97	2.06	2.20	2.30	2.41	2.58	2.83	3.26



a)



b)



c)

Figure 5.3. UV-Vis spectra (solid line) showing 2nd derivative of absorbance (dashed line) used to identify peak locations for P3HT in a) thin films, b) 200 nm nanotubes, and c) 100 nm nanotubes.

Hole Mobility

Based on analysis of the UV-Vis spectra indicating an increased effective conjugation length in P3HT nanotubules as compared to thin films, it might be reasonable to expect a concomitant increase in carrier mobility. Charge carrier transport is limited by the rate of intermolecular transport between polymer chains. Increased long range order in conjugated polymers correlates with a greater degree of intermolecular π -bond overlap, which increases the effective conjugation length of the material and hence carrier mobility.

The general SCLC model in Equation 3.5 has been shown to be applicable across both field regimes for semiconducting polymers [107, 145, 174]. Mobility values were $9.07 \times 10^{-3} \text{ cm}^2 \text{ V}^{-1} \text{ s}^{-1}$ and $5.75 \times 10^{-3} \text{ cm}^2 \text{ V}^{-1} \text{ s}^{-1}$ for the 200 nm and 100 nm nanotubule devices respectively [146]. These are in good agreement with thin film values for regioregular P3HT from transistor measurements that are consistently of the order of $\sim 10^{-2} \text{ cm}^2 \text{ V}^{-1} \text{ s}^{-1} \sim 10^{-3} \text{ cm}^2 \text{ V}^{-1} \text{ s}^{-1}$ [7, 10, 175]. Though the 200 nm samples are higher, the close agreement between values for all samples leads to a conclusion that indications of molecular order from the UV-Vis spectra do not correlate to any significant difference between the hole mobilities of the nanotubules and thin films.

Polarized FTIR

FTIR spectra of 100 nm nanotubules of P3HT are shown for the perpendicular and 30° polarization states in Figure 5.4. The full spectrum is shown in the inset, however the focus is on the vibrational band at $\sim 1220 \text{ cm}^{-1}$. This band has been associated with the C-C inter-ring vibration along the polymer backbone [176, 177]. A significant difference in the absorbance for this peak provides further evidence of polymer chain alignment. Using Equation 3.4, a dichroic ratio for this peak of 2.75 was

found. In general, a dichroic ratio of one implies no preferential orientation. A dichroic ratio greater than one indicates an orientation of the P3HT chain backbone parallel with the nanotube axis.

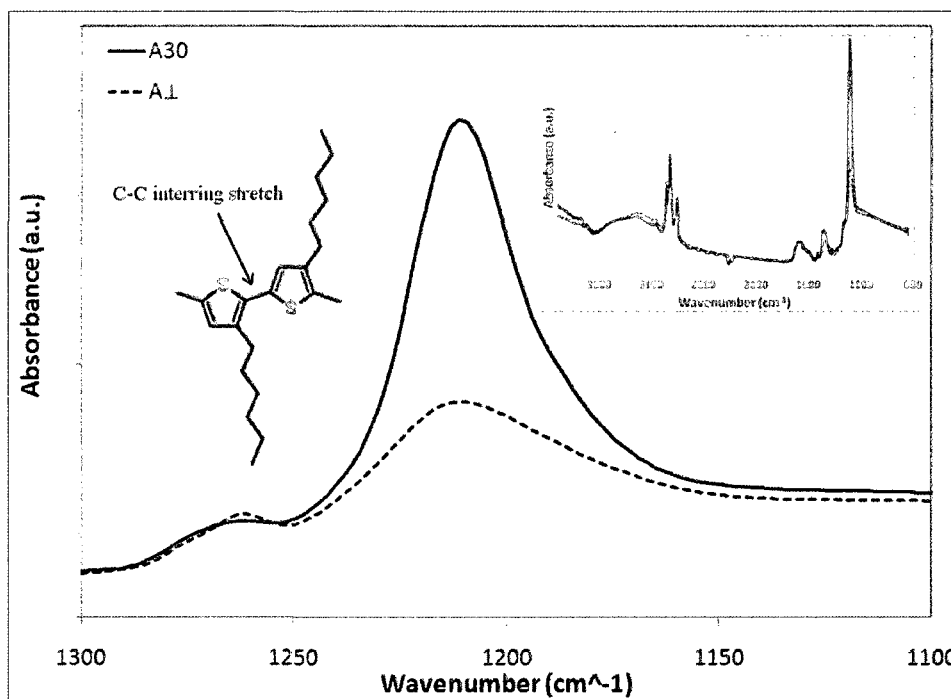


Figure 5.4. The C-C inter-ring vibrational band for the \perp (dashed line) and 30° (solid line) polarizations. The full FTIR spectra are shown in the inset.

Conclusions

P3HT nanotubes were fabricated via template wetting nanofabrication and their optoelectronic properties evaluated and compared with thin films of the same material. UV-Vis spectra showed narrowing and redshift of absorption bands in nanotubes relative to thin films indicative of increased effective conjugation length and long range order. This is further confirmed by the presence of a peak at ~ 1.97 eV found from 2nd derivative analysis of the spectra. Interestingly, two additional peaks not seen in thin films were observed from this fine structure analysis in spectra in the nanotubular configuration.

Further evidence of increased molecular order was found in the dichroism of the C-C inter-ring stretching vibration in polarized FTIR experiments. These experiments indicate a preferential alignment of the polymer backbone parallel with nanotube axis. Based on spectroscopy results, it was anticipated that some increase in carrier mobility would be observed in the P3HT nanotubes relative to thin films, however, significant improvement in mobilities was not found as values observed for regioregular P3HT nanotubes were consistently of the order of 10^{-3} to 10^{-2} $\text{cm}^2\text{V}^{-1}\text{s}^{-1}$, in good agreement with values published elsewhere as observed in field effect transistors [7, 10, 175]. No significant differences in either spectroscopic or electrical behavior were observed between the two different nanotube diameters examined. Thus, at least in this diameter range, it does not appear that nanotube diameter has an impact on the conformation or performance of P3HT.

CHAPTER 6

IMPACT OF PURIFICATION BY SOXHLET EXTRACTION OF POLYTHIOPHENE NANOTUBES

Introduction

Semiconducting and optoelectronic, π -conjugated polymers have been studied for a wide range of device applications with varying degrees of success, as device performance is often hindered by poor charge transport properties. These polymers typically have very limited exciton lifetimes and low charge carrier mobilities, due in part to the lack of molecular order in most thin films [44]. Residual organometallic compounds, monomers and short chain oligomers from the chemical synthesis process also act to reduce charge carrier transport properties [9, 155, 178-180].

Processing methods, including a variety of nanofabrication techniques and purification processes, can improve charge carrier transport by improving molecular ordering and removing impurities. Processing approaches employed to induce molecular order in semiconducting polymers have included the use of alignment substrates, [171] as well as a variety of nanofabrication techniques including electrospinning[19], nanofluidic-lithographic methods [172], template synthesis [82, 94], and template wetting [107, 112].

Polymer nanotubules and nanowires created using template wetting exhibit different material properties from thin films and other configurations of the same material. For example, some materials have shown curvature-induced molecular order and crystallinity within the nanopore [110], and in the case of conjugated polymers, enhanced carrier transport has been observed [107].

Impurities in organic electronic materials introduced during synthesis, along with a high degree of polydispersity, can act to accelerate device degradation, limit molecular ordering, and trap-free carriers [20, 179, 181]. One of the most widely studied semiconducting polymers is P3HT, which is typically synthesized by reacting halogenated 3-hexylthiophene monomers with organometallic catalysts [8, 9, 155, 178, 180]. Residual catalyst, monomer, or short chain oligomers in the product can significantly affect the performance of the material [9, 179, 180]. Significant improvements in polythiophene device performance have been achieved through improved synthesis procedures and extraction methods which produce narrower molecular weight distributions and materials with minimal metallic impurities [7, 9, 17, 155, 175, 178, 179, 182]. For example, Trznadel et al. demonstrated sequential Soxhlet extraction with a series of solvents as an effective means of both removing impurities from P3HT, as well as separating the polymer into relatively narrow molecular weight fractions [9]. For this work Soxhlet extraction procedure with P3HT was performed, and the optoelectronic properties were analyzed for the different molecular weight extracts in a confined, nanotubular configuration formed via template wetting nanofabrication.

Experimental

Materials

Regioregular P3HT with >98.5 % head-to-tail linkages (Rieke Metals Inc.) was obtained from Sigma-Aldrich. ACS reagent grade acetone, chloroform, dichloromethane, hexane, and tetrahydrofuran were also obtained from Sigma-Aldrich and were used as received. Commercially-available anodic porous alumina membranes (Whatman Co.) were used as templates. These were ~60 μm thick with pore densities of approximately of 10^{10} pores per cm^2 and 10^9 pores per cm^2 for templates with nominal pore diameters of 100 nm and 200 nm, respectively.

Methods

Soxhlet extraction was performed following a variation of the procedure described by Trznadel et al., which has since been utilized by several others [9, 179, 182]. Extraction was carried out using each of four solvents in order: acetone, hexane, dichloromethane, and tetrahydrofuran, until the filtrate appeared colorless. The extracting solvents were subsequently allowed to evaporate from collected samples, and the mass of each solid polymer fraction was recorded. Weight percentages of material extracted for each fraction are recorded in Table 6.1. These results are in good quantitative agreement with those obtained by Samitsu et al. using polymer from the same source employed in this work (Sigma Aldrich) [179], and in qualitative agreement with those of Trznadel et al., who used polymer synthesized in their lab [9]. It is the assumption of this work that the molecular weight distributions of each fraction obtained in this work are also qualitatively in agreement with those observed by Samitsu and Trznadel as well. Due to the limited solubility predicted for P3HT in acetone and hexane, the extracted material for these fractions is assumed to be made up of residual

catalyst material, unreacted monomer, and short chain oligomers [9, 179, 180]. The molecular weight dependence of solubility allows low molecular weight polymer to be extracted with dichloromethane, leaving the high molecular weight polymer to be extracted with tetrahydrofuran, as shown by Samitsu et al. (see Table 6.1) [179].

Table 6.1. Percentage of material extracted in each cycle of the Soxhlet extraction procedure for experimental work done here and elsewhere.

Solvent	Present work using Sigma Aldrich P3HT	Samitsu et al. [179] using Sigma Aldrich P3HT			Trznadel et al. [9] using lab synthesized P3HT
	wt %	wt %	Mn	Mw	wt %
Acetone	0.6	2.6			6.5
Hexane	4.3	1.7	4300	5000	9.7
Dichloromethane	17.9	12.2	9900	15000	33.1
Tetrahydrofuran	77.2	83.6	27400	110000	49.2
Chloroform	-	-			1.6

Samples were created using template wetting nanofabrication [107]. Wetting solutions were created from the as-received, unfiltered polymer (sample group denoted as UNF), as well as the polymer fractions obtained from the Soxhlet extraction process with dichloromethane (sample group DC) and tetrahydrofuran (sample group THF), by dissolving polymer from each sample group separately in chloroform at a concentration of 2 mg/ml. Chloroform was used universally as the wetting solvent, so as not to convolute the effects of the extraction process with those of the wetting solvent. Porous alumina templates with both 100 nm and 200 nm nominal pore diameters were wetted with 100 μ L of a specific wetting solution, and the solvent was allowed to evaporate. Residual polymer was removed from exterior template surfaces by means of reactive ion etching with helium plasma.

Samples were optically characterized using UV-Vis spectroscopy, providing a measure of the excitation energy for the various samples. For comparison with the templated nanostructures, thin films were cast on a smooth quartz substrate from the same chloroform-based solution used for the template wetting process.

Results and Discussion

Electronic Spectra

UV-Vis spectra for films, 200 and 100 nm diameter nanotubules are shown in Figure 6.1 with some quantitative measures of these spectra summarized in Table 6.2. The onset energy of absorption in spectra of thin drop cast films of the as received polymer (denoted UNF) and the THF fractions from the extraction process, shown in Figure 6.1a, are identical, at 1.89 eV. These values are slightly redshifted from what is observed in the film cast from the lower molecular weight dichloromethane fraction (DC) with an excitation energy of 1.92 eV. This shift is indicative of a slightly greater average conjugation length for both the THF fraction and UNF samples and is mostly likely attributed to the higher average molecular weight in these samples [9]. This same trend is also seen in spectra of the 100 and 200 nm nanotubular configurations, shown in Figs. 6.5b and c, though the difference between the DC fraction and two higher average molecular weight materials is slightly greater. A bathochromic shift in the onset of adsorption is observed for each fraction in nanotubules when compared to thin films of the same fraction, indicative of a greater average conjugation length in the nanotubules [9]. A smaller shift relative to the films is seen for the lower molecular weight DC fraction to 1.90 eV for both nanotubule diameters. No significant difference in the onset of absorption is seen between the two nanotubule diameters in any fraction.

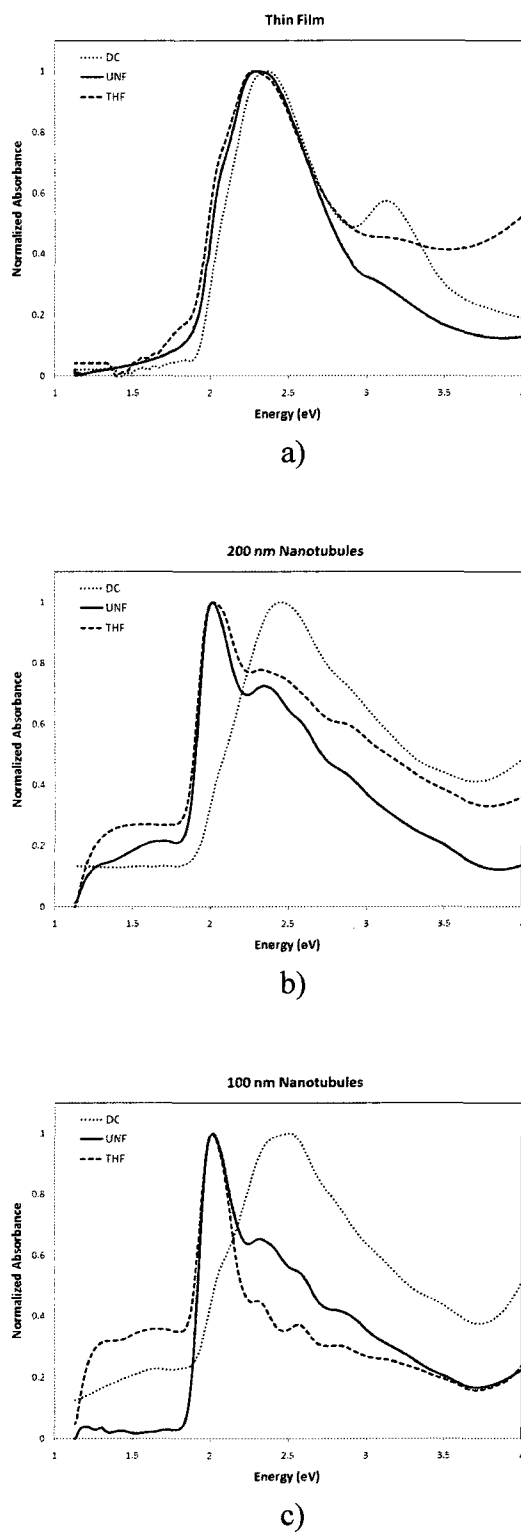


Figure 6.1. UV-Vis spectra of P3HT as received (UNF), and fractions extracted with dichloromethane (DC) and tetrahydrofuran (THF) via Soxhlet extraction a) cast into films, b) in 200 nm diameter nanotubes, and c) 100 nm diameter nanotubes.

Table 6.2. Quantitative comparison of P3HT thin film and nanotubule spectra, illustrating the peak narrowing and redshift of the nanotubule spectra relative to films.

Sample	Onset of Absorption (eV)	Fraction of Band Area from 1.8 to 2.25 eV	Width at 3/4 Max (eV)
UNF Film	1.89	27.3%	0.47
DC Film	1.92	19.1%	0.43
THF Film	1.89	26.0%	0.50
UNF 200 nm	1.85	37.6%	0.21
DC 200 nm	1.90	19.2%	0.63
THF 200 nm	1.85	31.9%	0.53
UNF 100 nm	1.84	37.7%	0.20
DC 100 nm	1.90	18.1%	0.64
THF 100 nm	1.84	46.3%	0.17

Another indication of the redshift in the overall absorption band is found by examining fraction of the total peak area (from 1.8 to 3.5 eV) found in the low energy narrow band observed in the THF and UNF nanotube samples, from 1.8 to 2.25 eV. For the THF and UNF fractions, this value increases from just over 25% of total peak area in the films to between 31.9 and 46.3% for the various nanotubes. Interestingly, little change in this value is observed between films and nanotubes cast from the lower molecular weight dichloromethane fraction.

It is also apparent from inspection of the spectra in Figure 6.1 that the absorption bands for the nanotube samples for the as received polymer and the THF fraction are significantly narrower than those of the thin films. The width of the bands and $\frac{3}{4}$ max drops from approximately 0.5 eV in the film to ~ 0.2 eV in the nanotubes for these material samples. The narrow part of the absorption band from 1.8 to 2.25 eV. This suggests narrower distributions of discrete electronic states are available, indicative of a higher degree of molecular ordering. The absorption peaks observed for nanotubes from the DC sample group do not show this same narrowing effect, and in fact actually broaden slightly.

The minima in the 2nd derivative provide the location of the constituent peaks that make up the absorption band, and are summarized in Table 6.3. For comparison, results reported by Trznadel et al. for the same analysis on films are shown as well [9, 133]. These are in excellent agreement with films cast from the same fractions in this work. Here little difference is seen between the film samples and nanotubes cast from the lower molecular weight dichloromethane fraction. The other nanotube samples however show a quite different fine structure with two additional peaks not seen in thin films at 1.97 and ~2.3 eV. Illustration of this is given in Figure 6.2, showing the second derivative overlaid with the spectrum for 200 nm nanotubes from the THF and DC fractions. The additional constituent peaks are indicative of a change in physical molecular structure from the film to the nanotube. The bathochromic shift of the lowest energy absorption feature is again evidence of increased order and a greater effective conjugation length. In comparing spectra of the two different diameter nanotubule samples, little difference is seen in relative peak. The differences are insufficient to draw any conclusions however about the effect of nanotubule diameter.

Table 6.3. Peak locations in UV-Vis absorption band identified from minima in 2nd derivative of absorption spectrum. Film data denoted with * is from Trznadel et al. [9].

Sample		Absorption Peak Energy (eV)							
UNF film		2.04	2.21		2.39	2.59	2.83	3.08	
DCfilm*		2.04	2.21		2.42	2.63			
DC film		2.04	2.24		2.40	2.65	2.80	3.10	
THF film*		2.02	2.21		2.42	2.63			
THF film		2.03	2.23		2.39	2.64	2.78	3.16	
UNF 200 nm	1.97	2.07	2.20	2.32	2.41	2.59	2.88	3.15	3.49
THF 200 nm	1.96	2.09	2.20	2.30	2.47	2.62	2.88	3.18	3.50
DC 200 nm		2.03	2.21	2.33	2.50		2.84	3.18	3.44
UNF 100 nm	1.97	2.06	2.20	2.30	2.41	2.58	2.83	3.26	3.51
THF 100 nm	1.98	2.09	2.21	2.30	2.35	2.57	2.84	3.14	3.52
DC 100 nm		2.04		2.33		2.56	2.81	3.09	3.46

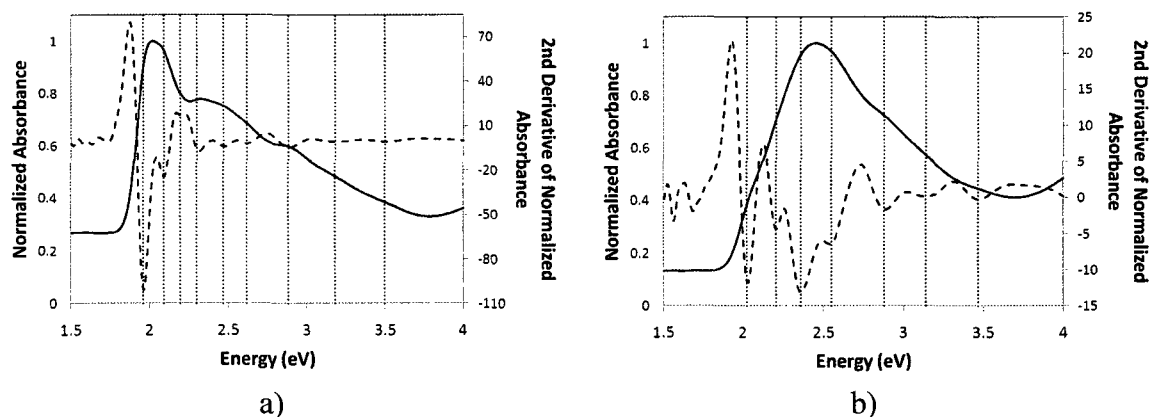


Figure 6.2. Representative UV-Vis spectra (solid line) showing the 2nd derivative of absorbance (dashed line) used to identify peak locations for P3HT in a) 200 nm nanotubes cast from the THF fraction and b) 200 nm nanotubes cast from the DC fraction. The vertical dotted lines represent minima in the 2nd derivative of the spectrum.

Electrical Characterization

Space charge limited current (SCLC) models are used in this work to model carrier transport in P3HT, and have been widely used for this and other semiconducting polymer systems [118, 141, 142, 145, 164, 165]. The general SCLC (Equation 3.5) has been shown to be applicable across both field regimes for semiconducting polymers [107, 145, 174].

Experimentally obtained data were found to agree well with the behavior described by Equation 3.5, which describes a transitional behavior from ohmic processes at low applied bias to space-charge-limited behavior at higher bias. Best fit curves to this model are shown on the data curves in Figure 6.3 [146]. In the as received polymer samples, the mobility was found to be $5.75 \times 10^{-03} \text{ cm}^2 \text{V}^{-1} \text{s}^{-1}$ for the 100 nm nanotubes and $9.07 \times 10^{-03} \text{ cm}^2 \text{V}^{-1} \text{s}^{-1}$ for the 200 nm nanotubes. As expected from previously described results, the THF fraction yielded similar results, $5.49 \times 10^{-03} \text{ cm}^2 \text{V}^{-1} \text{s}^{-1}$ and $6.77 \times 10^{-03} \text{ cm}^2 \text{V}^{-1} \text{s}^{-1}$ for the 100 and 200 nm nanotubes respectively. In each case, the 200 nm nanotubes exhibited greater hole mobility than the 100 nm nanotubes. Highest

mobilities were found for the DC fraction of $9.32 \times 10^{-3} \text{ cm}^2 \text{V}^{-1} \text{s}^{-1}$ for 100 nm and $1.94 \times 10^{-2} \text{ cm}^2 \text{V}^{-1} \text{s}^{-1}$ for 200 nm nanotubules. According to spectroscopic results, this fraction had the lowest effective conjugation length and largest distribution of electronic states. However, this fraction is also expected to have the lowest polydispersity, [9, 179] reducing any interstitial ordering defects that may occur due to dissimilar molecules increasing the mobility, but not significantly reducing the optical bandgap.

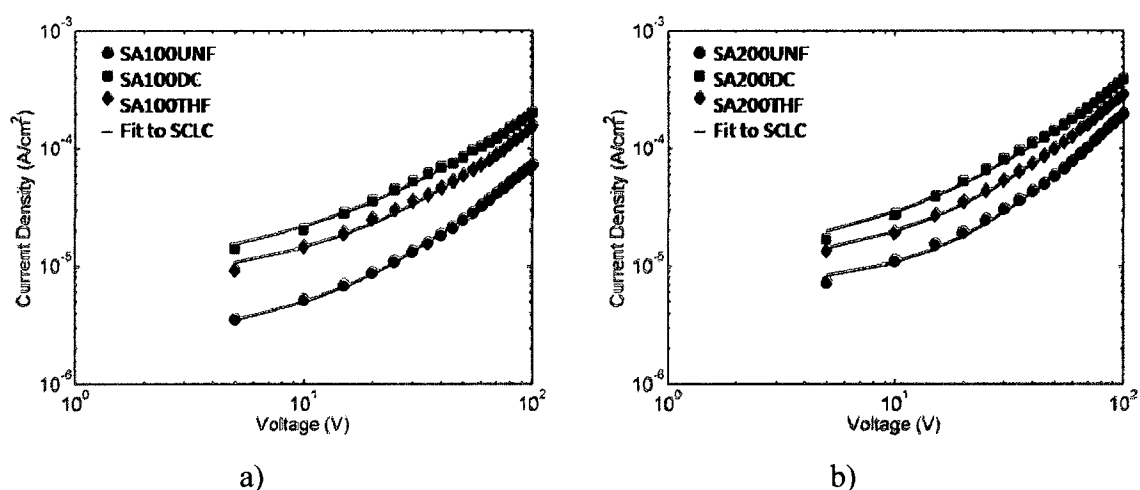


Figure 6.3. J - V characteristics for nanotube-based electronic devices created with various fractions of P3HT material for a) 100 nm and b) 200 nm nanotubes. Solid lines represent regression fits to Equation 3.5 [146].

Conclusion

Soxhlet extraction has been used to purify bulk P3HT material, yielding significant quantities of material for each of a low molecular weight DC and higher molecular weight THF fractions, with extracted mass percentages in good agreement with other work for polymer from the same manufacturer [179]. Small difference in the UV-Vis spectra were observed in thin films cast from these fractions, consistent with previously observed results and attributable to differences in the effective conjugation length due to the differing average molecular weights of the fractions [9]. Extracted

P3HT was used to successfully create semiconducting polymer nanotubes via template wetting nanofabrication, and electronic devices based on these nanotubes. In this configuration, a bathochromic shift in the absorption bands was observed relative to thin films, indicating a further increase in the degree of molecular order and effective conjugation length due to the physical configuration of the material. Additional peaks in the nanotubule samples, not seen in thin films, were also resolved from analyzing the second derivative of the absorption band, providing further evidence of a change in the electronic structure of the material in this configuration.

CHAPTER 7

WATCHING PAINT DRY: THE EFFECTS OF CASTING SOLVENT ON THE FORMATION OF CONJUGATED POLYMER NANOTUBES CREATED WITH TEMPLATE WETTING NANOFABRICATION

Introduction

Poor electrical interaction is a known problem in disordered conjugated polymers limiting the efficiency and performance in electronic devices made from these materials [183]. Improving the order, and thereby improving the charge transport, in conjugated polymers has been the focus of many studies. Improving the molecular ordering in semiconducting polymer devices is dependent on the ability for charge carriers to transfer from one chain to another efficiently. The effect and types of charge carrier interchain transport has been the focus of many studies into thin film devices that are highly dependent on this order [171]. Absorption of light in photovoltaic devices is also highly dependent on increasing the effective conjugation length by interchain π -orbital overlap [184].

One of the main factors that influence the conformation of polymer chains and thus the molecular ordering of a solid state device is the solvent used to dissolve the polymer [51, 68] and cast the device into a film [69]. Solvent effects on a polymer

depend on the solvent used, the polymer being deposited, and the fabrication process. Thin films cast from polythiophene derivatives depend highly on the evaporation rate [51]. P3HT, for example, has a rigid-rod molecular structure that will self-orient and aggregate resulting in a largely stacked system of thiophene rings between adjacent polymer chains [7, 10, 182, 185]. This alignment is seen more in drop-cast films than from films that are spin casted due to the evaporation rate of the solvent [51]. Slower evaporation allows for the polymer chains to reach a more thermodynamically favorable state [51] and reduces solvent quenching effects where the polymer chain retains a “memory” of its state in the solvent [10].

Poly(phenylene vinylene)s (PPVs) are largely amorphous and do not exhibit the same rigid rod conformation seen in polythiophenes [186]. This attributes to PPVs likelihood to form agglomerations in bad solvent where chains are folded but not interacting electrically [61]. Simulations and light scattering measurements have shown that the radius of gyration for MEH-PPV molecules in chloroform is much larger than in toluene which is identified as toluene samples forming tight coils while chloroform causes the polymer to an extended conformation [132, 186]. The effective conjugation length in MEH-PPV will be elongated when the solvent straightens the polymer redshifting the optical absorbance [61]. However, simply straightening a molecule does not always produce a redshift as MEH-PPV in chloroform will straighten the molecule and produce a torsion angle between phenyl rings causing a blueshift with respect to chlorobenzene which is better able to align the backbone [187]. Longer effective conjugation lengths lead directly to improved charge carrier transport [44] as well as a

lower energy optical bandgap [188]. This clearly shows that a solvent's ability to straighten a polymer chain is important when creating devices for these purposes.

Chapter 4 demonstrated that solution based template wetting was an effective means of creating nanotubes from P3HT and MEH-PPV while Chapter 5 demonstrated the change in the electronic structure of P3HT due to the curvature induced confinement. Here, solvent effects on solution based template wetting for MEH-PPV and P3HT are examined. Electronic transport within the nanostructures is characterized by the current-voltage characteristics. UV-Visible spectroscopy is used to approximate the optical bandgap, the highest electronic state concentration, and the electronic absorption bands. Polarized FTIR is used to discover alignment of the polymer chains relative to the pore walls. TGA analysis will be used to make qualitative comparisons of the solvent evaporation characteristics.

Experimental

Materials

Regioregular poly(3-hexylthiophene-2,5-diyl) with > 98.5 % head-to-tail linkages (P3HT), poly[2-methoxy-5-(2-ethylhexyloxy)-1,4-phenylenevinylene] (MEH-PPV, $M_{n,avg}$ 70,000 – 100,000) and ACS reagent grade chlorobenzene (CB), chloroform (CF), tetrahydrofuran (THF), and toluene (TOL) were obtained from Sigma-Aldrich and used as received. Solutions of each polymer were created by dissolution in either of CB, CF, THF, or TOL at a concentration of 2 mg/ml. Commercially available anodic porous aluminum oxide membranes (Whatman Co.) were used as templates. Templates were 60 μm thick with monodisperse pore diameters of 100 nm and 10^{10} pores per cm^2 .

Methods

Porous anodized aluminum oxide templates were wetted with solution volumes to create nanotubule wall thickness is under 5 nm to ensure that the bulk of the polymer deposition is through precursor wetting [189, 190]. All samples were allowed to evaporate ~18 hours to ensure complete solvent evaporation. Residual polymer on the surface of the template was removed with a nonreactive He plasma etch. Short etch times and the high aspect ratio of the pores is believed to prevent etching of the nanostructures in the pores [124]. SEM micrographs were taken after partially etching the alumina template in a 25 wt. % aqueous KOH solution. These micrographs are shown in Figure 7.1.

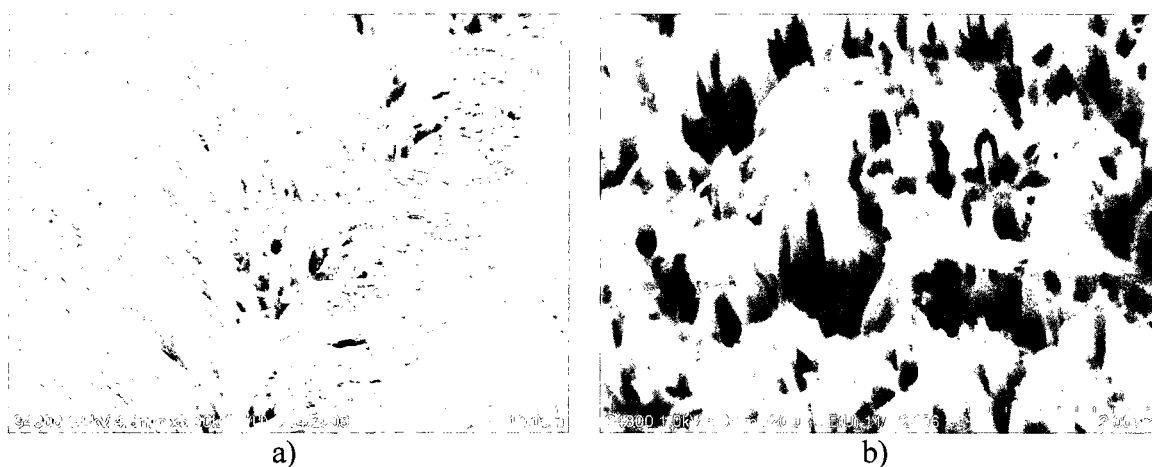


Figure 7.1. Scanning electron micrographs of a) MEH-PPV and b)P3HT nanotubes created using template wetting in 100 nm diameter alumina nanopores with chloroform as the solvent for the wetting solution.

Electronic devices were fabricated by depositing metallic contacts on each side of the templates, forming device structures with either MEH-PPV nanotubes or P3HT nanotubes. The work function, ϕ_m , of the chosen contact material from metals whose ϕ_m is within a few 0.1 eV of the top of the valence band, space-charge-limited (SCL) hole

conduction will dominate in the device, allowing for accurate examination of the hole transport properties [141]. Here, 150 nm thick Au ($\phi_m \approx 5.1$ eV) [144] electrodes were formed on each side of the wetted membranes after the plasma etch was completed. Conduction is assumed to be dominated by a single carrier (in this case, holes) throughout this work.

For the UV-Vis absorption analysis, templates were used directly after plasma etching. UV-Vis spectroscopy was performed using a Shimadzu UV 1650PC system in order to determine optical absorbance spectra and approximate band gaps of the material embedded within the nanoporous membranes by determining the low energy onset of absorption. Nanotube-template samples were analyzed by orienting them in the UV-Vis system such that the incident beam was normal to the template or film surface ensuring that the whole beam would transmit through the sample.

Polarized FTIR spectroscopy was used to study the degree of orientation of the MEH-PPV and P3HT polymer chains in the nanotubular configuration. A quantitative measure of chain orientation in the nanopore is the dichroic ratio, R , was readily solved for from the infrared absorbance using Equation 3.4.

Thermogravimetric analysis to determine the solvent dependent evaporation characteristics was performed by deposited a polymer/solvent solution onto an alumina pan and allowing to evaporate at 30° C in a nitrogen environment until the % weight/minute was less than 0.0 %/min which is the lowest rate of measure allowed by the analyzer. The start of the gel drying stage was calculated from the 2nd derivative curve of the mass per unit time.

Results and Discussion

Electrical Characterization

Current densities in the nanotube-based electronic devices were found to be in good agreement with both of the space-charge-limited conduction models described above, as R^2 values for the least-squares-regression were in excess of 0.995 for the standard [146]. Values of hole mobility were obtained by considering both the TF-SCLC behavior of current density in linear combination with ohmic behavior given in Equation 3.5.

Current densities for MEH-PPV devices vary strongly with solvent, while current densities in P3HT samples were relatively independent of solvent. Average current densities for each polymer are illustrated in Figure 7.2, along with corresponding fits to Equation 3.5 and resulting hole mobilities are shown in Table 7.1 [146].

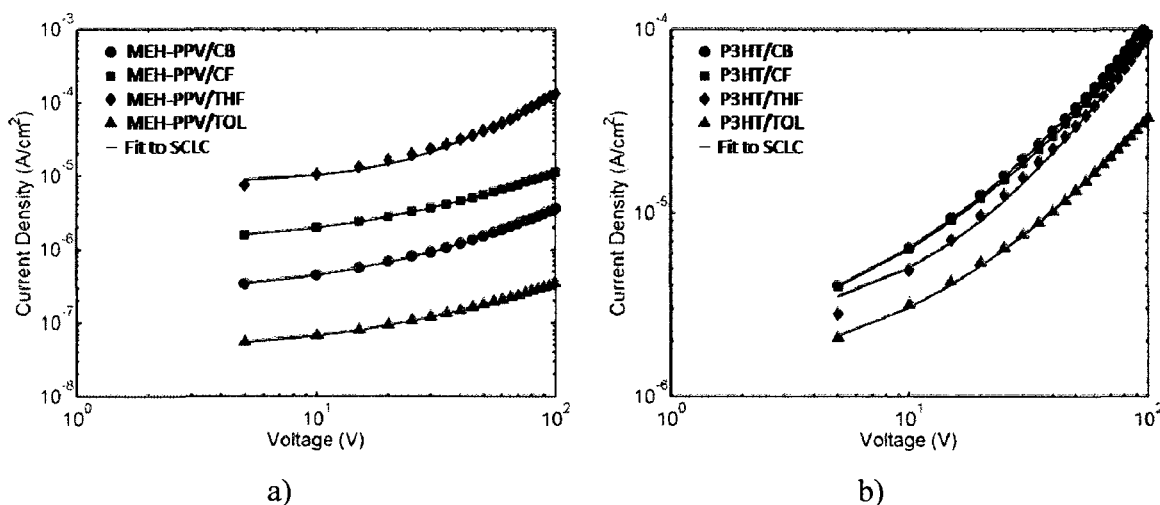


Figure 7.2. Average J - V characteristics for electronic devices fabricated from 100 nm nanotubes of a) MEH-PPV and b) P3HT, created by template wetting from various solvents. Solid lines represent least-squares-regression fits to Equation 3.5 [146].

Table 7.1. Hole mobility determined from analysis of space-charge-limited currents in MEH-PPV and P3HT nanotube-based electronic devices.

Following (3.5)	
Sample Group	$\mu_{p,avg}$ ($\text{cm}^2 \text{V}^{-1} \text{s}^{-1}$)
MEH-PPV/CB	3.24E-05
MEH-PPV/CF	2.39E-04
MEH-PPV/THF	9.31E-03
MEH-PPV/TOL	5.41E-06
P3HT/CB	7.67E-03
P3HT/CF	5.39E-03
P3HT/THF	6.70E-03
P3HT/TOL	1.38E-03

UV-Visible Spectroscopy

UV-Vis spectra for MEH-PPV and P3HT thin films and nanotubules fabricated from chlorobenzene, chloroform, tetrahydrofuran, and toluene are displayed in Figure 7.3. From this data peak locations and optical bandgaps (E_g) for each sample was calculated and is shown in Table 7.2. The thin film samples of MEH-PPV and P3HT are noticeably different from each other. The P3HT thin films exhibit a shoulder on the low energy side of the peak while the MEH-PPV thin films only show a broad single peak without noticeable features. This is indicative a fine structures assembling in the P3HT thin films that are largely absent from the MEH-PPV corresponding to the semi-crystalline and amorphous natures of P3HT and MEH-PPV respectively [32]. The 100 nm MEH-PPV nanotubules are, visually, quite similar to the thin films while the P3HT nanotubules have a noticeably redshifted and sharp peak. The P3HT curves seem to show very little variation between casting solvents while there is a visible shift in MEH-PPV samples.

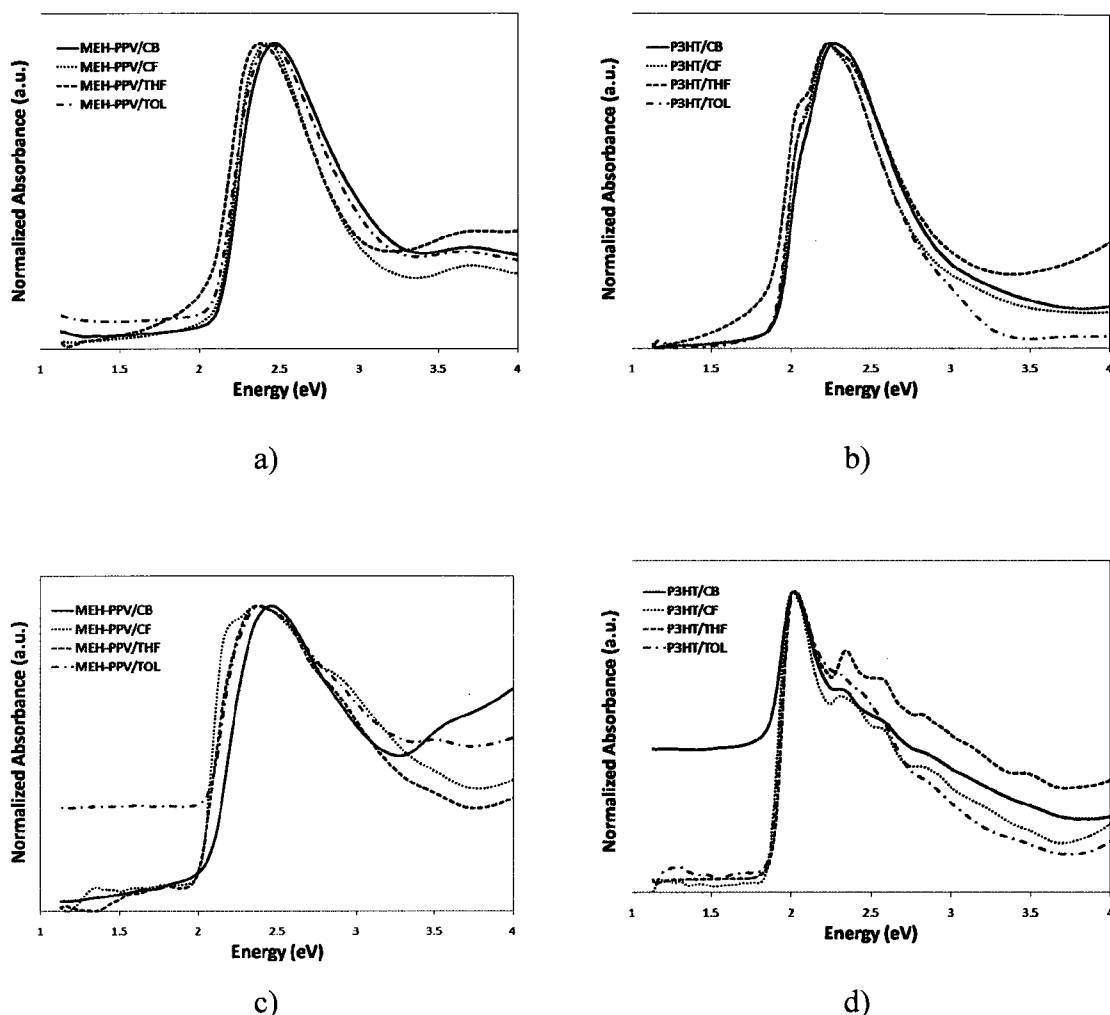


Figure 7.3. UV-Vis absorbance spectra for a) thin films and c) 100 nm nanotubes of MEH-PPV and b) thin films and d) 100 nm nanotubes of P3HT in four solvents.

The peak locations of MEH-PPV redshift in all solvents used. This indicated that the highest concentration of electronic states (or chromophores) is at a lower energy which indicates a longer effective conjugation length between the two fabrication techniques [187]. This result is repeated in the E_g that shows a shift that is similar in energy difference to the shift in peak location. This reduction in the onset energy is indicative of a narrowing of the optical bandgap [191]. The E_g of the THF and CF samples are noticeably lower than those of the CB and TOL samples. This gap between the aromatic (CB and TOL) and nonaromatic (CF and THF) solvents indicates that the

excitation energy can be influenced by the solvent choice for MEH-PPV. This is especially evident in the CF samples where the E_g is redshifted by more than 0.1 eV in the nanotubules. This solvent dependency in the optical bandgap stands in good agreement with the mobilities calculated for each sample set. Figure 7.4a demonstrates that a lower E_g will correspond to a higher mobility.

Table 7.2. Peak absorption and optical bandgap for MEH-PPV and P3HT thin films and 100 nm nanotubules determined from UV-Vis spectra.

Sample	Peak Absorption (eV)			Optical Bandgap (eV)		
	Thin Film	100 nm Nanotubules	Energy Shift	Thin Film	100 nm Nanotubules	Energy Shift
MEH-PPV/CB	2.48	2.45	0.03	2.12	2.06	0.06
MEH-PPV/CF	2.43	2.36	0.07	2.12	2.00	0.12
MEH-PPV/THF	2.38	2.37	0.01	2.07	2.00	0.07
MEH-PPV/TOL	2.45	2.37	0.08	2.10	2.04	0.06
P3HT/CB	2.28	2.00	0.28	1.91	1.84	0.07
P3HT/CF	2.23	2.01	0.22	1.89	1.84	0.05
P3HT/THF	2.23	2.02	0.21	1.88	1.85	0.03
P3HT/TOL	2.24	2.03	0.21	1.90	1.85	0.05

The P3HT peak location is highly redshifted in the nanotubules. This indicates a dominant chromophore that has a longer effective conjugation length [187]. This strong redshift of the peak location is not mirrored in a shift in E_g that is ~ 0.05 eV on average. Both of these measures are characteristic of a more highly packed structure. Further, the differences in peak locations and optical bandgaps between solvents are essentially the same for all solvents used. When compared to the mobility measurements in Figure 7.4b, the lack of variation in either the mobility or excitation energy indicates that the choice of solvent has little effect on the semi-crystalline P3HT. This lack of solvent dependency stands in sharp contrast to that seen in MEH-PPV samples.

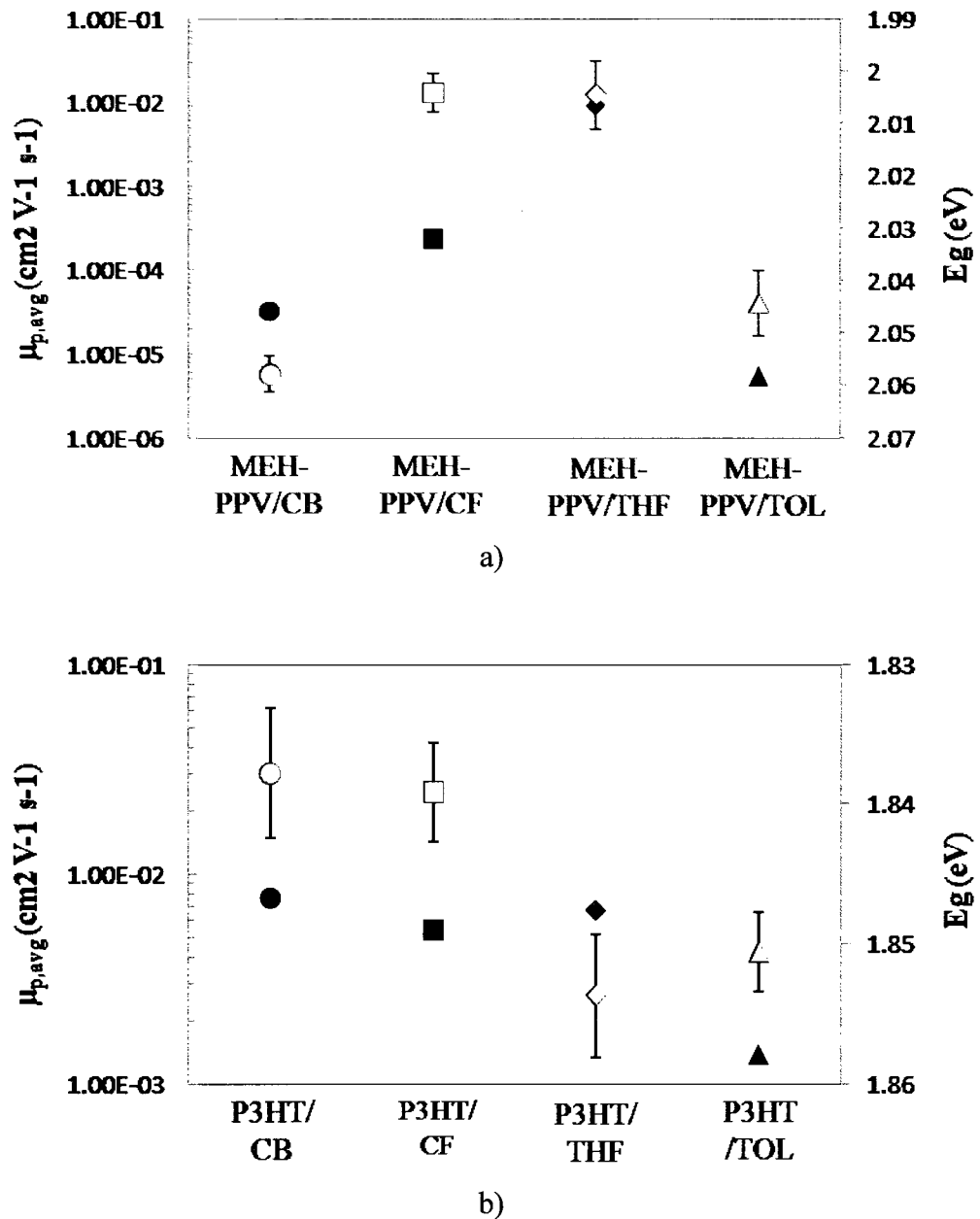


Figure 7.4. Hole mobility (μ_p) [146] and optical bandgap E_g for 100 nm nanotubes of a) MEH-PPV and b) P3HT. The closed symbols correspond to the μ_p and the open symbols correspond to E_g .

The absorbance band peaks are seen in the Tables 7.3 and 7.4 for P3HT and MEH-PPV, respectively, are taken from the minima of the 2nd derivatives of the spectra and indicate fine structure differences between the films and nanotubes [173]. The

bands show that P3HT have a low energy band that is absent from the films in all solvents. Couple this with the overall increase in order due to the peak location movement and it is clear that a curvature induced order is occurring. It can also be seen that there are whole peaks in the thin films that are absent in the nanotubules while the nanotubules have peaks absent from the P3HT films. This indicates a structure in the nanotubules that is not seen in the thin film devices.

Table 7.3. Peak locations in P3HT UV-Vis absorption band as identified from minima in 2nd derivative of absorption spectrum. Relative peak location is designated with a vertical dashed line.

Sample	Structure	Absorption peak energy (eV)								
P3HT/CB	Thin Film	2.03	2.20	2.38	2.55	2.75	2.88	3.10	3.28	
P3HT/CF	Thin Film	2.03	2.19	2.37	2.56	2.72	2.88	3.05	3.18	
P3HT/THF	Thin Film	2.02	2.20	2.39	2.57	2.73	2.89	3.03	3.19	
P3HT/TOL	Thin Film	2.02	2.19	2.37	2.59	2.72	2.84	3.02		
P3HT/CB	Nanotubule	1.99	2.13	2.21	2.33	2.58	2.88	3.13		
P3HT/CF	Nanotubule	1.97	2.07	2.20	2.32	2.41	2.59	2.88	3.15	
P3HT/THF	Nanotubule	1.97	2.08	2.12	2.21	2.33	2.50	2.59	2.83	3.15
P3HT/TOL	Nanotubule	1.99	2.11	2.18	2.30	2.44	2.59	2.83	3.14	

MEH-PPV bands are more surprising with, up to, two bands being seen in at energies lower than the lowest energy of the films. MEH-PPV once again shows a higher solvent dependency as the CF and THF samples lowest energy band is nonexistent in the CB and TOL samples. Thus, the lower E_g arises from an energy band that is not evident in devices created from the other two solvents. The overall electronic structure of the nanotubules is in agreement with the peaks found in the thin films with the exception of the lower energy bands. In contrast to P3HT, conclusions about any changes in inherent structure between the two fabrication techniques cannot be seen.

Table 7.4. Peak locations in MEH-PPV UV-Vis absorption band as identified from minima in 2nd derivative of absorption spectrum. Relative peak location is designated with a vertical dashed line.

Sample	Structure	Absorption peak energy (eV)								
MEH-PPV/CB	Thin Film	2.32	2.47		2.60	2.83	3.02	3.34		
MEH-PPV/CF	Thin Film	2.29		2.46	2.66	3.05				
MEH-PPV/THF	Thin Film	2.27		2.46	2.68	2.88	3.11			
MEH-PPV/TOL	Thin Film	2.28		2.45	2.57	2.82	3.09	3.36		
MEH-PPV/CB	Nanotubule	2.22	2.35		2.50	2.60	2.90	3.15	3.50	
MEH-PPV/CF	Nanotubule	2.13	2.23	2.32		2.46	2.60	2.88	3.15	3.50
MEH-PPV/THF	Nanotubule	2.10	2.17	2.31		2.42	2.56	2.87	3.15	3.50
MEH-PPV/TOL	Nanotubule	2.20	2.33		2.50	2.60	2.88	3.15	3.50	

Polarized Infrared Spectroscopy

FTIR measurements at the \perp and 30° polarization states were taken to determine the alignment of the polymers with the pore and are shown in Table 7.5. P3HT shows strong alignment in THF with an R of ~ 16 and moderate alignment in CF and no alignment in CB or TOL at $\sim 1220 \text{ cm}^{-1}$. This band is the interring C-C stretch [176, 177] of the P3HT indicating that the polymer back bone is aligned with the pore wall. MEH-PPV exhibits strong alignment in CF and THF ($R \sim 11-12$) with moderate alignment in TOL and no alignment in CB at $\sim 1210 \text{ cm}^{-1}$ which is the C-O stretch of the methoxy and/or ethylhexyloxy side chains with the phenyl ring [23]. An alignment of the side chains with the pore wall would be expected for the PPV backbone to be aligned perpendicular relative to the pore wall. This once again is in agreement with the bimodal solvent effects seen between the CF/THF devices and the CB/TOL devices.

Table 7.5. Dichroic ratio of MEH-PPV and P3HT nanotubules determined by polarized FTIR shown with the measured absorbances for each orientation. Dichroic ratio calculated using Equation 7.2.

Sample	A_{30}	A_{\perp}	R
MEH-PPV/CB	0.12	0.11	1.12
MEH-PPV/CF	6.28	0.73	11.07
MEH-PPV/THF	6.40	0.68	12.23
MEH-PPV/TOL	1.09	0.43	3.06
P3HT/CB	0.17	0.17	1.02
P3HT/CF	1.67	0.59	2.75
P3HT/THF	6.04	0.49	16.13
P3HT/TOL	0.14	0.10	1.44

The parallel and perpendicular arrangement of P3HT and MEH-PPV, respectively, leads to an understanding of the self-organization of the polymer chains within the nanopore. CF and THF are known to interact mostly with the side chains of these polymers while CB and TOL interact mostly with the aromatic rings [65, 187]. When the solvent dewets from the pore wall, a shearing force is induced on the deposited polymer [60, 82].

The shearing would then act on the part of the polymer chain (backbone vs. side chain) at which solvent exhibits it highest affinity. Forces acting on P3HT are likely to arrange it parallel to the pore wall as the regioregular structure would place equal force on each side of the polymer chain. MEH-PPV would behave differently as the force applied to the side chains would turn the molecule so that the side chains would orient in the direction of the retreating solvent. Solvents that interact mostly with the polymer backbone would exert less of a moment on the polymer as the center of mass for each polymer is closer to the backbone. A simplistic model would be that the side chains of MEH-PPV and P3HT are acting as a moment arms to turn the polymer chains into their

particular orientation. This effect would explain the amorphous characteristics of solution wetted PVDF [110] (as mentioned in Chapter 3) as the polymer does not have side chains to be effected by the drying solvent.

When comparing the mobility with the alignment numbers (Figure 7.5b), P3HT exhibits a very weak relationship with the dichroic ratio. This non-relation can be seen the most in CB devices that show no preferential alignment, but have the highest mobility. P3HT is known to form aggregates and precipitates during solvent evaporation [51]. Solution of P3HT were often observed to be cloudy and yellow or deep purple if not used soon after sonication indicating the formation of aggregates. Though these aggregates facilitate charge transfer, it would appear that the orientation of the aggregates with respect to the pore wall may be independent of the charge transfer and that the aggregation may hinder the overall alignment of the P3HT chains. In both the cases of mobility and E_g , P3HT devices are within an order of magnitude of each other so little change is seen overall.

In MEH-PPV nanotubules, the alignment measured by the dichroic ratio is in good agreement with the mobility and bandgap measurements (Figure 7.5a,c). As the MEH-PPV molecules align with the tube they are aligning with other MEH-PPV molecules so that they organizing in the same direction. This organization (or lack thereof) may drive the difference seen between the aromatic and nonaromatic solvents. It is of some note, that the MEH-PPV/TOL devices do exhibit a mild orientation, but do not seem to have an enhancement in the mobility. There is a lowering of the E_g energy for these samples relative to the MEH-PPV/CB devices indicating a longer effective conjugation length.

Overall, it is extremely likely that the dichroic ratio can be taken as a qualitative measure of the effective conjugation length of the polymer devices; such that a higher dichroic ratio is indicative of a longer effective conjugation length in the more amorphous MEH-PPV while it is largely independent of any properties seen in P3HT.

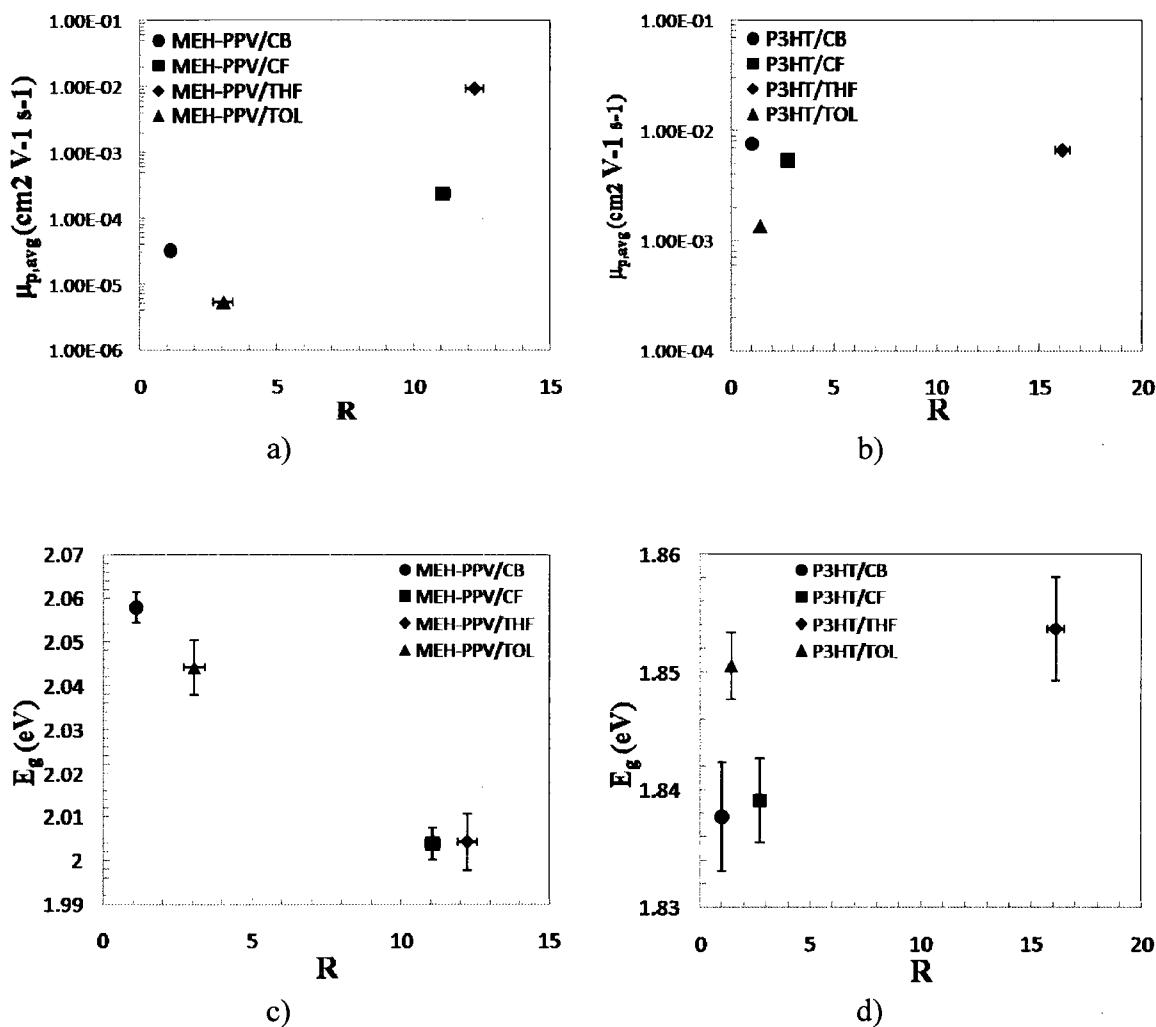


Figure 7.5. Mobility data [146] plotted as a function of dichroic ratio in a) MEH-PPV and b) P3HT as well as optical bandgap as a function of dichroic ratio in c) MEH-PPV and d) P3HT.

Solution Evaporation Characteristics

Thermogravimetric analysis of the drying P3HT and MEH-PPV films were carried out to determine the solvent evaporation characteristics of the solvents from the polymer. As a polymeric solution dries it goes through three phases: liquid evaporation, gel drying and a transition region between the two as illustrated in Figure 7.6. The gel drying time (t_{gel}) as a fraction of the total drying time (t_{total}) can be taken as a relative affinity of the solvent for the polymer.

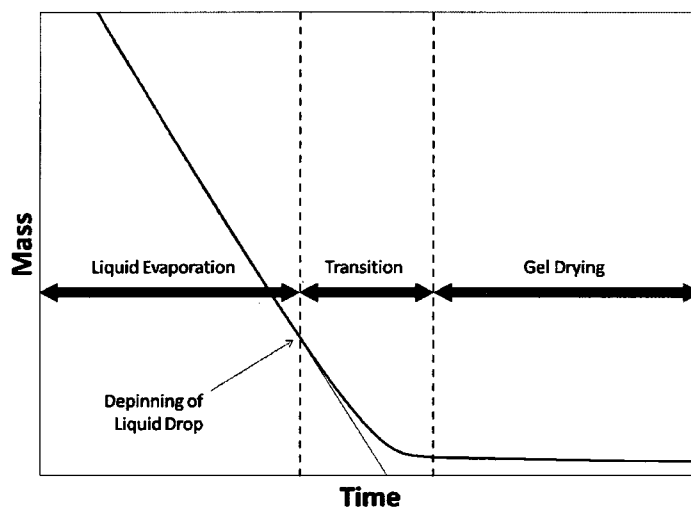


Figure 7.6. Illustration showing the three phases that make up the drying of the MEH-PPV and P3HT in various solvents.

When a sessile drop with a dispersion of particles dries, it will exhibit a linear drying rate until the drop depins. Once the drop has depinned, the evaporation will slow as the evaporation is a function of the radius of the drop which is contracting. This will lead to a characteristic tail at the end of the drying [192]. However, this tail is short in time and is a small portion of the overall drying as the bulk of the liquid is lost while the drop is pinned to the surface. In a polymeric solution, the tail will elongate as the solution transitions from a solution into a gel [69] in what is the analogue to the

dissolution steps of the polymer forming a gel before complete dissolution. If the t_{gel}/t_{total} fraction is the same between two different solvent, then the relative affinity is the same and the t_{gel} is simply a function of the boiling point of the solvent. If the fraction is higher in one solvent with respect to another, then the relative affinity is higher regardless of boiling point. This analysis serves as a way in which to analyze solvent evaporation of a polymeric solution between solvents of differing boiling point. This is important as solvent quenching and solvent annealing effects are known to alter the conformation of deposited MEH-PPV and P3HT [139].

Several studies have indicated that polymer chain organization and ordering can be increased by a process of slowing the solvent evaporation time [139]. This is accomplished by either using a higher boiling point solvent [71, 72] or by increasing the vapor pressure of the solvent in a specialized drying area [72, 74, 139]. While this effect is well known, it has not been found which of these two mechanisms is more effective or more suited to the fabrication of polymer nanostructures. In MEH-PPV, the high boiling point solvents (CB and TOL) have not shown the same electronic or orientation properties of the much lower boiling point solvent of CF and THF in this study. Therefore, the gel drying time fraction can give insights into the drying characteristics and the extension of which drying region is most beneficial to chain organization in template wetted structures.

The dichroic ratio, mobility, and optical bandgap for each device are plotted as a function of the relative affinity of the solvents for MEH-PPV and P3HT in Figure 7.7. In both P3HT and MEH-PPV, the evaporation of THF from the gel phase is shown to be longer than the liquid drying time with the P3HT/THF t_{gel} being $\sim 75\%$ of the overall

drying time. In MEH-PPV the t_{gel}/t_{total} is in good agreement with the properties of the devices with a higher ratio showing more alignment, lower E_g , and a higher mobility. These qualitative correlations indicate that the choice in solvent when fabricating nanostructures of MEH-PPV is very important as has been noted for films. This mirrors the trend of a good low boiling point solvent, like CF, will quench the polymer chain if allowed to evaporate quickly [71] but will take on an extended conformation with a long effective conjugation length if allowed to evaporate more slowly [69]. The only exception is the MEH-PPV/CB mobility in which highly organized aggregates are thought to form and prevent penetration of the longer molecular weights into the porous template [146].

In P3HT devices, a relation can be seen between the gel fraction and the dichroic ratio. This indicates that oriented nanostructures of P3HT are solvent dependent. However, the electronic properties do not seem to be solvent affected as no clear relationship can be seen in the optical bandgap or the mobility. This stands in contrast to studies that have shown that the solvent and deposition conditions have a large effect on the mobilities of P3HT films [71]. It would appear that the template wetting process on its own is responsible for the minor increases in E_g and mobility in P3HT. This is likely due to the semi-crystalline nature of P3HT.

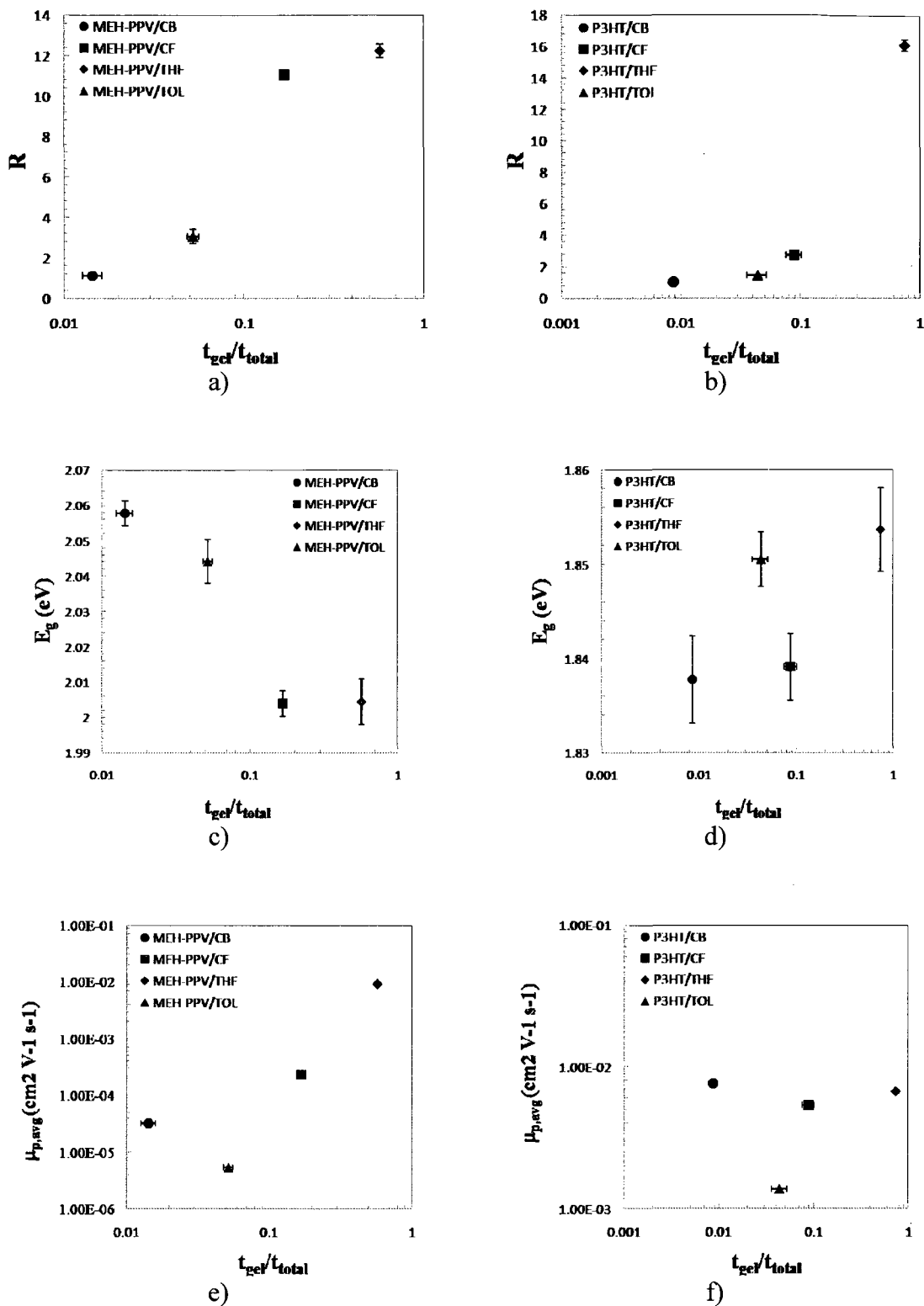


Figure 7.7. Gel drying fraction (t_{gel}/t_{total}) for MEH-PPV and P3HT polymer solutions compared with the a-b) dichroic ratio, c-d) optical bandgap (E_g), and e-f) hole mobility (μ_p) [146].

The gel drying time fraction analysis indicates that organization of conjugated polymers at the nanoscale can be increased by extending the gel drying time. This allows the polymer chains to exist in the slowly drying gel state and self-organize over an extended period of time. This viscous quasi-liquid gel state promotes the formation of aggregates on the surface of the pore wall, but in a regular direction. This effect is similar to that seen in thick films of P3HT where the slower evaporation of the film area below the surface leads to a more ordered structure [70, 185]. These results could also redirect the question of solvent choice as THF had the greatest impact on the structure of the polymer nanotubules, but is a known θ solvent that yields poorly extended chain conformations [187, 193]. Therefore, the solvent annealing effect could depend on both the conformation of the chain in solution and the ability to self-align in the gel phase. The effect is most apparent in the more amorphous MEH-PPV but can also be seen to have a minor effect on the structure of semi-crystalline P3HT.

Conclusion

Solution based template wetting has been shown to be an effective fabrication method for the production of nanotubular structure from MEH-PPV and P3HT. Solvent induced effects have been shown to have effects on effective conjugation length and orientation of conjugated polymers within a nanoporous template.

Semi-crystalline P3HT exhibited little or no change in properties due to solvent interaction and only a slight increase in optical bandgap. P3HT did show a large shift in the absorbance peak and the creation of absorbance bands that were not present in the drop cast thin film. This enhancement was seen across all solvent types and is most likely due to curvature induced order than the solvent choice.

Amorphous MEH-PPV was shown to be considerably different depending on the solvent choice with non-aromatic solvents inducing larger effects than aromatic solvents. Hole mobilities in MEH-PPV cast from THF were shown to be four orders of magnitude higher than in thin film devices [166, 167]. As shown here, solvent choice is an effective way to alter the properties of MEH-PPV in the nanopore.

The orientation of the conjugated polymers in the nanotube had an effect on the optical and electronic properties. For MEH-PPV, alignment in the pore was determined to be solvent dependent and had an obvious effect on the molecular order as it produced higher mobilities and low energy absorbance peaks that were not seen in non-aligned samples. Alignment in P3HT may have had an effect on the effective conjugation length as determined by mobility and optical measurements, but this enhancement was too small to be certain. Also, the choice of conjugated polymer will also determine the orientation relative to the pore wall as the side chains of the polymer are thought to have the more effect on the orientation. The regioregular P3HT only shows alignment in solvents that interact with the side chains causing a parallel orientation. A similar effect is seen in MEH-PPV where perpendicular alignment is mostly due to the shear forces on the side chains turning the polymer into the perpendicular orientation.

The relative affinity of the solvent to the polymer measured by the gel drying fraction was shown to increase solvent annealing effects by increasing the time the polymer was in gel so that self-orientation could take place over a longer time. The THF samples of both conjugated polymers exhibited that highest gel time relative to the total drying time. This is of interest as THF is generally considered to be a θ solvent and not ideal for the creation of ordered films [187, 193]. Though the THF may induce

conformational defects in the solvent phase, the gel drying time is thought to anneal any such defects in this study and allow for self-organization into a more ordered structure.

CHAPTER 8

CONCLUSION

Template wetting nanofabrication has been demonstrated as a simple, solution-based means of producing polymer nanotubes using nanoporous metal oxides and the conjugated polymers MEH-PPV and P3HT. The nanotubes were tested for optical and solvent drying characteristics in order to determine the structure within the nanoporous template. Enhancement of chain organization and alignment were found in both polymers to different degrees.

The nanotubes were studied via optical absorption which gave insight into the order of the polymer structure as well as the effective conjugation length. In general, all devices were found to have an optical bandgap lower than that of thin films. The P3HT E_g was found to be ~ 0.05 eV lower for all samples while the MEH-PPV E_g was redshifted ~ 0.08 eV. Hole mobilities in the MEH-PPV nanotubes improved when compared to thin films of that material, suggesting that confinement and curvature-induced molecular ordering of the polymer molecules may be present within the nanoscale pores. P3HT showed no significant improvement in hole mobility (when compared to the films) indicating that this polymer remains ordered in a single fashion in both the nanopore and in thin films. Nanotubes formed from a blend of MEH-PPV and P3HT showed properties intermediate to that of the individual polymers. The blend was highly influence by the P3HT as it could be modeled as 80% P3HT and 20% MEH-PPV

which is indicative of the higher absorption of the P3HT in the blend. FTIR analysis provided evidence that no chemical or electrical interactions occur between the two polymers when blended due to a high degree of phase separation as the IR spectrum closely resembled that of an average of the two constituents.

Further analysis in the optical and physical properties of P3HT found that this polythiophene derivative has an increased effective conjugation length and long range order as determined by the narrowing and redshift (~ 0.21 eV) of absorption bands in nanotubes relative to thin films. This is further confirmed by the presence of a low energy absorption peak not seen in thin film devices at 1.97 eV. Polarized FTIR experiments yielded a dichroic ratio of 2.75 indicating a moderate preferential alignment of the polymer backbone parallel with nanotube axis. Significant improvement in mobilities was not found as values observed for regioregular P3HT nanotubes were consistently of the order of published values observed in field effect transistors [7, 10, 175]. Differences in behavior observed between the two different nanotube diameters were not considered significant enough to make a clear determination as to structural changes between the two sizes.

Purification of bulk P3HT material via Soxhlet extraction yielded significant quantities of material for each of a low molecular weight DC and higher molecular weight THF fractions. Small differences in the UV-Vis spectra were observed in thin films cast from these fractions attributable to differences in the effective conjugation length due to the differing molecular weights of the fractions. Extracted P3HT was used to create polymer nanotubes that exhibited a bathochromic shift in the absorption bands relative to thin films. This indicates a further increase in the degree of molecular order

and effective conjugation length due to the physical configuration of the material. This shift was seen the most in the THF fraction which had a ~ 0.04 - 0.05 eV redshift. The DC fraction only exhibited a small, but resolvable, shift of ~ 0.02 eV. This would indicate that the increase in ordering found in higher molecular weights may not be applicable to lower molecular weights. Peaks in the nanotubule samples were not seen in thin films for the THF fractions provides further evidence of a change in the electronic structure of the material in this configuration. The DC fraction had low energy absorption peak at ~ 2.04 eV which is virtually identical to that of the thin films and further shows that the extent of ordering may be limited in lower molecular weights.

Solvent induced effects showed little effect on effective conjugation length and orientation of conjugated polymers within a nanoporous template between samples of semi-crystalline P3HT. Amorphous MEH-PPV showed large solvent effects in hole mobilities ranging from 10^{-6} $\text{cm}^2\text{V}^{-1}\text{s}^{-1}$ for samples made from toluene to 10^{-2} $\text{cm}^2\text{V}^{-1}\text{s}^{-1}$ for samples cast from Tetrahydrofuran. The effective conjugation length was also affected with the non-aromatic solvents exhibited a lower optical bandgap as well as a lower energy absorption peak at ~ 2.12 eV than the aromatic solvents. Enhanced ordering in MEH-PPV nanotubules was only seen in the lowest energy as peak location as it did not change appreciably and remained at ~ 2.21 eV.

Orientation of the conjugated polymers in the nanotube has an effect on the optical and electronic properties of MEH-PPV and P3HT to varying degrees. MEH-PPV alignment in the pore was determined to be solvent dependent and had an obvious effect on the molecular order producing higher mobilities and low energy absorbance peaks not seen in non-aligned samples. The aligned samples were cast from the non-aromatic

solvents indicating that solvent choice may play a large role in the orientation of the amorphous MEH-PPV. Alignment in P3HT had an effect on the effective conjugation length as determined by mobility and optical measurements, but this enhancement was smaller than MEH-PPV (~ 0.05 vs. ~ 0.08 eV). P3HT only showed alignment in the parallel orientation while MEH-PPV was found to have mostly perpendicular alignment which may be attributed to the side chains of the conjugated polymers.

The gel drying time was shown to increase solvent annealing effects by increasing the time the polymer have available to self-orient. THF samples of both polymers exhibited a gel drying fraction that ranged from 3 to 85 times longer than that of other solvents. The THF gel drying fraction, coupled with the improvements in mobility, optical bandgap, and dichroic ratio, indicate that the THF samples experience a longer solvent annealing time.

Enhancements seen in all nanotubes seemed to take place up to a certain level for both polymers suggesting that an upper limit to attainable device improvement may exist. However, this work makes it clear that template wetting nanofabrication can improve order and effective conjugation length on semiconducting conjugated polymers. Further improvements in amorphous polymers may be attained by the careful solvent selection and evaporation control. Semi-crystalline polymers may be minorly enhanced by solvent choice and orientation but these benefits do not seem to affect the electrical or optical characteristics.

Future Work

Future work on the topic should include a more in-depth study of the photoluminescent behavior of these polymers. Better understanding of the photo and

electroluminescence would provide a greater insight into effective conjugation lengths and band energies for nanostructured materials. Molecular modeling of the effects of solvation and evaporation would provide further insight into the true physical phenomena responsible for the observations made in this work. Further, the use of experimental techniques including X-ray diffraction, dynamic light scattering, thermal degradation, and polarized light UV-Vis could be used to gain a more thorough knowledge of the complete structure of these polymers when incorporated into the nanostructure.

It is known that increasing the effective conjugation length in optoelectric polymers will decrease the quantum efficiency of the luminescence. By increasing the order of the polymers in this study, their usefulness for organic, light emitting diodes (OLEDs) has been reduced. Therefore, a particularly interesting study may be to attempt to increase the disorder of conjugated polymer nanotubules formed via template wetting. One route to accomplish this may be to expose the nanotubes to the vapors of bad solvents to induce coiling or to cast them at temperatures near the boiling point of the solvent to induce solvent quenching.

REFERENCES

- [1] C. K. Chiang, C. R. Fincher, Y. W. Park, A. J. Heeger, H. Shirakawa, E. J. Louis, S. C. Gau, and A. G. MacDiarmid, "Electrical Conductivity in Doped Polyacetylene," *Physical Review Letters*, vol. 39, p. 1098, 1977.
- [2] C. K. Chiang, M. A. Druy, S. C. Gau, A. J. Heeger, E. J. Louis, A. G. MacDiarmid, Y. W. Park, and H. Shirakawa, "Synthesis of highly conducting films of derivatives of polyacetylene, (CH)_x," *J. Am. Chem. Soc.*, vol. 100, pp. 1013-1015, 1978.
- [3] A. G. MacDiarmid and A. J. Heeger, "Organic Metals and Semiconductors: The Chemistry of Polyacetylene, CH_x, and its derivatives," *Synthetic Metals*, vol. 1, pp. 101-118, 1979.
- [4] W. Barford, *Electronic and Optical Properties of Conjugated Polymers*. Oxford, England: Oxford University Press, 2005.
- [5] A. Tsumura, H. Koezuka, and T. Ando, "Macromolecular electronic device: Field-effect transistor with a polythiophene thin film," *Applied Physics Letters*, vol. 49, pp. 1210-1212, 1986.
- [6] H. E. Katz and A. J. Lovinger, "A soluble and air-stable organic semiconductor with high electron mobility," *Nature*, vol. 404, p. 478, 2000.
- [7] C. D. Dimitrakopoulos and D. J. Mascaro, "Organic thin-film transistors: A review of recent advances," *IBM Journal of Research and Development*, vol. 45, pp. 11-27, 2001.
- [8] X. Wu, T.-A. Chen, and R. D. Rieke, "Synthesis of regioregular head-to-tail poly[3-(alkylthio)thiophenes]. A highly electroconductive polymer," *Macromolecules*, vol. 28, p. 2101, 1995.
- [9] M. Trznadel, A. Pron, M. Zagorska, R. Chrzaszcz, and J. Pielichowski, "Effect of molecular weight on spectroscopic and spectroelectrochemical properties of regioregular poly(3-hexylthiophene)," *Macromolecules*, vol. 31, pp. 5051-5058, 1998.

- [10] H. Sirringhaus, P. J. Brown, R. H. Friend, M. M. Nielsen, K. Bechgaard, B. M. W. Langeveld-Voss, A. J. H. Spiering, R. A. J. Janssen, E. W. Meijer, P. Herwig, and D. M. de Leeuw, "Two-dimensional charge transport in self-organized, high-mobility conjugated polymers," *Nature*, vol. 401, pp. 685-688, 1999.
- [11] J. H. Burroughes, D. D. C. Bradley, A. R. Brown, R. N. Marks, K. Mackay, R. H. Friend, P. L. Burns, and A. B. Holmes, "Light-emitting diodes based on conjugated polymers," *Nature*, vol. 347, pp. 539-541, 1990.
- [12] D. Braun and A. J. Heeger, "Visible light emission from semiconducting polymer diodes," *Applied Physics Letters*, vol. 58, pp. 1982-1984, 1991.
- [13] G. Yu and C. Zhang, "Dual-function semiconducting polymer devices: Light-emitting and photodetecting diodes," *Applied Physics Letters*, vol. 64, p. 1540, 1994.
- [14] R. N. Marks, J. J. M. Halls, D. D. C. Bradley, R. H. Friend, and A. B. Holmes, "Photovoltaic response in poly(p-phenylene vinylene) thin-film devices," *Journal of Physics Condensed Matter*, vol. 6, pp. 1379-1394, 1994.
- [15] M. Granstrom, K. Petritsch, A. C. Arias, A. Lux, M. R. Andersson, and R. H. Friend, "Laminated fabrication of polymeric photovoltaic diodes," *Nature*, vol. 395, pp. 257-260, 1998.
- [16] A. Assadi, C. Svensson, M. Willander, and O. Inganäs, "Field-effect mobility of poly(3-hexylthiophene)," *Applied Physics Letters*, vol. 53, pp. 195-197, 1988.
- [17] Z. Bao, Y. Feng, A. Dodabalapur, and V. R. Raju, "High-Performance Plastic Transistors Fabricated by Printing Techniques," *Chemistry of Materials*, vol. 9, p. 1299, 1997.
- [18] H. Sirringhaus, T. Kawase, R. H. Friend, T. Shimoda, M. Inbasekaran, W. Wu, and E. P. Woo, "High-resolution inkjet printing of all-polymer transistor circuits," *Science*, vol. 290, pp. 2123-2126, 2000.
- [19] D. Li, A. Babel, S. A. Jenekhe, and Y. Xia, "Nanofibers of conjugated polymers prepared by electrospinning with a two-capillary spinneret," *Advanced Materials*, vol. 16, pp. 2062-2066, 2004.
- [20] S. R. Forrest, "The path to ubiquitous and low-cost organic electronic appliances on plastic," *Nature*, vol. 428, pp. 911-918, 2004.
- [21] J. M. Shaw and P. F. Seidler, "Organic electronics: Introduction," *IBM Journal of Research and Development*, vol. 45, pp. 3-8, 2001.
- [22] R. J. Visser, "Application of polymer light-emitting materials in light-emitting diodes, backlights and displays," *Philips Journal of Research*, vol. 51, pp. 467-477, 1998.

- [23] J. C. Scott, J. H. Kaufman, J. Salem, J. A. Goitia, P. J. Brock, and R. Dipietro, "MEH-PPV light-emitting diodes: Mechanisms of failure," *Molecular Crystals and Liquid Crystals Science and Technology Section A: Molecular Crystals and Liquid Crystals*, vol. 283, pp. 57-62, 1996.
- [24] N. Oyama, T. Tatsuma, T. Sato, and T. Sotomura, "Dimercaptan-polyaniline composite electrodes for lithium batteries with high energy density," *Nature*, vol. 373, pp. 598-600, 1995.
- [25] W. E. Howard and O. F. Prache, "Microdisplays based upon organic light-emitting diodes," *IBM Journal of Research and Development*, vol. 45, pp. 115-127, 2001.
- [26] U. Mitschke and P. Bäuerle, "The electroluminescence of organic materials," *Journal of Materials Chemistry*, vol. 10, pp. 1471-1507, 2000.
- [27] K. M. Coakley and M. D. McGehee, "Conjugated Polymer Photovoltaic Cells," *Chemistry of Materials*, vol. 16, pp. 4533-4542, 2004.
- [28] N. Karl, "Introduction," in *Organic Electronic Materials: Conjugated Polymers and Low Molecular Weight Organic Solids*, R. Farchioni and G. Grosso, Eds. Berlin: Springer-Verlag, 2001, pp. 215-239.
- [29] R. H. Friend, R. W. Gymer, A. B. Holmes, J. H. Burroughes, R. N. Marks, C. Taliani, D. D. C. Bradley, D. A. Dos Santos, J. L. Bredas, M. Logdlund, and W. R. Salaneck, "Electroluminescence in conjugated polymers," *Nature*, vol. 397, pp. 121-128, 1999.
- [30] M. Steinhart, J. H. Wendorff, A. Greiner, R. B. Wehrspohn, K. Nielsch, J. Schilling, J. Choi, and U. Gosele, "Polymer nanotubes by wetting of ordered porous templates," *Science*, vol. 296, p. 1997, 2002.
- [31] J. H. Schon, S. Berg, C. Kloc, and B. Batlogg, "Ambipolar Pentacene Field-Effect Transistors and Inverters," *Science*, vol. 287, p. 1022, 2000.
- [32] M. Jeffries-El and R. D. McCullough, "Regioregular Polythiophenes," in *Conjugated Polymers: Theory, Synthesis, Properties, and Characterization*, T. A. Skotheim and J. R. Reynolds, Eds. Boca Raton, FL: CRC Press, 2007.
- [33] H. Kuhn, "Free electron model for absorption spectra of organic dyes," *The Journal of Chemical Physics*, vol. 16, pp. 840-841, 1948.
- [34] H. Kuhn, "A quantum-mechanical theory of light absorption of organic dyes and similar compounds," *The Journal of Chemical Physics*, vol. 17, pp. 1198-1212, 1949.
- [35] G. Taubmann, "Calculation of the h \bar{A} ^{1/4}ckel parameter \hat{I}^2 from the free-electron model," *Journal of Chemical Education*, vol. 69, pp. 96-97, 1992.

- [36] J. S. de Melo and L. M. Silva, "Singlet and triplet energies of alpha-oligothiophenes: A spectroscopic, theoretical, and," *Journal of Chemical Physics*, vol. 111, p. 5427, 1999.
- [37] P. J. Brown, H. Sirringhaus, M. Harrison, M. Shkunov, and R. H. Friend, "Optical spectroscopy of field-induced charge in self-organized high mobility poly(3-hexylthiophene)," *Physical Review B*, vol. 63, p. 125204, 2001.
- [38] R. L. Christensen, A. Faksh, J. A. Meyers, I. D. W. Samuel, P. Wood, R. R. Schrock, and K. C. Hultsch, "Optical Spectroscopy of Long Polyenes," *The Journal of Physical Chemistry A*, vol. 108, pp. 8229-8236, 2004.
- [39] B. G. Sumpter, P. Kumar, A. Mehta, M. D. Barnes, W. A. Shelton, and R. J. Harrison, "Computational Study of the Structure, Dynamics, and Photophysical Properties of Conjugated Polymers and Oligomers under Nanoscale Confinement," *The Journal of Physical Chemistry B*, vol. 109, pp. 7671-7685, 2005.
- [40] E. A. Grulke, *Polymer Process Engineering*. Englewood Cliffs, New Jersey: Prentice Hall, 1994.
- [41] H. S. Nalwa, *Handbook of Advanced Electronic and Photonic Materials and Devices*, 2001.
- [42] R. E. Martin and F. Diederich, "Linear monodisperse π -conjugated oligomers: Model compounds for polymers and more," *Angewandte Chemie - International Edition*, vol. 38, pp. 1350-1377, 1999.
- [43] D. A. V. Bout, W.-T. Yip, D. Hu, D.-K. Fu, T. M. Swager, and P. F. Barbara, "Discrete Intensity Jumps and Intramolecular Electronic Energy Transfer in the Spectroscopy of Single Conjugated Polymer Molecules," *Science*, vol. 277, pp. 1074-1077, August 22, 1997 1997.
- [44] Y.-S. Chen and H.-F. Meng, "Intrachain carrier transport in conjugated polymer with structural and chemical defects," *Physical Review B*, vol. 66, p. 035202, 2002.
- [45] J. Kim, "Assemblies of conjugated polymers. Intermolecular and intramolecular effects on the photophysical properties of conjugated polymers," *Pure and Applied Chemistry*, vol. 74, pp. 2031-2044, 2002.
- [46] J. L. Brédas, D. Beljonne, V. Coropceanu, and J. Cornil, "Charge-transfer and energy-transfer processes in π -conjugated oligomers and polymers: A molecular picture," *Chemical Reviews*, vol. 104, pp. 4971-5003, 2004.
- [47] G. D. Scholes and G. Rumbles, "Excitons in nanoscale systems," *Nature Materials*, vol. 5, pp. 683-696, 2006.

- [48] A. O. Patil, A. J. Heeger, and F. Wudl, "Optical properties of conducting polymers," *Chemical Reviews*, vol. 88, pp. 183-200, 1988.
- [49] J. Roncali, "Molecular Engineering of the Band Gap of pi-Conjugated Systems: Facing Technological Applications," *Macromolecular Rapid Communications*, vol. 28, pp. 1761-1775, 2007.
- [50] J. L. Bredas, "Relationship between band gap and bond length alternation in organic conjugated polymers," *Journal of Chemical Physics*, vol. 82, p. 3808, 1985.
- [51] Z. Bao, A. Dodabalapur, and A. J. Lovinger, "Soluble and processable regioregular poly(3-hexylthiophene) for thin film field-effect transistor applications with high mobility," *Applied Physics Letters*, vol. 69, p. 4108, 1996.
- [52] A. R. West, *Basic Solid State Chemistry*, 2 ed. Chichester, England: John Wiley & Sons, LTD, 1999.
- [53] C. K. Chiang, M. A. Druy, S. C. Gau, A. J. Heeger, E. J. Louis, A. G. MacDiarmid, Y. W. Park, and H. Shirakawa, "Synthesis of highly conducting films of derivatives of polyacetylene, (CH)_x," *Journal of the American Chemical Society*, vol. 100, pp. 1013-1015, 1978.
- [54] H. Shirakawa, E. J. Louis, A. G. MacDiarmid, C. K. Chiang, and A. J. Heeger, "Synthesis of electrically conducting organic polymers: Halogen derivatives of polyacetylene, (CH)_x," *Journal of the Chemical Society, Chemical Communications*, pp. 578-580, 1977.
- [55] A. B. Holmes, D. D. C. Bradley, A. R. Brown, P. L. Burn, J. H. Burroughes, R. H. Friend, N. C. Greenham, R. W. Gymer, D. A. Halliday, R. W. Jackson, A. Kraft, J. H. F. Martens, K. Pichler, and I. D. W. Samuel, "Photoluminescence and electroluminescence in conjugated polymeric systems," *Synthetic Metals*, vol. 57, pp. 4031-4040, 1993.
- [56] B. Xu and S. Holdcroft, "Molecular control of luminescence from poly(3-hexylthiophenes)," *Macromolecules*, vol. 26, pp. 4457-4460, 1993.
- [57] W. J. Feast and R. H. Friend, "Synthesis and material and electronic properties of conjugated polymers," *Journal of Materials Science*, vol. 25, pp. 3796-3805, 1990.
- [58] M. D. McGehee and A. J. Heeger, "Semiconducting (Conjugated) Polymers as Materials for Solid-State Lasers," *Advanced Materials*, vol. 12, pp. 1655-1668, 2000.

- [59] J. Cornil, D. Beljonne, J. P. Calbert, and J. L. Brédas, "Interchain Interactions in Organic π -Conjugated Materials: Impact on Electronic Structure, Optical Response, and Charge Transport," *Advanced Materials*, vol. 13, pp. 1053-1067, 2001.
- [60] F. W. Billmeyer, *Textbook of Polymer Science*, 3 ed. New York: John Wiley & Sons, 1984.
- [61] R. Traiphol, N. Charoenthai, T. Sriksirin, T. Kerdcharoen, T. Osotchan, and T. Maturos, "Chain organization and photophysics of conjugated polymer in poor solvents: Aggregates, agglomerates and collapsed coils," *Polymer*, vol. 48, pp. 813-826, 2007.
- [62] S. A. Arnautov, E. M. Nechvolodova, A. A. Bakulin, S. G. Elizarov, A. N. Khodarev, D. S. Martyanov, and D. Y. Paraschuk, "Properties of MEH-PPV films prepared by slow solvent evaporation," *Synthetic Metals*, vol. 147, pp. 287-291, 2004.
- [63] R. Traiphol, P. Sanguansat, T. Sriksirin, T. Kerdcharoen, and T. Osotchan, "Spectroscopic Study of Photophysical Change in Collapsed Coils of Conjugated Polymers: Effects of Solvent and Temperature," *Macromolecules*, vol. 39, pp. 1165-1172, 2006.
- [64] C. R. C. B. Moreira, D. S. Machado, R. M. Souto-Maior, J. B. Filho, and M. C. dos Santos, "Solvatochromism on regiochemically substituted poly(Hexylthiophenes)," *Synthetic Metals*, vol. 84, pp. 811-812, 1997.
- [65] S. R. Amrutha and M. Jayakannan, "Probing the π -Stacking Induced Molecular Aggregation in π -Conjugated Polymers, Oligomers, and Their Blends of p-Phenylenevinylenes," *The Journal of Physical Chemistry B*, vol. 112, pp. 1119-1129, 2008.
- [66] T. Q. Nguyen, V. Doan, and B. J. Schwartz, "Conjugated polymer aggregates in solution: Control of interchain interactions," *Journal of Chemical Physics*, vol. 110, pp. 4068-4078, 1999.
- [67] J. Liu, Y. Shi, and Y. Yang, "Solvation-Induced Morphology Effects on the Performance of Polymer-Based Photovoltaic Devices," *Advanced Functional Materials*, vol. 11, pp. 420-424, 2001.
- [68] B. J. Schwartz, "CONJUGATED POLYMERS AS MOLECULAR MATERIALS: How Chain Conformation and Film Morphology Influence Energy Transfer and Interchain Interactions," *Annual Review of Physical Chemistry*, vol. 54, pp. 141-172, 2003.
- [69] S. Lee, J. Y. Lee, and H. Lee, "Solvent effects on the characteristics of conductive and luminescent polymers," *Synthetic Metals*, vol. 101, pp. 248-249, 1999.

- [70] G. Wang, J. Swensen, D. Moses, and A. J. Heeger, "Increased mobility from regioregular poly(3-hexylthiophene) field-effect transistors," *Journal of Applied Physics*, vol. 93, p. 6137, 2003.
- [71] J.-F. Chang, J. Clark, N. Zhao, H. Sirringhaus, D. W. Breiby, J. W. Andreasen, M. M. Nielsen, M. Giles, M. Heeney, and I. McCulloch, "Molecular-weight dependence of interchain polaron delocalization and exciton bandwidth in high-mobility conjugated polymers," *Physical Review B*, vol. 74, p. 115318, 2006.
- [72] R. J. Kline, M. D. McGehee, E. N. Kadnikova, J. Liu, J. M. J. Frechet, and M. F. Toney, "Dependence of Regioregular Poly(3-hexylthiophene) Film Morphology and Field-Effect Mobility on Molecular Weight," *Macromolecules*, vol. 38, pp. 3312-3319, 2005.
- [73] P. Kumar, A. Mehta, S. M. Mahurin, S. Dai, M. D. Dadmun, B. G. Sumpter, and M. D. Barnes, "Formation of Oriented Nanostructures from Single Molecules of Conjugated Polymers in Microdroplets of Solution: The Role of Solvent," *Macromolecules*, vol. 37, pp. 6132-6140, 2004.
- [74] K. Do Hwan, P. Yeong Don, J. Yunseok, K. Sungsoo, and C. Kilwon, "Solvent Vapor-Induced Nanowire Formation in Poly(3-hexylthiophene) Thin Films," *Macromolecular Rapid Communications*, vol. 26, pp. 834-839, 2005.
- [75] S. Iijima, "Helical microtubules of graphitic carbon," *Nature*, vol. 354, p. 56, 1991.
- [76] R. H. Baughman, A. A. Zakhidov, and W. A. de Heer, "Carbon Nanotubes--the Route Toward Applications," *Science*, vol. 297, p. 787, 2002.
- [77] M. Steinhart, J. H. Wendorff, and R. B. Wehrspohn, "Nanotubes à la Carte: Wetting of Porous Templates," *ChemPhysChem*, vol. 4, pp. 1171-1176, 2003.
- [78] M. Steinhart, R. B. Wehrspohn, U. Gosele, and J. H. Wendorff, "Nanotubes by template wetting: A modular assembly system," *Angewandte Chemie - International Edition*, vol. 43, pp. 1334 - 1344, 2004.
- [79] O. G. Schmidt and K. Eberl, "Thin solid films roll up into nanotubes," *Nature*, vol. 410, p. 168, 2001.
- [80] G. M. Whitesides, J. P. Mathias, and C. T. Seto, "Molecular self-assembly and nanochemistry: A chemical strategy for the synthesis of nanostructures," *Science*, vol. 254, pp. 1312-1319, 1991.
- [81] D. H. Reneker and I. Chun, "Nanometre diameter fibres of polymer, produced by electrospinning," *Nanotechnology*, vol. 7, pp. 216-223, 1996.
- [82] C. R. Martin, "Nanomaterials: a membrane-based synthetic approach," *Science*, vol. 266, pp. 1961-1966, 1994.

- [83] A. Formhals, "Process and Apparatus for Preparing Artificial Threads," U. S. P. Office, Ed. Germany: Sreiber-Gastell, R., 1934.
- [84] S. Megelski, J. S. Stephens, D. B. Chase, and J. F. Rabolt, "Micro- and Nanostructured Surface Morphology on Electrospun Polymer Fibers," *Macromolecules*, vol. 35, pp. 8456-8466, 2002.
- [85] H. Hou, Z. Jun, A. Reuning, A. Schaper, J. H. Wendorff, and A. Greiner, "Poly(p-xylylene) Nanotubes by Coating and Removal of Ultrathin Polymer Template Fibers," *Macromolecules*, vol. 35, pp. 2429-2431, 2002.
- [86] A. Babel, D. Li, Y. Xia, and S. A. Jenekhe, "Electrospun nanofibers of blends of conjugated polymers: Morphology, optical properties, and field-effect transistors," *Macromolecules*, vol. 38, pp. 4705-4711, 2005.
- [87] A. Greiner and J. H. Wendorff, "Electrospinning: A fascinating method for the preparation of ultrathin fibers," *Angewandte Chemie - International Edition*, vol. 46, pp. 5670-5703, 2007.
- [88] A. Babel and S. A. Jenekhe, "Morphology and field-effect mobility of charge carriers in binary blends of poly(3-hexylthiophene) with poly[2-methoxy-5-(2-ethylhexoxy)-1,4-phenylenevinylene] and polystyrene," *Macromolecules*, vol. 37, pp. 9835-9840, 2004.
- [89] C. R. Martin, "Membrane-Based Synthesis of Nanomaterials," *Chem. Mater.*, vol. 8, pp. 1739-1746, 1996.
- [90] C. J. Brumlik and C. R. Martin, "Template synthesis of metal microtubules," *J. Am. Chem. Soc.*, vol. 113, pp. 3174-3175, 1991.
- [91] C. A. Foss, G. L. Hornyak, J. A. Stockert, and C. R. Martin, "Template-Synthesized Nanoscopic Gold Particles: Optical Spectra and the Effects of Particle Size and Shape," *J. Phys. Chem.*, vol. 98, pp. 2963-2971, 1994.
- [92] J. D. Klein, R. D. Herrick, D. Palmer, M. J. Sailor, C. J. Brumlik, and C. R. Martin, "Electrochemical fabrication of cadmium chalcogenide microdiode arrays," *Chem. Mater.*, vol. 5, pp. 902-904, 1993.
- [93] Z. Cai and C. R. Martin, "Electronically conductive polymer fibers with mesoscopic diameters show enhanced electronic conductivities," *J. Am. Chem. Soc.*, vol. 111, pp. 4138-4139, 1989.
- [94] W. Liang and C. R. Martin, "Template-synthesized polyacetylene fibrils show enhanced supermolecular order," *J. Am. Chem. Soc.*, vol. 112, pp. 9666-9668, 1990.
- [95] C. R. Martin, L. S. Van Dyke, Z. Cai, and W. Liang, "Template synthesis of organic microtubules," *J. Am. Chem. Soc.*, vol. 112, pp. 8976-8977, 1990.

- [96] S. Demoustier-Champagne, J. Duchet, and R. Legras, "Chemical and electrochemical synthesis of polypyrrole nanotubules," *Synthetic Metals*, vol. 101, pp. 20-21, 1999.
- [97] R. V. Parthasarathy and C. R. Martin, "Template-Synthesized Polyaniline Microtubules," *Chem. Mater.*, vol. 6, pp. 1627-1632, 1994.
- [98] Z. Cai, J. Lei, W. Liang, V. Menon, and C. R. Martin, "Molecular and supermolecular origins of enhanced electric conductivity in template-synthesized polyheterocyclic fibrils. 1. Supermolecular effects," *Chem. Mater.*, vol. 3, pp. 960-967, 1991.
- [99] L. Dauginet-De Pra and S. Demoustier-Champagne, "Investigation of the electronic structure and spectroelectrochemical properties of conductive polymer nanotube arrays," *Polymer*, vol. 46, pp. 1583-1594, 2005.
- [100] J. Joo, B. H. Kim, D. H. Park, H. S. Kim, D. S. Seo, J. H. Shim, S. J. Lee, K. S. Ryu, K. Kim, J. I. Jin, T. J. Lee, and C. J. Lee, "Fabrication and applications of conducting polymer nanotube, nanowire, nanohole, and double wall nanotube," *Synthetic Metals*, vol. 153, pp. 313-316, 2005.
- [101] J. L. Duvail, P. Retho, V. Fernandez, G. Louarn, P. Molinie, and O. Chauvet, "Effects of the Confined Synthesis on Conjugated Polymer Transport Properties," *J. Phys. Chem. B*, vol. 108, pp. 18552-18556, 2004.
- [102] D. H. Park, B. H. Kim, M. K. Jang, K. Y. Bae, S. J. Lee, and J. Joo, "Synthesis and characterization of polythiophene and poly (3-methylthiophene) nanotubes and nanowires," *Synthetic Metals*, vol. 153, pp. 341-344, 2005.
- [103] C. Barrett, D. Iacopino, D. O'Carroll, G. De Marzi, D. A. Tanner, A. J. Quinn, and G. Redmond, "Synthesis of Pentacene Nanotubes by Melt-Assisted Template Wetting," *Chemistry of Materials*, vol. 19, pp. 338-340, 2007.
- [104] T. P. Nguyen, S. H. Yang, P. Le Rendu, and H. Khan, "Optical properties of poly(2-methoxy-5-(2-ethyl-hexyloxy)-phenylene vinylene) deposited on porous alumina substrates," *Composites Part A: Applied Science and Manufacturing*, vol. 36, pp. 515-519, 2005.
- [105] J. Cannon, S. D. Bearden Jr, S. Selmic, and S. A. Gold, "Semiconducting polythiophene nanotubes by template wetting nanofabrication," in *AICHE Annual Meeting, Conference Proceedings*, 2008.
- [106] S. Moynihan, D. Iacopino, D. O'Carroll, P. Lovera, and G. Redmond, "Template Synthesis of Highly Oriented Polyfluorene Nanotube Arrays," *Chemistry of Materials*, vol. 20, pp. 996-1003, 2008.

- [107] J. P. Cannon, S. D. Bearden, F. M. Khatkhatay, J. Cook, S. Z. Selmic, and S. A. Gold, "Confinement-induced enhancement of hole mobility in MEH-PPV," *Synthetic Metals*, vol. 159, pp. 1786-1791, 2009.
- [108] J. P. Cannon, S. D. Bearden, and S. A. Gold, "Characterization of Conjugated Polymer/Anodic Aluminum Oxide Nanocomposites Fabricated Via Template Wetting," *Composites Part A: Applied Science and Manufacturing*, vol. In Press, Accepted Manuscript.
- [109] M. Steinhart, S. Murano, A. K. Schaper, T. Ogawa, M. Tsuji, U. Gosele, C. Weder, and J. H. Wendorff, "Morphology of polymer/liquid-crystal nanotubes: Influence of confinement," *Advanced Functional Materials*, vol. 15, pp. 1656-1664, 2005.
- [110] M. Steinhart, S. Senz, R. B. Wehrspohn, U. Gosele, and J. H. Wendorff, "Curvature-Directed Crystallization of Poly(vinylidene difluoride) in Nanotube Walls," *Macromolecules*, vol. 36, pp. 3646-3651, 2003.
- [111] S. Schlitt, A. Greiner, and J. H. Wendorff, "Cylindrical Polymer Nanostructures by Solution Template Wetting," *Macromolecules*, vol. 41, pp. 3228-3234, 2008.
- [112] G. A. O'Brien, A. J. Quinn, D. A. Tanner, and G. Redmond, "A single polymer nanowire photodetector," *Advanced Materials*, vol. 18, pp. 2379-2383, 2006.
- [113] J. Cannon, S. Selmic, and S. Gold, "Optoelectronic Polymer Nanowires by Templating Process," in *AICHE Annual Meeting*, San Francisco, CA, 2006.
- [114] S. Hotta, S. D. D. V. Rughooputh, A. J. Heeger, and F. Wudl, "Spectroscopic studies of soluble poly(3-alkylthienylenes)," *Macromolecules*, vol. 20, pp. 212-215, 1987.
- [115] Y. Furukawa, A. Sakamoto, and M. Tasumi, "Raman and infrared studies on the molecular structures of poly(1,4-phenylenevinylene) and poly(2,5-thienylenevinylene)," *The Journal of Physical Chemistry*, vol. 93, pp. 5354-5356, 1989.
- [116] S. Shi and F. Wudl, "Synthesis and characterization of a water-soluble poly(p-phenylenevinylene) derivative," *Macromolecules*, vol. 23, pp. 2119-2124, 1990.
- [117] J. Paloheimo, H. Stubb, P. Yli-Lahti, and P. Kuivalainen, "Field-effect conduction in polyalkylthiophenes," *Synthetic Metals*, vol. 41, pp. 563-566, 1991.
- [118] D. Chirvase, Z. Chiguvare, M. Knipper, J. Parisi, V. Dyakonov, and J. C. Hummelen, "Electrical and optical design and characterisation of regioregular poly(3-hexylthiophene-2,5diyl)/fullerene-based heterojunction polymer solar cells," *Synthetic Metals*, vol. 138, pp. 299-304, 2003.

- [119] A. W. Adamson and A. P. Gast, *Physical Chemistry of Surfaces*, Sixth ed. New York: Wiley-Interscience, 1997.
- [120] K. Grundke, "Wetting, Spreading and Penetration," in *Handbook of Applied Surface and Colloid Chemistry*. vol. 2, K. Holmberg, Ed.: John Wiley & Sons, Ltd, 2002, pp. 119-142.
- [121] G. Callegari, A. Calvo, J. P. Hulin, and F. Brochard-Wyart, "Dewetting versus Rayleigh Instability inside Capillaries," *Langmuir*, vol. 18, pp. 4795-4798, 2002.
- [122] M. Steinhart, R. B. Wehrspohn, U. Gosele, and J. H. Wendorff, "Nanotubes by template wetting: A modular assembly system," *Angewandte Chemie - International Edition*, vol. 43, pp. 1334-1344, 2004.
- [123] X. Feng and Z. Jin, "Spontaneous formation of nanoscale polymer spheres, capsules, or rods by evaporation of polymer solutions in cylindrical alumina nanopores," *Macromolecules*, vol. 42, pp. 569-572, 2009.
- [124] D. K. Chambers, B. Raut, D. Qi, C. B. O'Neal, and S. Z. Selmic, "The effect of helium plasma etching on polymer-based optoelectronic devices," *Thin Solid Films*, vol. 517, pp. 5743-5746, 2009.
- [125] J. McMurry, *Organic Chemistry*. Pacific Grove: Brooks/Cole, 1999.
- [126] R. B. Woodward, "Structure and absorption spectra. III. Normal conjugated dienes," *Journal of the American Chemical Society*, vol. 64, pp. 72-75, 1942.
- [127] L. F. Fieser, M. Fieser, and S. Rajagopalan, "ABSORPTION SPECTROSCOPY AND THE STRUCTURES OF THE DIOSTEROLS," *The Journal of Organic Chemistry*, vol. 13, pp. 800-806, 1948.
- [128] K. F. Wong, M. S. Skaf, C. Y. Yang, P. J. Rossky, B. Bagchi, D. Hu, J. Yu, and P. F. Barbara, "Structural and electronic characterization of chemical and conformational defects in conjugated polymers," *Journal of Physical Chemistry B*, vol. 105, pp. 6103-6107, 2001.
- [129] R. J. Anderson, D. J. Bendell, and P. W. Groundwater, *Organic Spectroscopic Analysis*. Cambridge, UK: The Royal Society of Chemistry, 2004.
- [130] M. Nic, J. Jirat, and B. Kosata, "Compendium of Chemical Terminology," in *IUPAC*, 2.1.5 ed: Blackwell Science, 2008.
- [131] L. Breban, L. Lutsen, G. Vanhoyland, J. D'Haen, J. Manca, and D. Vanderzande, "Thermally induced order in PPV derivatives," *Thin Solid Films*, vol. 511-512, pp. 695-700, 2006.

- [132] T. Huser, M. Yan, and L. J. Rothberg, "Single chain spectroscopy of conformational dependence of conjugated polymer photophysics," *Proceedings of the National Academy of Sciences of the United States of America*, vol. 97, pp. 11187-11191, 2000.
- [133] P. J. Brown, D. S. Thomas, A. Köhler, J. S. Wilson, J. S. Kim, C. M. Ramsdale, H. Sirringhaus, and R. H. Friend, "Effect of interchain interactions on the absorption and emission of poly(3-hexylthiophene)," *Physical Review B - Condensed Matter and Materials Physics*, vol. 67, pp. 642031-6420316, 2003.
- [134] B. Smith, *Fundamentals of Fourier Transform Infrared Spectroscopy*. Boca Raton, FL: CRC Press, 1996.
- [135] B. H. Stuart, *Infrared Spectroscopy: Fundamentals and Applications*. Chichester, West Sussex: John Wiley & Sons Ltd., 2004.
- [136] J. L. Koenig, "Application of Infrared Spectroscopy to Polymers," in *Applied Infrared Spectroscopy*, D. Kendall, Ed. New York, NY: Reinhold Publishing Corporation, 1966.
- [137] P. J. Hendra and W. F. Maddams, "Fourier Transform Infrared and Raman Spectroscopies in the Study of Polymer Orientation," in *Polymer Spectroscopy*, A. H. Fawcett, Ed. Chichester, West Sussex: John Wiley & Sons, Ltd., 1996.
- [138] R. Zbinden, *Infrared Spectroscopy of High Polymers*. New York: Academic Press, 1964.
- [139] G. Li, Y. Yao, H. Yang, V. Shrotriya, G. Yang, and Y. Yang, "Solvent annealing" effect in polymer solar cells based on poly(3-hexylthiophene) and methanofullerenes," *Advanced Functional Materials*, vol. 17, pp. 1636-1644, 2007.
- [140] N. P. Cheremisinoff, *Product Design and Testing of Polymeric Materials*. New York, NY: Marcel Dekker, Inc., 1990.
- [141] I. D. Parker, "Carrier tunneling and device characteristics in polymer light-emitting diodes," *Journal of Applied Physics*, vol. 75, pp. 1656-1666, 1994.
- [142] I. H. Campbell, P. S. Davids, D. L. Smith, N. N. Barashkov, and J. P. Ferraris, "Schottky energy barrier dependence of charge injection in organic light-emitting diodes," *Applied Physics Letters*, vol. 72, pp. 1863-1865, 1998.
- [143] M. Onoda, K. Tada, A. A. Zakhidov, and K. Yoshino, "Photoinduced charge separation in photovoltaic cell with heterojunction of p- and n-type conjugated polymers," *Thin Solid Films*, vol. 331, pp. 76-81, 1998.

- [144] I. H. Campbell, T. W. Hagler, D. L. Smith, and J. P. Ferraris, "Direct measurement of conjugated polymer electronic excitation energies using metal/polymer/metal structures," *Physical Review Letters*, vol. 76, p. 1900, 1996.
- [145] Z. Chiguvaré, J. Parisi, and V. Dyakonov, "Current limiting mechanisms in indium-tin-oxide/poly(3-hexylthiophene)/aluminum thin film devices," *Journal of Applied Physics*, vol. 94, pp. 2440-2448, 2003.
- [146] J. P. Cannon, "CHASING μ ," in *College of Engineering and Science*. vol. Doctor of Philosophy Ruston, La: Louisiana Tech University, 2009.
- [147] A. G. MacDiarmid, "\"Synthetic metals\": A novel role for organic polymers (Nobel Lecture)," *Angewandte Chemie, International Edition*, vol. 40, pp. 2581-2590, 2001.
- [148] S. R. Forrest and M. E. Thompson, "Introduction: Organic Electronics and Optoelectronics," *Chemical Reviews (Washington, DC, United States)*, vol. 107, pp. 923-925, 2007.
- [149] J. M. Shaw and P. F. Seidler, "Organic electronics. Introduction," *IBM Journal of Research and Development*, vol. 45, pp. 3-9, 2001.
- [150] I. McCulloch, "Thin films: Rolling out organic electronics," *Nature Materials*, vol. 4, pp. 583-584, 2005.
- [151] A. J. Heeger, "Nobel lecture: semiconducting and metallic polymers: the fourth generation of polymeric materials," *Reviews of Modern Physics*, vol. 73, pp. 681-700, 2001.
- [152] J. R. Sheats, "Manufacturing and commercialization issues in organic electronics," *Journal of Materials Research*, vol. 19, pp. 1974-1989, 2004.
- [153] P. W. M. Blom and M. J. M. De Jong, "Device operation of polymer light-emitting diodes," *Philips Journal of Research*, vol. 51, pp. 479-494, 1998.
- [154] T. W. Kelley, P. F. Baude, C. Gerlach, D. E. Ender, D. Muires, M. A. Haase, D. E. Vogel, and S. D. Theiss, "Recent Progress in Organic Electronics: Materials, Devices, and Processes," *Chemistry of Materials*, vol. 16, pp. 4413-4422, 2004.
- [155] T. A. Chen, X. Wu, and R. D. Rieke, "Regiocontrolled synthesis of poly(3-alkylthiophenes) mediated by Rieke zinc. Their characterization and solid-state properties," *Journal of the American Chemical Society*, vol. 117, p. 233, 1995.
- [156] D. H. Hwang, M. J. Park, S. K. Kim, N. H. Lee, C. Lee, Y. B. Kim, and H. K. Shim, "Characterization of white electroluminescent devices fabricated using conjugated polymer blends," *Journal of Materials Research*, vol. 19, pp. 2081-2086, 2004.

- [157] T. Ahn, H. Lee, and S. H. Han, "Electroluminescence characteristics of polymer blend PBET and MEH-PPV," *Molecular Crystals and Liquid Crystals Science and Technology Section A: Molecular Crystals and Liquid Crystals*, vol. 377, pp. 391-394, 2002.
- [158] M. Jonforsen, I. Ahmad, T. Johansson, J. Larsson, L. S. Roman, M. Svensson, O. Inganäs, and M. R. Andersson, "Photodiodes made from poly(pyridopyrazine vinylene):polythiophene blends," *Synthetic Metals*, vol. 119, pp. 185-186, 2001.
- [159] S. H. Yang, T. P. Nguyen, P. Le Rendu, and C. S. Hsu, "Optical and electrical properties of PPV/SiO₂ and PPV/TiO₂ composite materials," *Composites Part A: Applied Science and Manufacturing*, vol. 36, pp. 509-513, 2005.
- [160] W. J. Lee, J. W. Lee, and C. G. Kim, "Characteristics of an electromagnetic wave absorbing composite structure with a conducting polymer electromagnetic bandgap (EBG) in the X-band," *Composites Science and Technology*, vol. 68, pp. 2485-2489, 2008.
- [161] Y. Dong, J. Lu, F. Yan, and Q. Xu, "Optical study of poly(3-decylthiophene)/cds nanocomposites," *Polymer Composites*, vol. 30, pp. 723-730, 2009.
- [162] L. Flandin, G. Bidan, Y. Brechet, and J. Y. Cavaillès, "New nanocomposite materials made of an insulating matrix and conducting fillers: Processing and properties," *Polymer Composites*, vol. 21, pp. 165-174, 2000.
- [163] D. Qi, K. Kwong, K. Rademacher, M. O. Wolf, and J. F. Young, "Optical emission of conjugated polymers adsorbed to nanoporous alumina," *Nano Letters*, vol. 3, pp. 1265-1268, 2003.
- [164] G. G. Malliaras, J. R. Salem, P. J. Brock, and C. Scott, "Electrical characteristics and efficiency of single-layer organic light-emitting diodes," *Physical Review B*, vol. 58, p. R13411, 1998.
- [165] V. R. Nikitenko, H. Heil, and H. von Seggern, "Space-charge limited current in regioregular poly-3-hexyl-thiophene," *Journal of Applied Physics*, vol. 94, pp. 2480-2485, 2003.
- [166] I. H. Campbell, D. L. Smith, C. J. Neef, and J. P. Ferraris, "Consistent time-of-flight mobility measurements and polymer light-emitting diode current-voltage," *Applied Physics Letters*, vol. 74, p. 2809, 1999.
- [167] I. H. Campbell, D. L. Smith, C. J. Neef, and J. P. Ferraris, "Charge transport in polymer light-emitting diodes at high current density," *Applied Physics Letters*, vol. 75, pp. 841-843, 1999.
- [168] C. R. Martin, "Nanomaterials: a membrane-based synthetic approach," *Science (Washington, D. C.)*, vol. 266, pp. 1961-6, 1994.

- [169] Y.-S. Chen and H.-F. Meng, "Intrachain carrier transport in conjugated polymer with structural and chemical defects," *Physical Review B: Condensed Matter and Materials Physics*, vol. 66, pp. 035202/1-035202/5, 2002.
- [170] S. P. Economopoulos, G. K. Govaris, C. L. Chochos, N. P. Tzanetos, A. K. Andreopoulou, J. K. Kallitsis, P. Yianoulis, and V. G. Gregoriou, "Synthesis and Characterization of Conjugated Polymers and Their Blends for Optoelectronic Applications," *Macromolecular Symposia*, vol. 205, pp. 19-31, 2004.
- [171] H. Sirringhaus, R. J. Wilson, R. H. Friend, M. Inbasekaran, W. Wu, E. P. Woo, M. Grell, and D. D. C. Bradley, "Mobility enhancement in conjugated polymer field-effect transistors through chain alignment in a liquid-crystalline phase," *Applied Physics Letters*, vol. 77, pp. 406-408, 2000.
- [172] C. De Marco, E. Mele, A. Camposeo, R. Stabile, R. Cingolani, and D. Pisignano, "Organic light-emitting nanofibers by solvent-resistant nanofluidics," *Advanced Materials*, vol. 20, pp. 4158-4162, 2008.
- [173] O. Inganäs, W. R. Salaneck, J. E. Åsterholm, and J. Laakso, "Thermochromic and solvatochromic effects in poly(3-hexylthiophene)," *Synthetic Metals*, vol. 22, pp. 395-406, 1988.
- [174] M. A. Lampert, "Simplified Theory of Space-Charge-Limited Currents in an Insulator with Traps," *Physical Review*, vol. 103, p. 1648, 1956.
- [175] Z. Bao, A. Dodabalapur, and A. J. Lovinger, "Soluble and processable regioregular poly(3-hexylthiophene) for thin film field-effect transistor applications with high mobility," *Applied Physics Letters*, vol. 69, pp. 4108-4110, 1996.
- [176] E. A. Bazzouai, G. L'Amour, S. Aeiyaeh, J. Aubard, J. P. Marsault, and P. C. Lacaze, "SERS spectra of polythiophene in doped and undoped states," *Journal of Physical Chemistry*, vol. 99, pp. 6628-6634, 1995.
- [177] G. Louarn, J. P. Buisson, S. Lefrant, and D. Fichou, "Vibrational studies of a series of α -oligothiophenes as model systems of polythiophene," *Journal of Physical Chemistry*, vol. 99, pp. 11399-11404, 1995.
- [178] R. D. Rieke and T. A. Chen, "Regiocontrolled synthesis utilizing highly reactive zinc leads to poly(alkylthiophene) with the highest regioregularity, the smallest band gap, and the highest intrinsic conductivity," *Polymer Preprints, Division of Polymer Chemistry, American Chemical Society*, vol. 34, p. 426, 1993.
- [179] S. Samitsu, T. Shimomura, S. Heike, T. Hashizume, and K. Ito, "Effective production of poly(3-alkylthiophene) nanofibers by means of whisker method using anisole solvent: Structural, optical, and electrical properties," *Macromolecules*, vol. 41, pp. 8000-8010, 2008.

- [180] M. Trznadel, A. Pron, and M. Zagorska, "Preparation and properties of fractionated regioregular poly(3-alkylthiophenes)," *Synthetic Metals*, vol. 101, pp. 118-119, 12 July 1998 through 18 July 1998 1999.
- [181] A. Menon, H. Dong, Z. I. Niazimbetova, L. J. Rothberg, and M. E. Galvin, "Polydispersity Effects on Conjugated Polymer Light-Emitting Diodes," *Chemistry of Materials*, vol. 14, pp. 3668-3675, 2002.
- [182] J. A. Merlo and C. D. Frisbie, "Field effect transport and trapping in regioregular polythiophene nanofibers," *Journal of Physical Chemistry B*, vol. 108, pp. 19169-19179, 2004.
- [183] P. W. M. Blom, M. J. M. de Jong, and J. J. M. Vleggaar, "Electron and hole transport in poly(p-phenylene vinylene) devices," *Applied Physics Letters*, vol. 68, p. 3308, 1996.
- [184] M. Al-Ibrahim, O. Ambacher, S. Sensfuss, and G. Gobsch, "Effects of solvent and annealing on the improved performance of solar cells based on poly(3-hexylthiophene): Fullerene," *Applied Physics Letters*, vol. 86, pp. 201120-3, 2005.
- [185] X. T. Hao, T. Hosokai, N. Mitsuo, S. Kera, K. K. Okudaira, K. Mase, and N. Ueno, "Control of the interchain π - π interaction and electron density distribution at the surface of conjugated poly(3-hexylthiophene) thin films," *Journal of Physical Chemistry B*, vol. 111, pp. 10365-10372, 2007.
- [186] C. K. Lee, C. C. Hua, and S. A. Chen, "Single-chain and aggregation properties of semiconducting polymer solutions investigated by coarse-grained Langevin dynamics simulation," *Journal of Physical Chemistry B*, vol. 112, pp. 11479-11489, 2008.
- [187] M. Zheng, F. Bai, and D. Zhu, "Photophysical process of MEH-PPV solution," *Journal of Photochemistry and Photobiology A: Chemistry*, vol. 116, pp. 143-145, 1998.
- [188] P. Buvat and P. Hourquebie, "Enhanced infrared properties of regioregular poly(3-alkylthiophenes)," *Macromolecules*, vol. 30, pp. 2685-2692, 1997.
- [189] D. Ausserré, A. M. Picard, and L. Léger, "Existence and Role of the Precursor Film in the Spreading of Polymer Liquids," *Physical Review Letters*, vol. 57, p. 2671, 1986.
- [190] L. Leger, M. Erman, A. M. Guinet-Picard, D. Ausserre, and C. Strazielle, "Precursor Film Profiles of Spreading Liquid Drops," *Physical Review Letters*, vol. 60, p. 2390, 1988.

- [191] S. H. Jin, S. Y. Kang, M. Y. Kim, Y. U. Chan, J. Y. Kim, K. Lee, and Y. S. Gal, "Synthesis and electroluminescence properties of poly(9,9-di-n-octylfluorenyl-2,7-vinylene) derivatives for light-emitting display," *Macromolecules*, vol. 36, pp. 3841-3847, 2003.
- [192] R. D. Deegan, "Pattern formation in drying drops," *Physical Review E - Statistical Physics, Plasmas, Fluids, and Related Interdisciplinary Topics*, vol. 61, pp. 475-485, 2000.
- [193] T.-Q. Nguyen, I. B. Martini, J. Liu, and B. J. Schwartz, "Controlling Interchain Interactions in Conjugated Polymers: The Effects of Chain Morphology on Exciton Annihilation and Aggregation in MEH-PPV Films," *The Journal of Physical Chemistry B*, vol. 104, pp. 237-255, 1999.